Institute of Geophysics
Polish Academy of Sciences

PUBLICATIONS
OF THE INSTITUTE OF GEOPHYSICS
POLISH ACADEMY OF SCIENCES

Geophysical Data Bases, Processing and Instrumentation

428 (D-75)

MONOGRAPHIC VOLUME

Analysis of Measurements and Modelling of the Biologically Active UV Solar Radiation for Selected Sites in Poland – Assessment of Photo-medical Effects

Agnieszka E. Czerwińska
and Janusz W. Krzyścin

Warsaw 2020 (Issue 2)

INSTITUTE OF GEOPHYSICS
POLISH ACADEMY OF SCIENCES

PUBLICATIONS
OF THE INSTITUTE OF GEOPHYSICS
POLISH ACADEMY OF SCIENCES

Geophysical Data Bases, Processing and Instrumentation

428 (D-75)

MONOGRAPHIC VOLUME

Analysis of Measurements and Modelling of the Biologically Active UV Solar Radiation for Selected Sites in Poland – Assessment of Photo-medical Effects

Agnieszka E. Czerwińska
and Janusz W. Krzyścin

Warsaw 2020

ISBN 978-83-66254-00-8 eISSN-2299-8020
DOI: 10.25171/InstGeoph_PAS_Publs-2020-002

Photo “Measurement point Kąty Rybackie” on the front cover by A.E. Czerwińska

Editorial Office
Instytut Geofizyki Polskiej Akademii Nauk
ul. Księcia Janusza 64, 01-452 Warszawa

C O N T E N T S

Editorial note

This publication is a revised version of A.E. Czerwinska's doctoral thesis defended at the Institute of Geophysics, Polish Academy of Sciences, under the supervision of Professor J.W. Krzyścin.

Abstract

This publication presents scenarios how to balance pro-health and detrimental effects of the UV radiation during controlled heliotherapy in order to minimize harm (erythema appearance and DNA damage) and maximize gain (increase of vitamin D level, psoriasis clearance). Referring to the literature, there is a need of finding a methodology to assess the potential risk and benefit at the moment of exposition to natural UV radiation.

A method is presented of a transition from erythemally weighted UV radiation to other biological weighted radiation (such as DNA damage, psoriasis clearance, and synthesis of vitamin D_3) with the use of measurements by broadband biometers (commonly used in meteorological stations) and hand-held UV index meters. The procedure has been developed analyzing the long-term measurements with the Brewer spectrophotometer at Belsk. The look-up tables containing the ratio between irradiance weighted with no-erythemal action spectra (DNA damage, psoriasis clearance, vitamin D_3 synthesis) and erythemal irradiance have been determined. The calculation algorithm has been built with the use of data collected in the years 2000–2010 and verified with the data collected in the years 2011–2014. An agreement of the modelled values with the observed ones has been found. The correspondence between the modeled and the observed vitamin and DNA-damage irradiance becomes slightly worse for the solar zenith angles greater than 65°. For the antipsoriatic irradiance, the model/observation agreement appears satisfying for the whole range of solar zenith angles considered. The calculation algorithm can be effectively used to mimic vitamin and DNA-damage irradiance between 9 am and 4 pm (local time) in the spring-summer period. It is the period when more time is spent outdoors and the algorithm has the highest accuracy in the personal doses calculations. Moreover, the algorithm has also been prepared to calculate non-erythemal daily doses based on the daily erythemal doses. The procedure can be effectively used to calculate antipsoriatic, DNA-damage and vitamin daily doses from standard measurements with broadband biometers used in the UV monitoring.

The erythemal daily doses of the UV radiation measured in the years 1976–2014 at Belsk are transformed to non-erythemal daily doses (vitamin D_3 synthesis, DNA damage, psoriasis clearance). The monthly and yearly trends of daily doses are calculated. It is found that the trend reversed in 2005 from increasing to decreasing one. Taking this into consideration, an original method is proposed for examining the trend significance. The method is based on the generation of hypothetical time series with statistical features resembling those in the measurement time series. The statistical significance of the trends in the periods 1976-2005 and 2005-2014 is determined, analyzing the trend values of many hypothetical time series (100,000). The trend overturning in 2005 is found at Belsk in all-analyzed biologically active UV radiation. Increasing trends in the period 1976-2005 in seasonal and monthly sums of the daily doses were replaced by the decreasing trend in the years 2005-2014, which can be more apparent in seasonal sums. The sources of such trend overturning are discussed. It seems that changes of the aerosol/clouds properties are responsible for the UV trend pattern.

During Baltic 2014 field campaign, which was conducted by the author, the measurements of the UV index are used to prepare pro-healthy scenarios of safe tanning to gain the recommended dose of the vitamin D_3 level due to solar radiation. A possibility of the antipsoriatic

heliotherapy on the Baltic coast is also examined. It is found that individual hand-held UV index meters can be used to assess in-situ UV radiation doses. The sufficient daily dose of vitamin D_3 from the skin synthesis could be received only if sunscreens are used after 20-30 minutes of sunbathing without any sun protection. Dermatologists suggest that sunscreens should be used all the time, which in turn causes inadequate vitamin D_3 level. The examination of the antipsoriatic doses received during the Baltic 2014 campaign proves that it is possible to conduct the antipsoriatic heliotherapy there. The antipsoriatic heliotherapy was previously commonly conducted in the selected health-care centres in the Canary Islands and at the Dead Sea.

The last chapter analyzes a city agglomeration of Warsaw impact on the erythemaly weighted UV radiation. Differences between erythemal doses collected by the Brewer spectrophotometers in Warsaw and at Belsk are calculated. Mean difference between both spectrophotometers midday 6 h (symmetrically around noon) doses for the clear sky is about 5%, while it was around 1%, when they were working together at the same location (Belsk). Modelled values (from the clear-sky radiation transfer model) showed that the midday 6 h doses, due to the difference in geographic location, are 2% lower in Warsaw. It allows for concluding that the specific city aerosol induces only 2% decline of erythemal radiation, which is similar to that caused by the geographic location difference. For all sky conditions the mean difference in the midday 6 h doses between two location was only 1% greater than that for the clear sky. Thus, the city agglomeration of Warsaw does not generate any specific cloudiness that could weaken the UV radiation. Pro-healthy heliotherapy is possible also in such large agglomeration and can be as effective as in the suburbs.

ANALIZA POMIARÓW I MODELOWANIE BIOLOGICZNIE CZYNNEGO PROMIENIOWANIA UV SŁOŃCA DLA WYBRANYCH MIEJSC W POLSCE – OCENA EFEKTÓW FOTOMEDYCZNYCH

Streszczenie

W niniejszej publikacji przedstawiono scenariusze zbilansowania pro-zdrowotnych i szkodliwych skutków promieniowania UV, podczas kontrolowanego naświetlania promieniami słonecznymi, tak aby ograniczyć jego szkodliwy wpływ (niszczenie struktury DNA, rumień) i osiągnąć maksymalne korzyści, takie jak wzrost poziomu witaminy D_3 w organizmie, czy też leczenie zmian łuszczycowych. W literaturze wskazywana jest potrzeba prowadzenia działań w tym zakresie, a także znalezienia metody pomiarowej, która pozwoli na równoczesną ocenę zagrożeń i korzyści już w trakcie ekspozycji na naturalne promieniowanie UV.

W pracy określono metodykę, jak z pomiarów promieniowania erytemalnego z zastosowaniem, np. szerokopasmowych biometrów powszechnie używanych na stacjach meteorologicznych lub tanich indywidualnych mierników indeksu UV, wyznaczyć biologicznie czynne napromienienie związane z niszczeniem struktur DNA, skórną syntezą witaminy D_3 oraz usuwaniem zmian łuszczycowych. Procedura została opracowana wykorzystując pomiary spektrofotometrem Brewera w Belsku. Wyznaczono tabele ilorazów pomiędzy natężeniem napromienienia niszczącego DNA, antyłuszczycowego i witaminalnego, a natężeniem napromienienia erytemalnego. Algorytm obliczeniowy został zbudowany na podstawie danych zebranych w latach 2000–2010 i zweryfikowany z zastosowaniem widm promieniowania UV zmierzonych w latach 2011–2014. Stwierdzono zgodność wartości modelowanych z wartościami obserwacyjnymi. Dla napromienienia witaminalnego i niszczącego DNA zgodność natężeń zaczyna się pogarszać dla kątów zenitalnych Słońca powyżej 65°. Dla napromienienia antyłuszczycowego zgodność jest dobra dla wszystkich kątów zenitalnych Słońca. Procedurę obliczeniową można efektywnie wykorzystać dla wyznaczania natężeń napromienienia witaminalnego i niszczącego DNA w godzinach 9:00–16:00 (czas lokalny) w sezonie wiosenno-letnim. Jest to okres, na który zwykle przypada aktywność człowieka na wolnym powietrzu i procedura będzie przydatna do oceny indywidualnego napromienienia człowieka. Ponadto opracowano tabele ilorazów i algorytm obliczeniowy dla dawek dziennych. Na podstawie zgodności wartości obserwacyjnych z modelowanymi oraz biorąc pod uwagę fakt, że odchylenia standardowe zwykle nie przekraczają kilku procent wartości średniej, stwierdzono, że procedurę obliczeniową można efektywnie wykorzystać dla wyznaczania dziennych dawek napromienienia o skuteczności antyłuszczycowej, niszczenia DNA i witaminalnej, mając do dyspozycji zmierzone dawki dzienne erytemalne.

Stosując wspomnianą wcześniej metodykę i mając do dyspozycji serię pomiarową dziennych dawek napromienienia erytemalnego z lat 1976–2014 w COG Belsk wyznaczono dzienne dawki napromienienia dla innych efektów biologicznych. Następnie obliczono trendy promieniowania UV o skuteczności erytemalnej, witaminalnej, antyłuszczycowej i niszczenia DNA. Zaobserwowano, że w roku 2005 trend zmienia się z rosnącego na malejący. W związku

z tym zastosowano niestandardową metodę badania trendu. Metoda opierała się na generacji potencjalnie możliwych serii czasowych o cechach zbliżonych do serii pomiarowej, a następnie wyznaczeniu istotności statystycznej współczynnika liniowego trendu w latach 1976–2005 i 2005–2014 na podstawie własności zespołu składającego się z wielu takich hipotetycznych serii (w naszym przypadku 100 000). Około 2005 roku obserwuje się zmianę kierunku trendu w biologicznie czynnym napromienieniu w Belsku. Wyraźny, rosnący trend w latach 1976–2005 w sezonowych i miesięcznych sumach napromienienia zostaje zastąpiony przez malejący trend w latach 2005–2014, który jest najlepiej widoczny w sezonowych sumach napromienienia. Trendy te są mniej wyraźne w sumach miesięcznych. Wykazano, że zmiana nie jest wynikiem odwrócenia trendu w całkowitej zawartości ozonu, a prawdopodobnie spowodowana jest wzrostem zachmurzenia lub grubości optycznej aerozolu atmosferycznego.

Stosując opracowane w pracy algorytmy przeliczeniowe, oraz wykorzystując wyniki wykonanych przez autora pomiarów w trakcie kampanii Bałtyk 2014, przedstawiono prozdrowotne scenariusze opalania w celu osiągnięcia właściwej dawki witaminy D_3, a także przeprowadzenia helioterapii antyłuszczycowej nad Morzem Bałtyckim. Na podstawie wykonanych obliczeń i pomiarów stwierdzono, że w warunkach bezchmurnego nieba wyniki pomiarów indeksu UV wyselekcjonowanymi tanimi ręcznymi miernikami są zgodne z wartościami modelowanymi indeksu UV otrzymanymi z równania transferu promieniowania w atmosferze. Ponadto w warunkach zachmurzonego nieba indywidualne mierniki mogą służyć do oceny warunków napromienienia w miejscu opalania. Na podstawie obliczonych personalnych dawek napromienienia witaminalnego stwierdzono, że stosując krem z filtrem SPF 30 (zalecanym przez dermatologów) podczas całego pobytu na słońcu, nie jest możliwe osiągnięcie dawki, odpowiadającej wymaganemu dziennemu zapotrzebowaniu na witaminę D_3. Obliczono także dawki antyłuszczycowe i ustalono, że latem nad Bałtykiem można stosować helioterapię antyłuszczycową.

Kolejnym etapem było określenie, w jakim stopniu warszawska aglomeracja miejska wpływa na promieniowanie ultrafioletowe o skuteczności erytemalnej. Różnica w poziomie promieniowania pomiędzy Warszawą, a miejscowością mniej zanieczyszczoną, jaką jest Belsk, została stwierdzona na podstawie danych pomiarowych ze spektrofotometrów Brewera, działających jednocześnie w tych miejscowościach. Średnia różnica wskazań obydwu przyrządów, dla bezchmurnego nieba, nie przekroczyła 5%, podczas gdy ta różnica wyniosła ponad 1% w sytuacji, kiedy przyrządy działały w Belsku. Modelowe obliczenia pokazały, że średnia różnica wynikająca z położenia geograficznego wynosi 2%. Na tej podstawie stwierdzono, że wpływ specyficznego aerozolu miejskiego na biologicznie czynne promieniowanie ultrafioletowe jest niewielki (~2%) i porównywalny do różnicy, wynikającej z położenia geograficznego. Dla pomiarów wykonywanych w każdych warunkach atmosferycznych średnia różnica dawek okołopołudniowych pomiędzy dwoma stacjami była o 1% wyższa niż dla nieba bezchmurnego, przy jednoczesnym wzroście wartości współczynnika zmienności, co było wynikiem wpływu lokalnego zachmurzenia na poziom promieniowania UV. Stwierdzono, że warszawska aglomeracja miejska nie generuje specyficznego zachmurzenia osłabiającego promieniowanie UV. Przeprowadzenie helioterapii prozdrowotnej w Warszawie jest zatem możliwe i tak samo efektywne, jak w miejscowościach podwarszawskich.

1. INTRODUCTION

1.1 Historical overview – the Sun and the human

Before the UV radiation was discovered, scientists in many countries had been observing various phenomena associated with the solar radiation for many centuries (Hockberger 2002). And so, already in 1275, the Dominican Albertus Magnus described an experiment in which he noticed that under the influence of sunlight, silver dissolved in nitric acid turned black. In 1556 Georg Fobricius, an Italian alchemist, noticed that silver chloride turned black under the influence of sunlight. On the other hand, in 1614 Angelo Sala observed that silver nitrate grated to powder turned black under the influence of sunlight. In 1777 a Swedish chemist Charles Willam Scheele discovered that paper impregnated with silver chloride turned black more effectively in blue and violet light (the shortest part of the visible light spectrum) upon exposure to solar radiation passed through a prism. Eventually, the UV radiation was discovered simultaneously by a German physicist Johann Wilhelm Ritter and a British chemist Wilhelm Hyde Wallastone in 1801. They noted that invisible rays just beyond the purple end of the visible spectrum (400–700 nm) were even more effective in reactions with silver compounds. To emphasise the reactive nature of these rays and to distinguish them from "heat rays" (as infrared radiation was defined) W. Ritter named them "deoxidising rays". The name evolved over time to "chemical rays" by which the UV rays were known in the 19th century. Finally, the name ultraviolet was adopted, which was created from the Latin phrases; "ultra" (above) and violet. In 1902 Samuel Pierpont Langley (the inventor of the bolometer improving measurements of the energy transmitted by solar radiation) discovered that UV radiation is attenuated by 40% while passing through the atmosphere, and the cause of this phenomenon was explained in 1909 by A. Miethe and E. Lehmann who noted that the absorbing factor is most probably the presence of ozone and oxygen in the upper layer of the atmosphere. Furthermore, in 1919 Carl Dorno described that the intensity of the UV radiation changes with the time of day and season of the year, and in 1921 Charles Fabry and Henri Buisson determined the spectral distribution of solar radiation and the absorption characteristics of ozone. In 1924 Gordon Dobson invented a spectrophotometer to measure column amount of ozone, i.e. the so-called total ozone in the atmosphere (following modification of its electronic components, the spectrophotometer is still the basic instrument for measuring ozone in the atmosphere). The Robertson–Berger meter, constructed in the 1970s, was the precursor of the currently commonly used broadband UV-B radiometers.

The health benefits as well as health damages of solar radiation have been discussed for many centuries. At the beginning of the 19th century, the therapeutic effects of solar radiation were noted in children with rickets. Research on rickets led to the discovery of vitamin D. Concurrently, it was noted that the long-term effects of UV radiation on the skin may be damaging.

The first description of psoriasis appeared in the first century AD and its author was Aulus Cornelius Celsus (Szramka-Pawlak 2008). In the Middle Ages, psoriasis was commonly confused with leprosy, thus patients were excluded from social life. In 1798 Robert Willan described psoriasis as a separate disease entity and was the first to use its current Latin name – *psoriasis*. In 1845 Ferdinand von Hebra made the final distinction between psoriasis and leprosy. Moreover, in the 1860s Heinrich Koebner and Heinrich Auspitz contributed to the understanding of some psoriatic lesions mechanisms (the so-called Koebner phenomenon and Auspitz sign). In 1892 Duncan Bulkley described *psoriasis* as a chronic disease associated with the weakening of the immune system and suggested the heredity of the disease.

In the 17th century, in England, Daniel Whistler and Francis Glisson were the first to scientifically describe rickets which since then was called the "English disease" (Sajkowska and Paradowska 2014). The disease was primarily characterised by knee valgus and the so-called "frog belly"; however, other symptoms associated with the calcium metabolism disorder in the

body were also observed. In the 18th century the French physician Levacher Feutrie presented the course and the various forms of rickets (Wicha 2012). In 1822, Polish physician and biologist Jędrzej Śniadecki was the first to demonstrate the theory that rickets could be treated by exposure to solar radiation in the study titled "On the Physical Upbringing of Children" (Śniadecki 2002). He suggested that infants should be exposed to sunlight to prevent rickets. In 1865 Armand Trosseau confirmed the relationship between rickets and insufficient sun exposure. He also sought the causes of the disease in poor diet and suggested consuming fish oil. In 1890 Theobald Palm established that the occurrence of the disease is related to light intensity. Simultaneously, reports on the harmful effects of sunlight appeared as early as 1858 (Albert and Ostheimer 2002). Jean-Martin Charcot noted that solar radiation caused skin erythema.

The technological development in the field of construction of artificial UV radiation sources resulted in significant progress in the treatment of psoriasis and rickets in the 19th century. In 1802 Humphry Davy invented the first artificial ultraviolet source, an arc lamp. Furthermore, in 1892 Leo Arons designed a low-pressure lamp and in 1906 a high-pressure mercury lamp was created by Richard Küch (Raab 1997).

In the 20th century, medical breakthroughs in the field of dermatology occurred. At that time Nils Ryberg Finsen (1860–1904) was the precursor of photo- and heliotherapy. He proposed the treatment of cutaneous tuberculosis utilising arc lamps modified by himself or sunlight focused by lenses. The scientific achievements of N.R. Finsen were highly rated, and in 1903 he received the Nobel Prize in Medicine. Following publication of N.R. Finsen's works, heliotherapy and phototherapy were proposed for the treatment of nearly every skin disease: acne, alopecia areata, pruritus of various origins, and since 1905 psoriasis. In the 1920s, N.R. Finsen's students, Oscar Bernhard and Auguste Rollier, stated that during progressive tanning, combined with outdoor activities, rest and good nutrition, the health of tuberculosis patients improved. In 1906 Ernst Kromayer demonstrated a mercury quartz lamp with a cooling system to enable irradiation by direct application to the sore area. The lamp was commonly used in dermatology for many years. In 1910 Carl von Bach invented and subsequently, in 1913, improved the mercury quartz lamp which by its spherical shape resembled artificial sun. Also in 1913 a Polish doctor Jan Raczyński presented the results of his research, by which he concluded that the sun exposure affects the calcium metabolism in the body. In 1919 a German doctor Kurt Huldschinsky suggested utilising an artificial source of ultraviolet (quartz lamp) for the treatment of rickets. In the 1920s Edward Mellanby discovered that rickets was probably related to a fat-soluble nutrient. In 1921 he called this substance vitamin D (it was the fourth marked vitamin). In addition, in 1923 Harry Goldblatt and Katherine Soames explained the mechanism for production of this vitamin in the body through the skin synthesis. Alfred F. Hess conducted extensive research on vitamin D on the basis of which, in 1925, he concluded that only direct exposure to solar rays results in the desired effect in the treatment of rickets. In the same year William H. Goeckermann proposed the use of photosensitising substances in antipsoriatic phototherapy. A.F. Hess requested the assistance of a chemist Adolf Windaus to determine the chemical structure of vitamin D. Based on numerous laboratory studies Adolf Windaus determined this structure for which he was awarded the Nobel Prize in Chemistry in 1928. Furthermore, in the 1930s, A. Windaus and, independently, F.A. Askew and co-workers isolated ergocalciferol and cholecalciferol (inactive forms of vitamin D_2 and D_3) from irradiated food. In 1936 researchers from the German pharmaceutical company Merck obtained synthetic vitamin D. Additionally, in 1941 Frank L. Apperly noted a relationship between increased sun exposure and reduced incidence of several types of cancer.

In the 1920s phototherapy was extremely popular, while at the beginning of the 20th century some disturbing publications considering the effects of excessive tanning on the increased occurrence of skin cancers started to appear. The first publication by James N. Hyde appeared in

1906 and subsequently in 1907 William Dubreuilh suggested that skin cancers were more common in labourers who worked outside. Also W.T. Corlett in 1915, C.N. Paul in 1918, and J.N. McCoy in 1920 confirmed the observations of the relationship between UV radiation and skin cancer. These reports were confirmed on the basis of laboratory tests on animals by George M. Findlay in 1928 (Albert and Ostheimer 2003). In the 1940s and 1950s the studies were repeated numerous times with similar results. It therefore became widely known that ultraviolet radiation is damaging and the protective measures against its adverse effects were sought. The first sunscreen was presented as early as 1928 in the United States. In 1942 Stephen Rothman and Jack Rubin demonstrated a sunscreen which was not only chemically stable, fragrance-free and did not leave stains on clothes, but was also effective. During the World War II, sunscreens were used to protect American soldiers against strong radiation in tropical areas. Active ingredients of the creams, which also protected against UV-A, were used for the first time in the late 1950s. In 1972 the American Health Service recommended placing a sun protection factor (SPF) on cream labels.

In the 1970s William Watson ultimately confirmed the hypothesis on the heredity of psoriasis. In 1971 Mark R. Haussler and colleagues isolated the first active metabolite of vitamin D (calciphediol), and then the final active form (calcitriol) was identified. Over time, it was discovered that psoriasis is associated with the human immune system. At that time, Parrish et al. (1974) applied UV-A therapy using a photosensitising substance – psoralen. In the 1980s the TL-01 fluorescent lamp emitting narrow-band UV-B radiation 311 ±1 nm was produced. It was determined that the therapy using these fluorescent lamps brings good results. In 1980 Michael F. Holick noted that topically applied vitamin D was effective for the treatment of psoriasis (Holick 1989). It was also the first time that the brothers Cedrik F. Garland and Frank C. Garland published the hypothesis that vitamin D protects against the occurrence of colorectal carcinoma. In 1981 John A. Parrish presented the spectrum of biological effectiveness of UV radiation in removing psoriatic lesions (Parrish and Jaenicke 1981).

Currently, phototherapy is used for the treatment of diseases such as psoriasis, atopic dermatitis, *lichenoides chronica* dandruff and itching of various origins. In addition to phototherapy, UV radiation is also used for treating rickets in children, physiological jaundice in newborns as well as seasonal depression. Appropriate balancing of the negative and positive effects of ultraviolet radiation on the human body is currently the subject of global debate (Baggerly et al. 2015).

1.2 Ultraviolet radiation

Ultraviolet radiation is classified as electromagnetic radiation, the wavelength range of which is between visible and X-ray radiation (Fig. 1).

Based on the energy level and the impact of UV radiation on the human body, it is most often divided into UV-C (100–280 nm), UV-B (280–315 nm), and UV-A (315–400 nm) radiation. UV-C is completely absorbed by oxygen and ozone molecules in the atmosphere. On the other hand, 95% of UV-B is absorbed by the ozone layer in the stratosphere. UV-B rays are primarily responsible for the destruction of DNA structures, causing certain types of skin cancers. UV-B radiation also leads to erythema on the skin which usually appears one day after the exposure to solar radiation. Moreover, UV-B radiation initiates the synthesis of vitamin D_3 in the human skin. Conversely, UV-A radiation is absorbed by the ozone layer only to a small extent. Part of the radiation in this range which penetrates through the ozone layer is scattered or absorbed in the troposphere by aerosol molecules; however, the vast majority reaches the Earth's surface. The damaging effects of the UV-A radiation are only visible after a long time. This type of radiation is believed to cause skin photoaging (wrinkles, loss of skin elasticity) and to contribute indirectly to the destruction of DNA structures (Bowszyc-Dmochowska 2010),

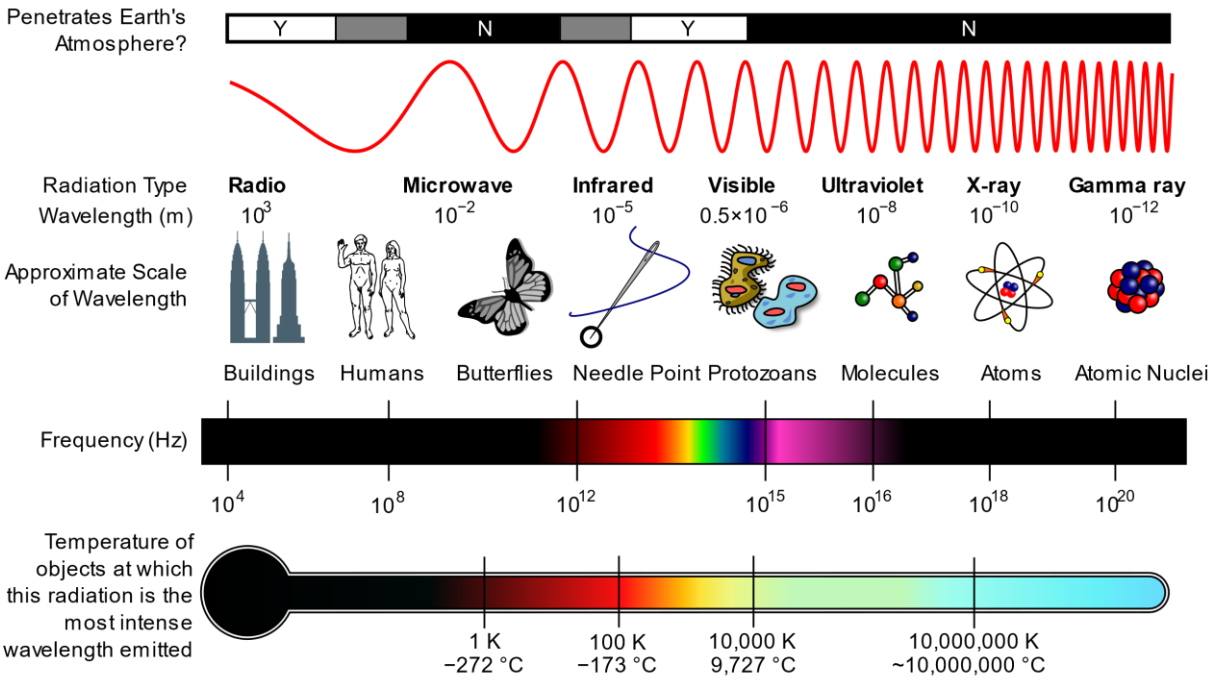

Fig. 1. Type of electromagnetic radiation depending on the wavelength (source: https://commons.wikimedia.org/w/index.php?curid=2974242).

simultaneously causing changes of the skin colour, i.e. suntan. UV-A radiation penetrates deeply and reaches the dermis, while UV-B stops in the epidermis.

The intensity of ultraviolet radiation reaching the surface of the Earth depends on many factors:

- total ozone in the atmosphere – ozone absorbs some of the UV radiation;
- the solar zenith angle (SZA) – dependent on the time of the day, season of the year, and the latitude. Most radiation reaches the surface of the Earth when the Sun is highest above the horizon, i.e. during solar noon and within the range of two hours before and two hours after noon in the cloudless sky;
- altitude above sea level – the intensity of UV radiation increases with the altitude above sea level (7% per km);
- degree of cloudiness – the effect of clouds on ultraviolet radiation is diverse. A uniform cloud layer weakens (reflects or scatters) some of the solar radiation. At the same time, clouds located on different levels in the atmosphere may cause an increase in the UV radiation near the surface of the Earth by multi-reflection of rays between the cloud layers;
- ground albedo – some surfaces (such as water, sand, snow) reflect solar rays causing the increase of UV radiation intensity;
- presence of atmospheric aerosols – they reduce radiation as a result of scattering or absorption.

1.3 Biologically active solar radiation

Biologically active solar radiation is associated with the effectiveness of causing specific biological effects (e.g. erythema or suntan) after exceeding some threshold doses, which are characteristic for a given organism. The organism's response to radiation depends on the wavelength incident on the skin. Usually, the shorter the wave the stronger the biological response. The

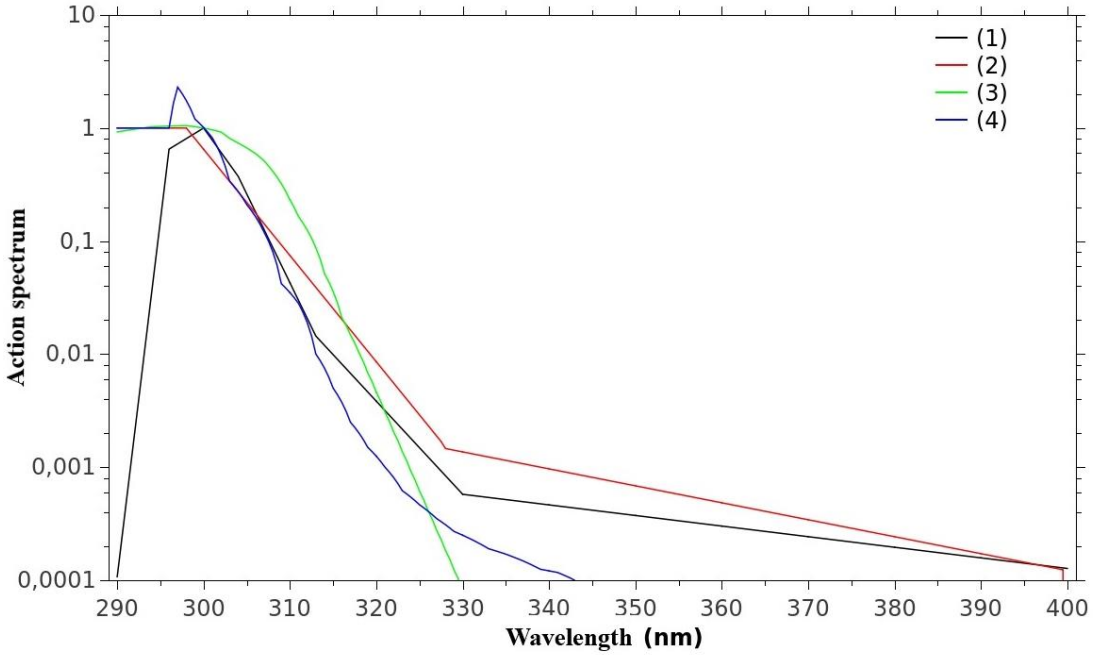

Fig. 2. Functions of biological efficacy depending on the wavelength for biological effects considered in the present study: (1) removal of psoriatic lesions (Krzyścin et al. 2014), (2) occurrence of erythema (as recommended by The International Commission on Illumination (CIE 1987)), (3) synthesis of vitamin D_3 in the body (according to CIE recommendations (CIE 2006)), (4) destruction of the DNA structure (Setlow 1974).

action spectrum determines the intensity of the induction of a particular biological effect as a function of the wavelength.

Figure 2 demonstrates the biological efficacy functions depending on the wavelength for the biological effects considered in the present study.

To determine the biologically effective intensity of irradiation [W/m^2], the spectral radiation intensity should be multiplied by the biological efficacy function (action spectrum), and subsequently the resulting values should be integrated over the entire spectral range. Biologically effective dose is an integral of the intensity of irradiation over a given time interval. Doses are expressed in J/m^2.

1.3.1 UV radiation with erythemal efficacy

UV radiation with erythemal efficacy is the type of radiation causing the appearance of erythema on the skin. Erythema (originating from the Greek *erythema*) is an inflammatory reaction of the skin resulting from the excessive exposure to solar radiation and involving vasodilatation at the site of exposure. The visible effect is redness, reaching its maximum within 24 hours following the exposure. Redness is accompanied by other symptoms such as burning, oedema, as well as malaise, nausea, headache and sometimes fever. After three days, the symptoms usually disappear, and the skin darkens and desquamates (Bowszyc-Dmochowska 2010).

To establish the duration of sunbathing without sunburn, the so-called minimal erythema dose (MED) was determined, i.e. a threshold dose, after which erythema occurs on the skin. This dose depends on the individual sensitivity of human skin. It is generally accepted that there are six skin phototypes, and the threshold doses have been defined for each of them (Fitzpatrick 1988). Table 1 presents the division into phototypes and the MED values corresponding to each phototype.

Table 1
Skin phototypes with the corresponding minimal erythema doses (MED)

Type	Characteristics	Reaction to sunlight	MED [J_{ERYT}/m^2]
I	Pale white skin, often with freckles, blue/green/hazel eyes, blond/red hair	It always burns, it is difficult to tan	200–300
II	Fair skin, blue/green eyes	It burns easily, it is difficult to tan	250–350
III	Darker white skin	It tans after the initial burn	300–500
IV	Light brown skin	Minimal burns, it tans easily	450–600
V	Brown skin	It rarely burns, it tans easily and strongly	600–1000
VI	Dark brown/black skin	It never gets burned, it always gets a lot of tan	1000–2000

The UV index (*UVI*) is dimensionless (the erythemal irradiance in W/m^2 multiplied by 40 m^2/W) and denotes the maximum daily value of erythemal irradiance (usually around local noon). The World Health Organisation (WHO) defined protection measures to be applied at specific UV index levels (Fig. 3, http://www.who.int/uv/en/).

Sunscreen is one of the most important sun protection measures. The active ingredients of creams can reflect and scatter UV radiation (minerals) or absorb and convert it into heat (chemical ingredients). Current cream formulas usually combine both types of ingredients which enables high protection. The sun protection factor (SPF) allows us to assess what protection a given cream provides, i.e. how effectively the erythemal dose could be reduced (Reisch 2002). It is assumed that sunscreens let 1/SPF part of radiation through (Norval and Wulf 2009). The SPF index is determined experimentally in laboratories. To simplify, it is assumed that the application of a cream with an SPF = X filter prolongs the time of safe tanning X times (Brannon 2015). Sunscreen also provides protection against UV-A radiation; however, the system for assessing the degree of protection is still not clearly defined.

Fig. 3. Protection measures to be applied depending on the UV index (according to WHO).

1.3.2 UV radiation with vitamin D efficacy

UV radiation with vitamin D efficacy concerns the vitamin D_3 synthesis in the human body. Skin synthesis of vitamin D_3 involves the transformation of subcutaneous cholesterol, 7-dehydrocholesterol, into previtamin D_3 due to solar radiation in the UV-B range. As a result of metabolic reactions, it is transformed into the inactive form of vitamin D_3, cholecalciferol (Webb 2006). The first stage of vitamin D activation (obtained from food or skin synthesis) takes place in the liver by hydroxylation, as a result of which the active metabolite 25-(OH)D (calcifediol) is produced. Further biochemical changes in the kidneys lead to the formation of the active form of vitamin D – 1,25-$(OH)_2$D, calcitriol (Sajkowska and Paradowska 2014). Serum calcifediol concentration is used as an indicator of the body's supply of vitamin D. In the case of deficiencies, supplementation is used. Vitamin D is administered primarily in the form of medicines containing vitamin D_2 (ergocalciferol) or D_3 (cholecalciferol). In the case of liver diseases or other conditions, supplementation also involves medicines containing the metabolite of vitamin D, calcifediol. In Poland, in the period from September to April it is advised to orally take from 800 to 2000 IU (international units) per day, i.e. 20–50 mg/day (Płudowski et al. 2013).

The standard daily dose (1SDD) of the vitamin D effective radiation is utilised in the assessment of amount of vitamin D_3 sythetised due to UV overexposure. This is essential to produce a dose in the body, which corresponds to the oral administration of 1000 IU (25 mg) of vitamin D_3. According to the Holick's rule, this dose can be received by exposing 1/4 of the body surface to 1/4 MED (Dowdy et al. 2010). As a consequence of a lack of agreement regarding analytical formulae of the vitamin D_3 efficacy spectrum in connection to the metabolic transformations of vitamin D_3 in the body, several 1SDD values have been suggested (Norval et al. 2010). Krzyścin et al. (2011a) proposed a dose of 1SDD = 100 $J_{VIT\text{-}D3}/m^2$ for a value of MED = 300 J_{ERYT}/m^2 (this MED value is in the range for phototype II, Table 1), taking into account the Holick's rule and the results of the work by Dowdy et al. (2010). To standardise the indicators used in the further parts of the text, 1SDD dose = 100 $J_{VIT\text{-}D3}/m^2$ will be referred to as MVD_3D (the minimal vitamin D_3 dose).

In light of recent research, evaluation of the appropriate vitamin D_3 level in the human body has gained significant interest. Until recently, it was believed that vitamin D_3 deficiency results only in the malfunction of the skeletal system and contributes to the development of rickets and osteoporosis. The first reports on other roles of vitamin D_3 than the control of calcium and phosphorus metabolism were released in 1980 by Cedric and Frank Garland; however, those were treated with caution (Sajkowska and Paradowska 2014). The results concerning the relation between vitamin D_3 and the prevention of large bowel cancer were released again in 2006, when more attention was given to this issue (Garland et al. 2006). In recent years, intensive research has shown that vitamin D_3 deficiencies can also lead to functional anomalies in the muscular, digestive and nervous systems (Holick and Chen 2008). Furthermore, a connection between the prevalence of other types of cancers and vitamin D_3 deficiency was also determined (WHO 2008).

Dermatologists and WHO recommend avoiding sun exposure at times when UV radiation is the strongest and in case of necessity to go outside sunscreen must be strictly used (Baggerly et al. 2015). The research conducted so far on the relation between the use of sunscreen and a reduced level of vitamin D in the human body does not give unambiguous results. Some researchers suggest that the use of sunscreens can effectively block the synthesis of vitamin D in the skin (Matsuoka et al. 1987, 1988; Sayre and Dowdy 2007, Springbett et al. 2010). In fact, people who use such creams on a daily basis may have even higher levels of vitamin D than people who do not apply them (Kligman et al. 1989; Marks et al. 1995; Farrerons et al. 2001). Norval and Wulf (2009) explain this paradox by the fact that people who use sunscreen tend to spend more time outdoors on sunny days than those who do not use photoprotection. Moreover,

sunscreen is usually applied incorrectly (uneven distribution of the cream, no re-application during the day).

1.3.3 UV radiation with anti-psoriatic efficacy

UV radiation with anti-psoriatic efficacy, mainly in the UV-B range, causes the removal of psoriatic lesions. Psoriasis is an autoimmune or a genetic skin disease. It is a persistent condition with periods of remission. Psoriasis is considered to be a social disease because of the fact that it involves approx. 2% of the population and due to its persistent nature (Szramka-Pawlak 2008). Patients have problems carrying out basic activities and the disease often affects them mentally and influences their relations with other people (Horn et al. 2007). Treatment of focal lesions using UV radiation can be conducted by artificial exposure to UV-B radiation: selective ultraviolet phototherapy (SUP), narrow UV-B range (the use of the TL-01 311 nm ±1 nm fluorescent lamps), UV-A radiation utilising medicines sensitising to this type of radiation (photochemotherapy – PUVA), and heliotherapy (exposure to sun radiation) sometimes combined with thalassotherapy (saline or sea baths).

Krzyścin et al. (2014), proposed the analytical formula for the efficacy spectrum for removing psoriatic lesions. They also determined a standard dose equal to 317.9 J_{AP}/m^2 corresponding to the dose obtained during a single exposure to the TL-01 fluorescent lamps in a dermatological cabin. Index "AP" means that in the calculation, the light spectrum has been weighted by the anti-psoriatic action spectrum. To unify the indicators in the further parts of the text, such dose will be marked as MAPD (minimal anti-psoriatic dose).

1.3.4 UV radiation with the destructive effect on DNA

Two primary types of malignant skin cancer occur as a consequence of destruction of the DNA structure under the influence of UV-B radiation, i.e. basal-cell and spinocellular. The development of skin malignancies is associated with long-term or repeated exposure to ultraviolet radiation. In healthy skin, the DNA regenerates rapidly following a short exposure. Malignancy occurs when damaged or mutated cells multiply, thus covering an increasingly larger area of the skin (Wolnicka-Głubisz and Płonka 2007). A different type of cancer related to ultraviolet radiation is malignant melanoma; however, its formation is influenced by more factors than exposure to excessive UV radiation alone (Noonan et al. 2012). In contrast to other biological effects mentioned earlier, no threshold dose has been established, after which the DNA structure is destroyed.

1.4 Purpose and scope of the study

Currently in Poland over 90% of people suffer from vitamin D_3 deficiency (Płudowski et al. 2014). Appropriate levels have only been observed in pregnant women, newborns and young children, for whom supplementation is recommended as a must. The lifestyle of Poles also does not lead to obtaining the appropriate level of this vitamin. Polish people tend to spend most of their time indoors, particularly between 11 am and 3 pm local time, when the UV radiation is the strongest. Additionally, the geographical location of Poland results in the fact that the dose from the skin synthesis, corresponding to the daily recommended amount of 1000 IU of vitamin D_3 administered orally, can only be obtained in the period from April to September. It seems that the most advantageous time to reduce the deficiency is the vacation period, when people tend to spend more time outdoors. One can also take advantage of this period by carrying out anti-psoriatic heliotherapy.

Broadband biometers are popular devices used in monitoring erythermal radiation (e.g. SL501, or Kipp and Zonen UVS-ET), which measure the erythemal strength of solar irradiation.

The strength of UV irradiation in the whole spectral range is measured by spectrophotometers but the high price precludes their common use. Hence, with the aim to determine radiation doses with non-erythemic biological efficacy, it is necessary to appropriately convert erythemal doses to doses with different biological efficacy.

The study reported here presents scenarios on how to use the health-promoting UV radiation exposures safely by analysing measurement data obtained from standard measures (biometers and personal hand-held UV index meters).

Detailed goals are as follows:

- development of a model for converting erythemal doses into biologically active doses pertaining vitamin D synthesis, anti-psoriatic and DNA damaging effects;
- determination of a method for defining and assessing the non-linear trend of the long-term solar radiation with various biological efficacies utilising the developed model as well as the original method for testing statistical significancy of trends;
- development of initial health-promoting scenarios to reduce the vitamin D_3 deficiency and to carry out anti-psoriatic heliotherapy using low-cost personal hand-held UV index meters;
- assessment whether urban environment, on the example of Warsaw, has an impact on the conditions for heliotherapy.

Chapter 2 demonstrates a model that enables the conversion of erythemal doses into irradiance doses with vitamin D synthesis, anti-psoriatic and DNA damaging efficacy. For this purpose, a conversion algorithm has been constructed for the above-mentioned biological effects on the basis of the results of the UV spectral measurements using the Brewer spectrophotometer at Belsk in 2000–2014. By using radiation spectra, biologically efficient UV irradiation intensity is determined during this period. The quotients of irradiance intensities with different biological efficacy and erythemal irradiance intensity depending on the solar zenith angle, and total ozone are determined. The model for calculating daily doses is constructed on a similar basis.

Data from years 1976–2014, which will be used to estimate the long-term variability of biologically active UV radiation, are analysed in Chapter 3. The considered measurement series of the erythemal doses is one of the longest series in the world. Daily data from the Belsk Observatory database, are used to calculate the total doses: monthly, annual and seasonal (from April to September). Erythemal data and UV indexes are also used to calculate irradiation doses for other biological effects by employing the algorithm proposed in Chapter 2. To determine the uncertainty of the trend of biologically active radiation in years 1976–2014, the "bootstrap" method is utilised.

Chapter 4 includes the results of research on the possibilities of carrying out phototherapy at the Baltic Sea during a more than two-week stay in Kąty Rybackie on the Vistula Spit, where the UV index was measured, using personal (carefully selected), low-cost hand-held meters. The results of the measurements are used to calculate erythemal, vitaminal and anti-psoriatic doses by the model developed in Chapter 2. The conducted calculations will help to answer the question of how to plan a stay on a beach to obtain the appropriate dose of vitamin D_3 safely and to assess an opportunity of anti-psoriatic heliotherapy by the Baltic Sea.

In Chapter 5, with the help of the measurement data obtained from the Brewer's spectrophotometers in years 2013–2014, the erythemal irradiation doses in Warsaw and at the Central Geophysical Observatory (CGO) Belsk are compared. Haberlie et al. (2015) proved that a city can have an impact on increasing overcast, while Acosta and Evans (2000) claimed that the doses of the UV radiation can be more than 20% lower in a city than in exurban areas. On the basis of the comparison carried out in this work, an influence of air pollution in Warsaw on the conditions for heliotherapy is evaluated.

Baggerly et al. (2015) claimed that it is essential to create a tool to assess the negative and positive effects of ultraviolet radiation in order to obtain the greatest benefits, while minimising health risks. Thanks to the algorithm presented, safe scenarios will be proposed for independent determination of the heliotherapy duration, using commonly available and low-cost meters of UV index, allowing psoriasis healing and the adequate level of vitamin D_3 synthesis.

2. ALGORITHMS FOR EVALUATING THE INTENSITIES AND DOSES OF BIOLOGICALLY ACTIVE SOLAR RADIATION

Broadband erythemal meters used at the UV monitoring stations supply the daily dose and the maximum daily erythemal irradiance (UV index). The current chapter describes a method for converting the erythemal values into values for other selected biological effects: synthesis of vitamin D_3 in the human skin, removal of psoriatic lesions, and destruction of the DNA structure. While constructing the computational algorithm for the above-mentioned biological effects, the results of measurements of the UV spectrum using the Brewer spectrophotometer at Belsk in 2000–2014 were used. With the help of the radiation spectrum, the biologically effective UV irradiation intensity, the so-called dose rate (*DR*), was determined during this period. Subsequently, the relationship between vitaminal *DR* (anti-psoriatic and DNA) and erythemal *DR* was established depending on the solar zenith angle (SZA) and total ozone (TO_3). The computational algorithm was built based on the data collected between 2000–2010 and verified utilising the UV radiation spectrum measured between 2011–2014.

In recent years, the correlation between radiation with erythemal and vitaminal efficacy has been studied (Kimlin et al. 2007; McKenzie et al. 2009; Pope et al. 2008; Fioletov et al. 2009) to determine the vitaminal doses based on erythemal doses obtained from standard (broadband) radiometers operating at monitoring stations. Considering the high cost of UV spectrophotometers, measurements of the UV spectra and thereby direct determination of doses for effects other than the erythemal ones are only possible in few places, e.g. in Poland, at the Institute of Geophysics of the Polish Academy of Sciences stations (Belsk and Warsaw). The functions of transition from erythemal to vitaminal doses were previously determined based on numerical simulations (using the solar radiation transfer model in the Earth's atmosphere) for a clear sky at given total ozone and atmospheric aerosol properties. In the present study, the *DR* measurements were used for selected biological effects and *DR* erythemal → *DR* other than erythemal transition functions were determined depending on the SZA and TO_3. Subsequently, the procedure was repeated for daily doses. In the consecutive chapters, the aforementioned functions for the vitaminal, anti-psoriatic and DNA weighted solar irradiation will be applied in simulations of daily doses other than erythemal based on the measurements using standard broadband erythemally weighted UV meters.

2.1 Model

The dose rate at moment t, $DR_{\mathrm{BIOL}}(t)$, for the selected biological effect (BIOL) was obtained from the following formula:

$$DR_{\mathrm{BIOL}} = \int_{\lambda} Spectrum(t,\lambda) \cdot AS_{\mathrm{BIOL}}(\lambda) d\lambda \tag{1}$$

where $Spectrum(t, \lambda)$ is the spectral irradiation in W/(m^2 nm), $AS_{\mathrm{BIOL}}(\lambda)$ denotes the relative (i.e. usually normalised to 1 for wavelength, where the biological effect is maximal) action spectrum for the BIOL effect. The following action spectra were used:

- erythemal – ERYT (according to the CIE 1987 recommendations);

- vitamin – VIT-D_3 (according to the CIE 2006 recommendations) normalised to 1 at 300 nm (Fioletov et al. 2009);
- anti-psoriatic – AP (Krzyścin et al. 2014);
- destruction of DNA – DNA (Setlow 1974 – $IE_{DNA} = 1$ for $\lambda < 298$ nm).

The aforementioned spectra of biological efficacy have been presented in Fig. 2 in Chapter 1.

Utilising the UV spectra obtained from measurements using a Brewer spectrophotometer in the years 2000–2010, the $DR_{BIOL}(t)$ ratios were determined:

$$DR_{VIT\text{-}D3}/DR_{ERYT},\ DR_{AP}/DR_{ERYT},\ DR_{DNA}/DR_{ERYT}.$$

The number of spectra analysed in years 2000–2010 is presented in Fig. 4.

The corresponding TO_3 and SZA values were determined for each UV spectrum. To calculate the solar zenith angle, astronomical formulas were applied for the position of the Sun at the moment of the spectrum measurement for the wavelength of 310 nm (measurement of the full spectrum takes 4 minutes). Measurement of TO_3 with the Brewer spectrophotometer is conducted many times a day and is independent of the UV spectrum measurement. TO_3 values measured at the moments closest to the time of the spectrum measurement were determined based on the principle that the closest TO_3 readings were from the DirectSun observations having the highest accuracy and if there is a lack of such readings, then TO_3 values were selected from zenith-sky observations.

Subsequently, the mean values of the ratios and their standard deviations in the function of *total ozone-solar zenith angle* in the ranges of TO_3 from 240 DU to 520 DU every 10 DU and SZA from 25° to 90° every 5° were determined. For instance, the mean value of the ratio for the pair ***i*** (total ozone) and ***j*** (angle) was obtained from averaging all of the values obtained in the case when the measured value of TO_3 meets the condition $250\ \text{DU} + 10\ \text{DU}*(\boldsymbol{i} - 1) \le TO_3 < 250\ \text{DU} + 10\ \text{DU}*\boldsymbol{i}$, and at the time of the measurement the solar zenith angle meets the condition $25° + 5°\ (\boldsymbol{j} - 1) \le \text{SZA}\ 25° + 5°\ \boldsymbol{j}$. In the Appendix (Tables 1A–3A), the mean values of ratios for pairs TO_3-SZA are presented for DR_{DNA}/DR_{ERYT}, DR_{AP}/DR_{ERYT}, $DR_{VIT\text{-}D3}/DR_{ERYT}$, respectively. Furthermore, the standard deviations for the aforementioned relations between dose rates with various biological efficacies are shown in Tables 4A–6A.

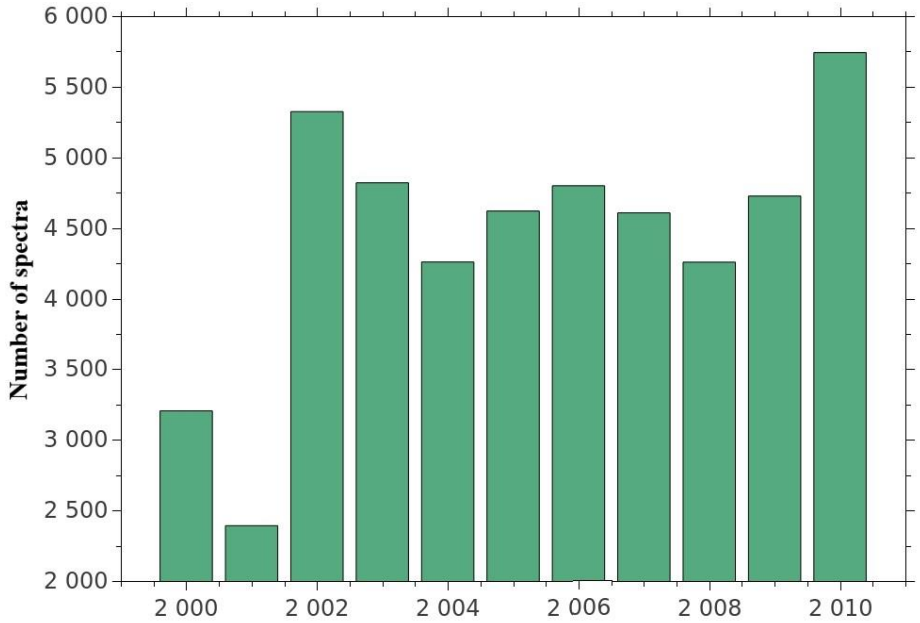

Fig. 4. Number of spectra analysed in the years 2000–2010.

Standard deviations usually do not exceed a few percent of the mean value; therefore, *DR* other than erythemal can be estimated with accuracy better than 10% based on the measured *DR* values for erythemal irradiation. In further parts of the text, modelled values of non-erythemal dose rates will be determined from the measured values of erythemal dose rates according to the following algorithm:

$$DR_{\mathrm{BIOL}}(t) = F_{\mathrm{BIOL}}(\mathrm{TO_3},\mathrm{SZA}) \cdot DR_{\mathrm{ERYT}}(t) \tag{2}$$

where the $F_{\mathrm{BIOL}}(\mathrm{TO_3}, \mathrm{SZA})$ value is determined from the interpolation between the matrix values for the appropriate biological effect. Depending on the chosen effect, one of the Tables (1A, 2A or 3A) is selected.

To determine the $F_{\mathrm{BIOL}}(\mathrm{TO_3}, \mathrm{SZA})$ value, the bilinear interpolation in triangles was utilised for the any $\mathrm{TO_3}$ and SZA values. For this purpose, triangles including a point with coordinates $\mathrm{TO_3}$, SZA were selected from the matrix. The location of the vertices of the triangle is shown in Fig. 5.

Subsequently, the interpolation formulas found at: http://www1.eonfusion.com/manual/index.php /Formulae_for_interpolation were applied.

$$F_{\mathrm{BIOL}}(\mathrm{TO_3}, \mathrm{SZA}) = \mathrm{A} * \mathrm{TO_3} + \mathrm{B} * \mathrm{SZA} + \mathrm{C} \tag{3}$$

where:

DET = determinant of the matrix = $\mathrm{TO_3}$ _1 * SZA _2 – $\mathrm{TO_3}$ _2 * SZA _1 + $\mathrm{TO_3}$ _2 * SZA _3 – $\mathrm{TO_3}$ _3 * SZA _2 + $\mathrm{TO_3}$ _3 * SZA _1 – $\mathrm{TO_3}$ _1 * SZA _3

A = ((SZA _2 – SZA _3) * $DR_{\mathrm{BIOL}}/DR_{\mathrm{ERYT}}$_1 + (SZA _3 – SZA _1) * $DR_{\mathrm{BIOL}}/DR_{\mathrm{ERYT}}$_2 + (SZA _1– SZA _2) * $DR_{\mathrm{BIOL}}/DR_{\mathrm{ERYT}}$_3) / DET

B = (($\mathrm{TO_3}$ _3 – $\mathrm{TO_3}$ _2) * $DR_{\mathrm{BIOL}}/DR_{\mathrm{ERYT}}$_1 + ($\mathrm{TO_3}$ _1 – $\mathrm{TO_3}$ _3) * $DR_{\mathrm{BIOL}}/DR_{\mathrm{ERYT}}$_2 + ($\mathrm{TO_3}$ _2 – $\mathrm{TO_3}$ _1) * $DR_{\mathrm{BIOL}}/DR_{\mathrm{ERYT}}$_3) / DET

C = (($\mathrm{TO_3}$ _2 * SZA _3 – $\mathrm{TO_3}$ _3 * SZA _2) * $DR_{\mathrm{BIOL}}/DR_{\mathrm{ERYT}}$_1 + ($\mathrm{TO_3}$ _3 * SZA _1 – $\mathrm{TO_3}$ _1 * SZA _3) * $DR_{\mathrm{BIOL}}/DR_{\mathrm{ERYT}}$_2 + ($\mathrm{TO_3}$ _1 * SZA _2 – $\mathrm{TO_3}$ _2 * SZA _1) * $DR_{\mathrm{BIOL}}/DR_{\mathrm{ERYT}}$_3) / DET

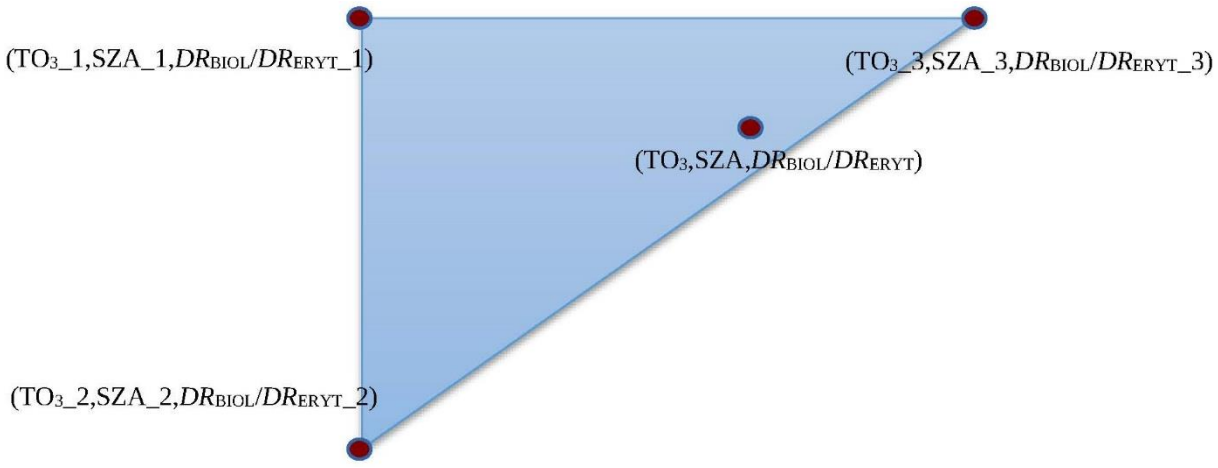

Fig. 5. Interpolation triangle for determining the F_{BIOL} function ($\mathrm{TO_3}$, SZA).

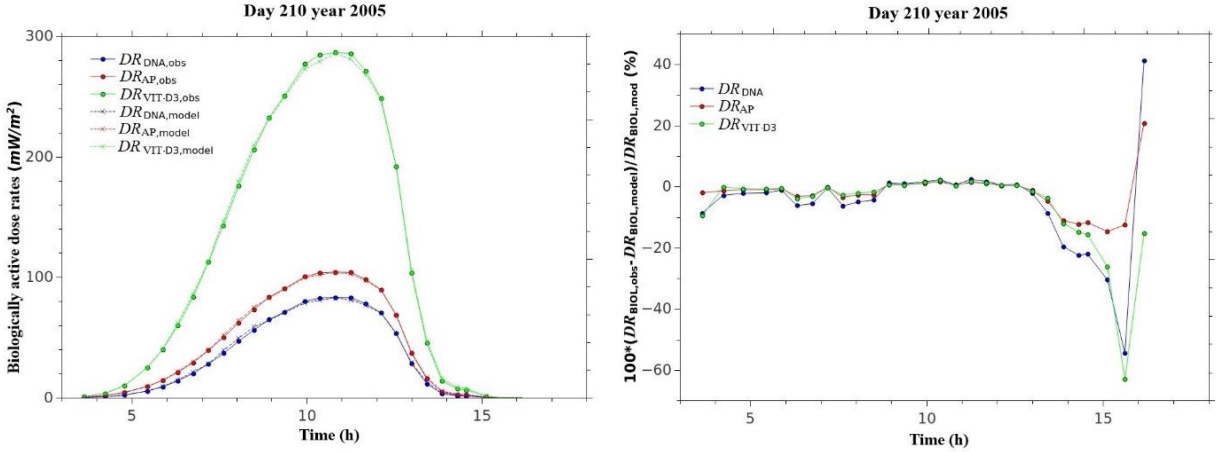

Fig. 6. Exemplary daily course of biologically effective UV irradiance for a sunny day (left panel). Normalised deviation of the observed values from the modelled ones in % (right panel).

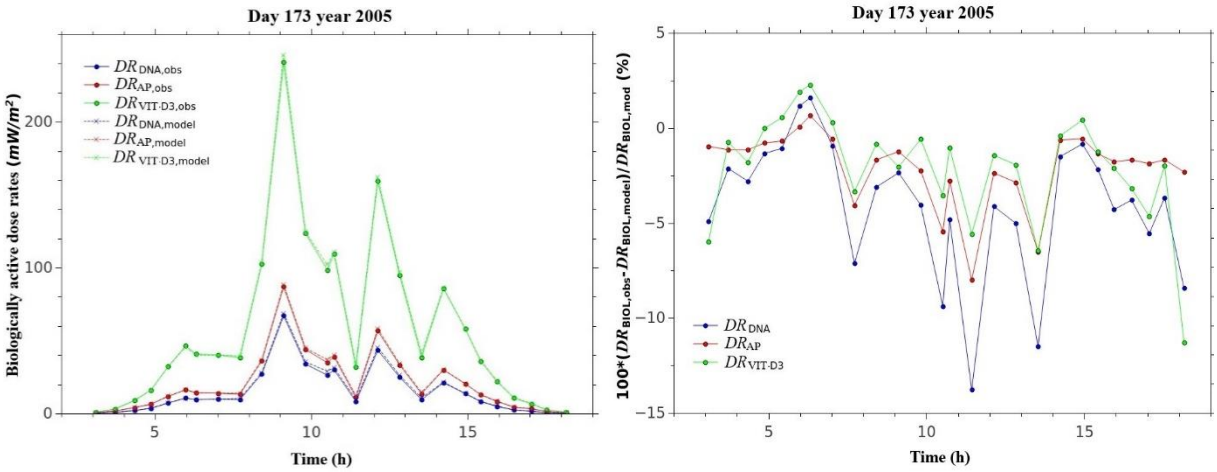

Fig. 7. Exemplary daily course of biologically effective UV radiation for a day with variable cloudiness (left panel). Normalised deviation of the observed values from the modelled ones in % (right panel).

Examples of daily courses of DR_{BIOL} from observations (solid line) and calculated using Eq. (3) (dashed line) are demonstrated in Figs. 6 and 7.

As it can be observed in Fig. 6, the model works well for a cloudless sky. The modelled values practically do not differ from the observed ones for the scale used in the figure. Around 3 pm (GMT) the complete overcast occurred. At this time, a considerable change was noted in the normalised deviation of the observed values from the modelled ones (increase in absolute values above 10%).

In addition, as it can be seen in Fig. 7, the model maps the *DR* value with efficacy different from erythemal based on DR_{ERYT} in variable cloudiness conditions well. The absolute value of the normalised deviation of the observed values from the model ones increases with decreasing DR_{ERYT} values.

2.2 Model verification

To verify the model, the values of irradiance were calculated for the spectra collected at Belsk in the years 2011–2014. Outlier values, i.e. spectra, which for small SZA (< 50°) provided the relationship $DR_{VIT\text{-}D3} \sim DR_{ERYT}$, were removed from the dataset. It was confirmed that some of the measurements could have been conducted during episodes with extreme overcast. An ex-

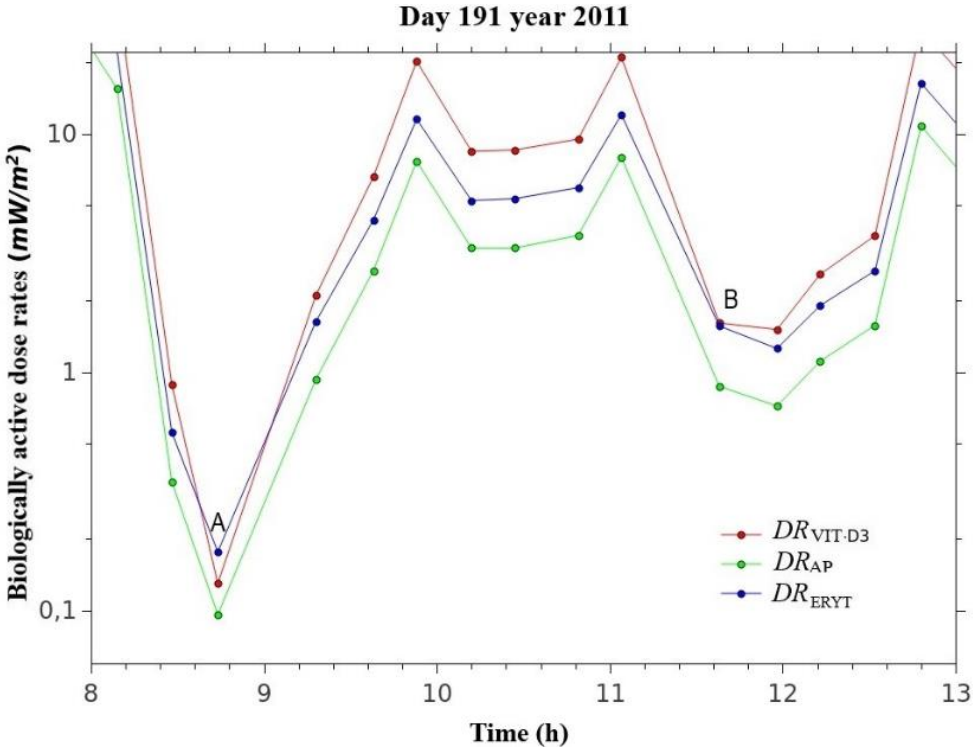

Fig. 8. Exemplary daily course of biologically effective dose rates for a day with episodes of extreme overcast.

amplary daily course for such a day is illustrated in Fig. 8. Measurements at moments A and B were included in the "outliers" category.

Model verification involved the comparison of the values calculated from the spectral measurements by the Brewer spectrophotometer with model values according to Eqs. (2) and (3).

The percentage deviation between these values was determined:

$$\frac{DR_{\mathrm{BIOL,model}} - DR_{BIOL,\mathrm{obs}}}{DR_{\mathrm{BIOL,obs}}} \cdot 100\% \tag{4}$$

where $DR_{\mathrm{BIOL,model}}$ is the modelled value, and $DR_{\mathrm{BIOL,obs}}$ is the value calculated from the spectral measurements.

Subsequently, the dependence of the calculated deviation value on the *DR* value obtained from the measurement, total ozone as well as the solar zenith angle was determined.

The above dependencies are presented in Figs. 9–20 and in Table 2.

On the scatterplots (Figs. 9, 13, and 17) the perfect agreement line, diagonal of the square, is shown in red. In other figures, besides the percentage deviation values, there are the mean value of the ratios (red line) and the smoothed ratios (green curve) by the LOWESS (**Lo**cally **We**ighted **S**catterplot **S**moothing) method (Cleveland 1979).

For dose rate, weighted by the DNA action spectrum, the coefficient of determination r^2 was 0.998, which indicates a very good fit. The mean percentage deviation of the modelled values from the observed values (Table 2) is 7.85% ± 5.83 (1 σ). From the graph of the percentage deviation as a function of the solar zenith angle (SZA) and from Table 2, it can be observed that the difference between the observed and modelled values increases with SZA. Above SZA of 65°, the rate of the difference increases. The same behaviour is found for $TO_3 > 400$ DU.

For dose rate, weighted by the anti-psoriasis (AP) action spectrum, the coefficient of determination r^2 was 0.999, which indicates a very good fit. The mean percentage deviation of the

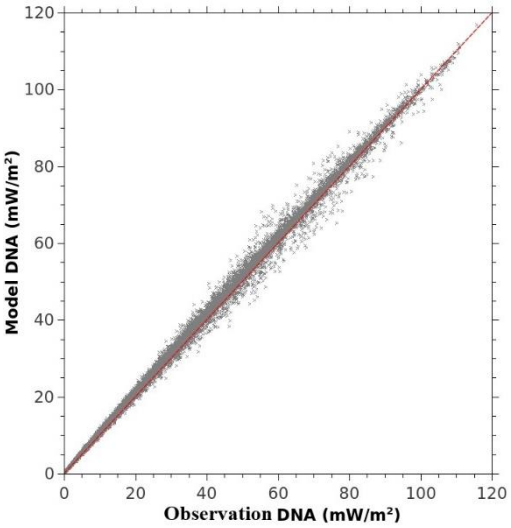

Fig. 9. Modelled DR values for DNA as a function of the measured values.

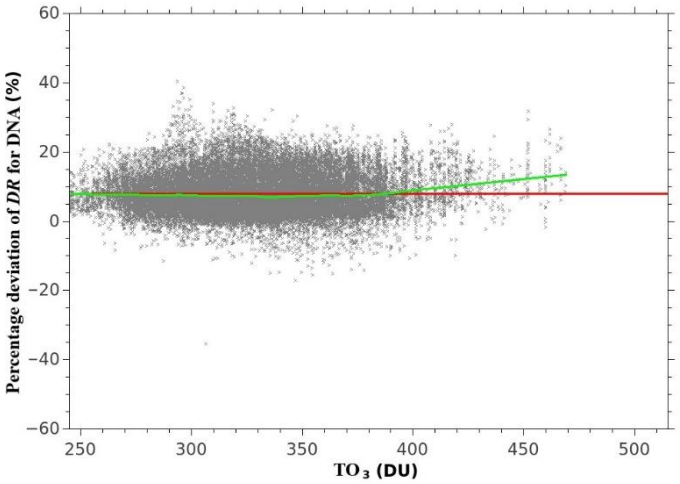

Fig. 10. Percentage deviation of DR modelled from DR measured for DNA as a function of total ozone.

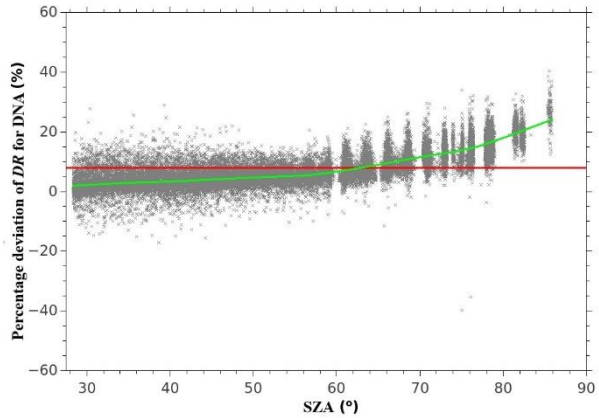

Fig. 11. Percentage deviation of DR modelled from DR measured for DNA as a function of solar zenith angle.

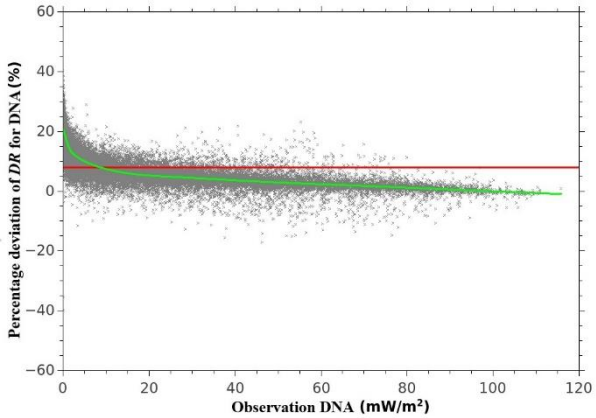

Fig. 12. Percentage deviation of DR modelled from DR measured for DNA as a function of the measured DR value.

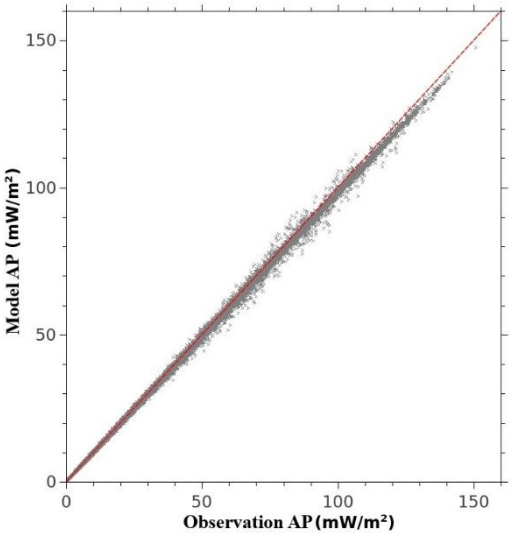

Fig. 13. Modelled DR values for AP as a function of measured values.

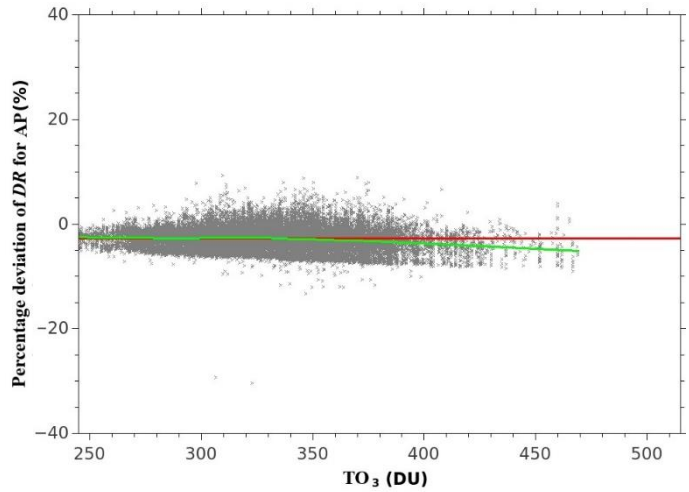

Fig. 14. Relationship for AP analogously to the one presented in Fig. 10.

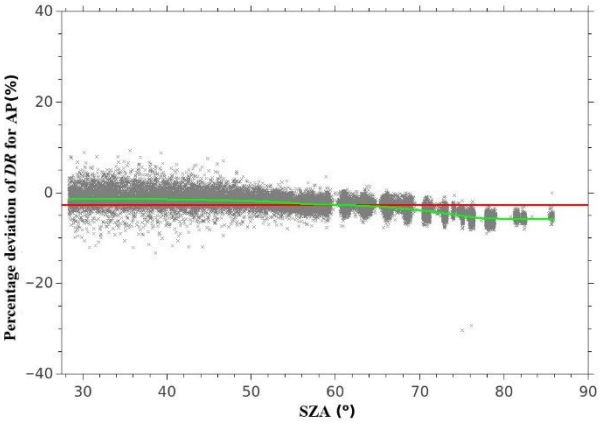

Fig. 15. Relationship for AP analogously to the one presented in Fig. 11.

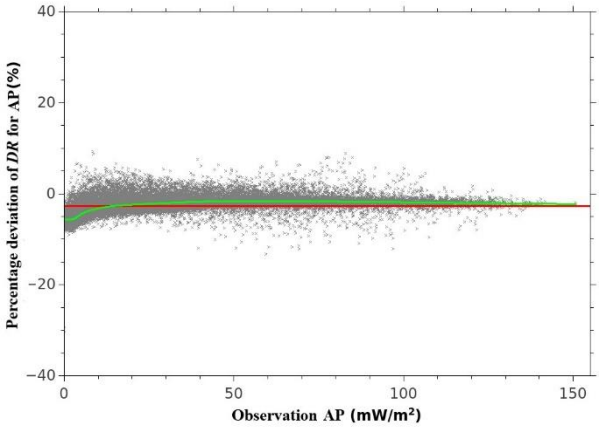

Fig. 16. Relationship for AP analogously to the one presented in Fig. 12.

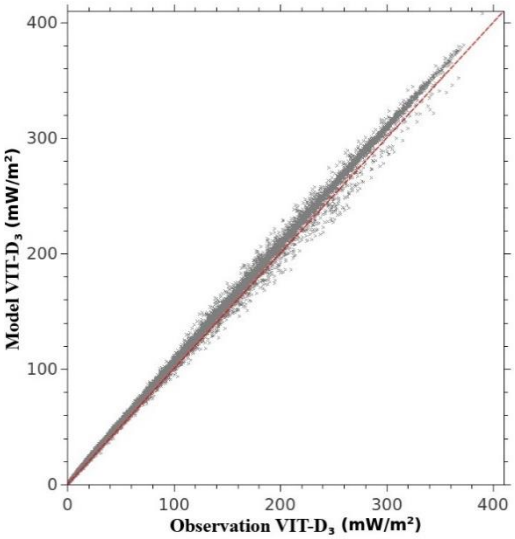

Fig. 17. Modelled DR values for VIT-D_3 as a function of measured values.

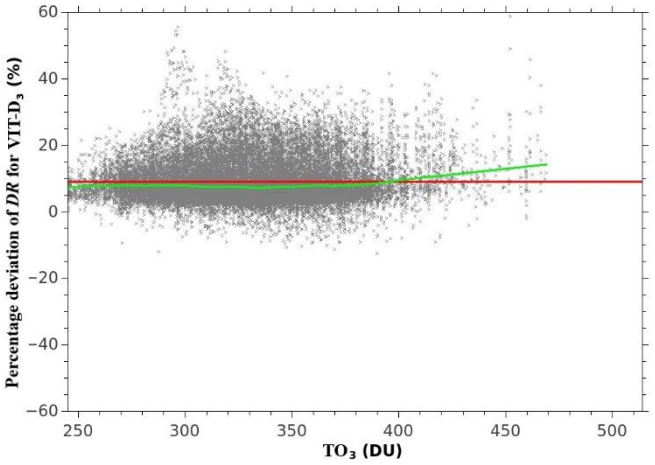

Fig. 18. Relationship for VIT-D_3 analogously to the one presented in Fig. 10.

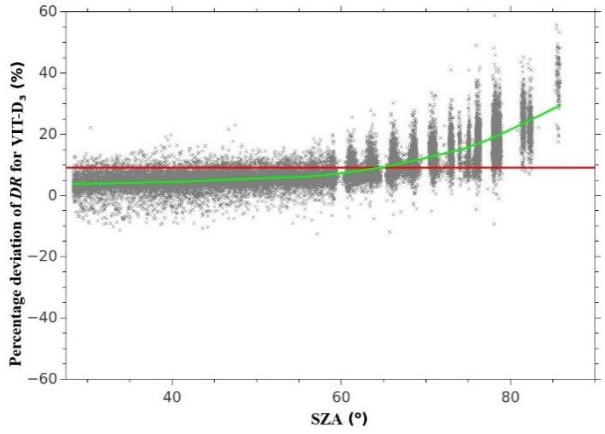

Fig. 19. Relationship for VIT-D_3 analogously to the one presented in Fig. 11.

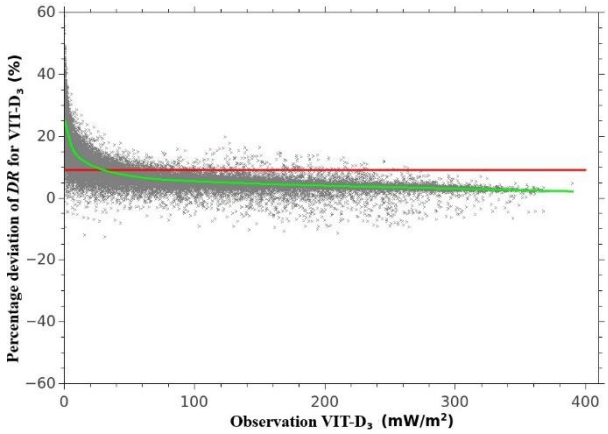

Fig. 20. Relationship for VIT-D_3 analogously to the one presented in Fig. 12.

Table 2

The values of the mean value and standard deviation of the percentage deviation according to Eq. (4) for various ranges of the solar zenith angle and biological effects

Solar zenith angle (SZA)	Mean value			Standard deviation (σ)		
	DNA	Psoriasis	Vit. D_3	DNA	Psoriasis	Vit. D_3
all	7.85	–2.80	8.96	5.83	2.07	6.59
< 35	2.98	–1.14	3.87	4.34	2.12	2.87
35–45	3.70	–1.32	4.43	3.85	1.81	2.73
45–55	4.82	–1.82	5.53	2.97	1.29	2.42
55–65	6.90	–2.68	7.53	3.07	1.08	2.99
65–75	11.22	–3.72	12.04	3.46	1.16	4.18
75–85	16.01	–5.71	18.89	4.17	0.99	6.24
<35–65	4.87	–1.84	5.58	3.77	1.65	3.08

modelled values from the observed values (Table 2) is –2.80% ± 2.07 (1 σ). As in the case of *DR* values for DNA, it can be found that for AP the model and observation agreement decreases for SZA > 65°. However, in the case of DR_{AP}, the difference does not exceed 10% even for SZA > 75° (Table 2).

For dose rate, weighted with the vitaminal (VIT-D_3) action spectrum, the coefficient of determination r^2 was 0.999, which indicates a very good fit. The mean percentage deviation of the modelled values from the observation values (Table 2) is 8.96% ± 6.59 (1 σ). The graph of the percentage deviation as a function of SZA reveals that the difference between the observed and modelled values increases with SZA, especially for SZA > 65° (Table 2). For total ozone above 400 DU, the percentage deviation increases marginally.

Figure 21 demonstrates the time (GMT) of the occurrence of SZA = 65° at Belsk for subsequent days in 2010. The period in the spring and summer season when SZA < 65° occurs during the whole day of human activity outdoors, i.e. from approximately 7 am (GMT) till 2 pm (GMT), when DR_{BIOL} reaches high values.

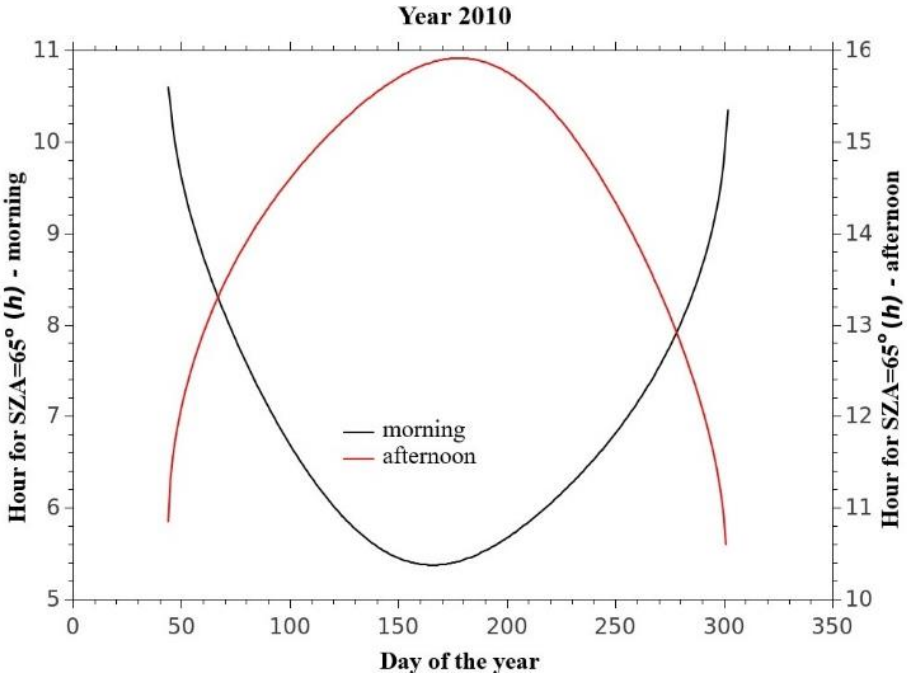

Fig. 21. Relationship between the time of occurrence of the solar zenith angle 65° at Belsk and the day in 2010.

For SZA < 65°, models 2 and 3 reproduce measurement values best (see Table 2). Therefore, DR_{BIOL} other than erythemal can be effectively modelled through a period of frequent outdoor activities.

2.3 Model for daily doses

Daily UV doses for the selected biological effect (BIOL), $D_{BIOL}(d)$, were determined by integrating the dose rates, $DR_{BIOL}(t)$:

$$D_{\mathrm{BIOL}}(d) = \int_{\mathrm{sunrise}}^{\mathrm{sunset}} DR_{\mathrm{BIOL}}\,(t)dt \tag{5}$$

where $DR_{BIOL}(t)$ was determined from Eq. (1), t denotes time (in seconds), and "sunrise" and "sunset" are the time of the sunrise and sunset on a given day d, respectively. Analytical formulas for biological efficacy were used as in Subchapter 2.1.

For each day with UV spectrum measurements in the April–September period, the corresponding TO_3 value and the minimum (at noon) solar zenith angle were determined. Astronomical formulas for the highest position of the Sun during the day (solar noon) were used to calculate SZA. TO_3 values were calculated as mean values from measurements between 9 am and 12 pm (GMT), i.e. around the midday sun. Then the mean ratios between $D_{BIOL}(d)$ and their standard deviations as a function of *total ozone-solar zenith angle* in the range of TO_3 from 240 DU to 520 DU every 10 DU and SZA from 25° to 55° were determined.

In the Appendix, in Tables 7A–9A, the mean values of ratios for *total ozone-solar zenith angle* pairs for D_{DNA}/D_{ERYT}, D_{AP}/D_{ERYT}, $D_{VIT\text{-}D3}/D_{ERYT}$ are demonstrated, respectively. In addition, Tables 10A–12A depict standard deviations for the aforementioned ratios between daily doses of UV radiation with different biological efficacies.

Standard deviations usually do not exceed a few percent of the mean value. Therefore, daily doses different than erythemal can be estimated with accuracy better than 10% based on the measured daily dose values for erythemal irradiation.

Modelled values of the daily doses for non-erythemal irradiation can be determined from the values of daily doses of erythemal irradiation depending on TO_3 and SZA according to the following algorithm:

$$D_{\mathrm{BIOL}}(d) = G_{\mathrm{BIOL}}(\mathrm{TO_3}, \mathrm{SZA}) * D_{\mathrm{ERYT}}(d) \tag{6}$$

where the $G_{BIOL}(TO_3, SZA)$ value is determined by interpolation between the matrix values of $D_{ERYT} \Rightarrow D_{BIOL}$. Depending on the biological effect considered, one of the Tables (7A, 8A or 9A) could be selected.

To determine $G_{BIOL}(TO_3, SZA)$ the bilinear interpolation in triangles is used for any TO_3 and SZA. For this purpose, Eq. (3) is utilised, where instead of DR_{BIOL}, D_{BIOL} is used.

Table 3 presents the values of the mean percentage deviation between modelled and observed doses (calculated analogously to Eq. (4)) and their standard deviations depending on the solar noon zenith angle. Similarly to the values of dose rate, an increase in the value of the percentage deviation was observed along with increasing SZA. The mean value of the percentage deviation does not exceed 1.5%.

Figures 22 and 23 show exemplary courses of observed (solid line) and calculated D_{BIOL} using Eq. (6) (dashed line) in July for the year when cloudless days prevailed (2005) or the year with variable clouds conditions (2007), respectively.

Both figures demonstrate that the model works well for both sunny days and the days with variable cloudiness conditions. In Fig. 22, a smaller variability in the values of the daily doses can be noticed than in Fig. 23. With lower radiation variability, the normalised deviation of the

observed values from the modelled ones does not exceed 5%. For high variability of cloudiness conditions, the maximum normalised deviations reach 10% for days with significantly strong attenuation of radiation due to clouds.

Table 3

The mean values and the standard deviation of the percentage difference between modelled/observed daily doses for various ranges of minimum solar zenith angles and biological effects for the period April–September

Solar zenith angle (SZA)	Mean value			Standard deviation		
	DNA	Psoriasis	Vit. D_3	DNA	Psoriasis	Vit. D_3
all	0.27	0.07	0.13	4.77	2.16	3.63
< 35	0.0003	–0.06	–0.02	4.52	2.05	3.26
35–45	0.29	0.09	0.09	4.92	2.35	3.76
45–55	1.09	0.42	0.66	5.15	2.06	4.34

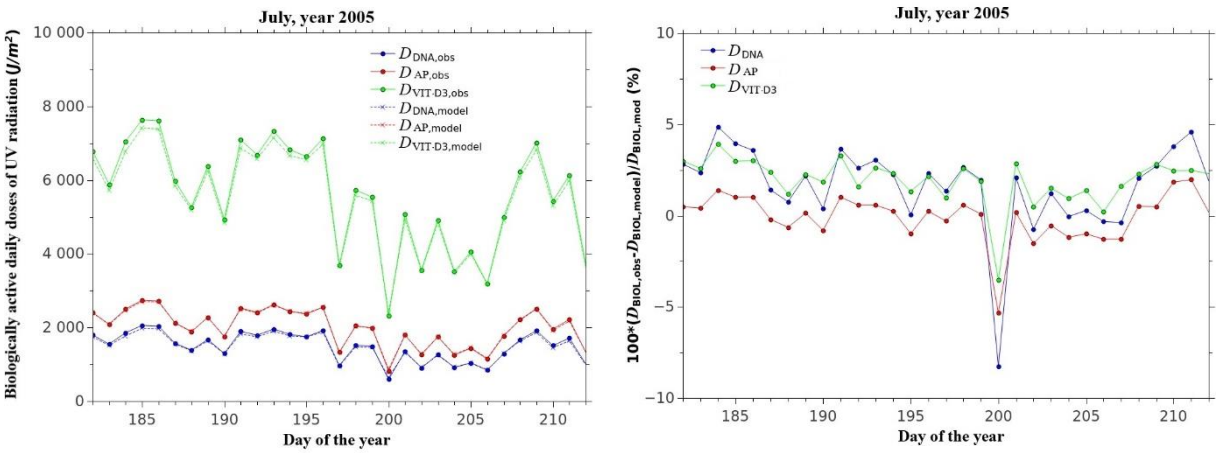

Fig. 22. Exemplary course of biologically active daily doses of UV radiation for July 2005 – left panel. Normalised deviation of the observed daily doses from the modelled ones in % – right panel.

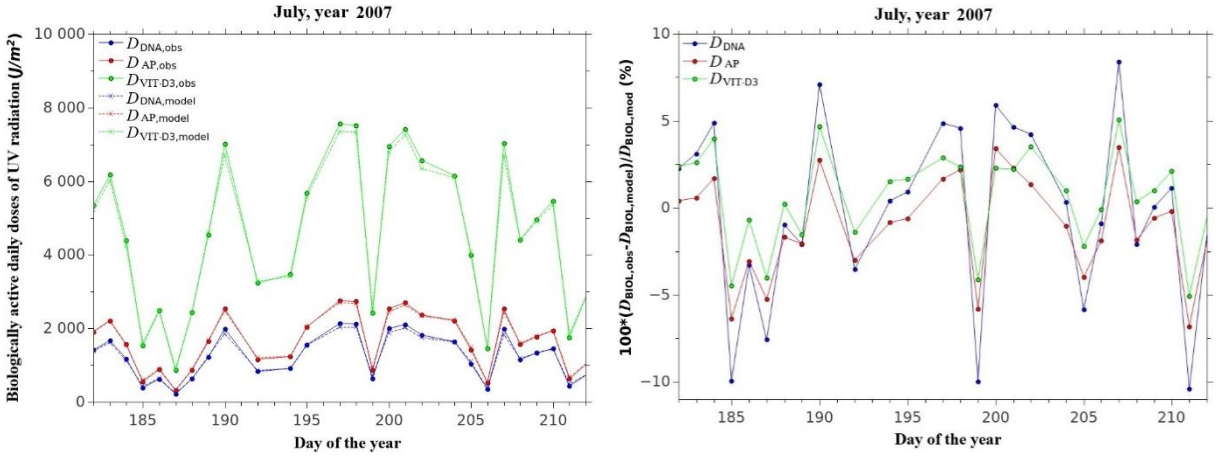

Fig. 23. Exemplary course of biologically active daily doses of UV radiation for July 2007 – left panel. Normalised deviation of the observed daily doses from the modelled ones in % – right panel.

2.4 Summary and conclusions

The current chapter presents the procedure for determining DR_{BIOL} for non-erythemal biological effects based on erythemal *DR*. The calculations take into account the action spectra of biological effects such as:

- synthesis of vitamin D_3 in the human body,
- psoriaris clearness,
- destruction of the DNA structure.

Using the measurement data obtained from the Belsk's Brewer spectrophotometer in the period 2000–2010, the DR_{BIOL}/DR_{ERYT} quotient matrices are built depending on the solar zenith angle and total ozone. The above relationships are used in the construction of the computational model (Eq. (2)), which has been verified on the basis of data for the years 2011–2014.

Compatibility of the modelled values with the observational ones is found:

- for DR_{DNA} and $DR_{VIT\text{-}D3}$, the modelled values begin to decline from the observed ones for SZA > 65°;
- for DR_{AP}, the agreement is good for all solar zenith angles;

The computational procedure can be effectively used to determine DR_{DNA} and $DR_{VIT\text{-}D3}$ between 9:00 and 16:00 (local time) in the spring and summer season. This is the period during which the human activity in the open air is usually the highest and the procedure will be useful for the assessment of personal doses. Anti-psoriasis intensity according to model described by Eq. (2) can be determined in the whole SZA range.

Furthermore, a computational procedure has been developed to determine the daily dose for non-erythemal radiation based on daily doses of erythemal radiation. The action spectra, used previously for the determination of DR_{BIOL}, were taken into account in the calculations.

The D_{BIOL}/D_{ERYT} quotients are calculated depending on SZA (at the local noon) and TO_3. Next, the above relationships were used in the construction of the computational model described by Eq. (6). It was concluded that the computational procedure can be effectively used to determine daily UV doses with efficacy different from the erythemal one, having the measured D_{ERYT} daily erythemal doses at disposal. This conclusion is based on the compatibility of the observed values with the modelled values, and taking into account the fact that standard deviations usually do not exceed a few percent of the mean value.

3. LONG-TERM CHANGES IN BIOLOGICALLY ACTIVE RADIATION AT BELSK

Measurements of UV radiation with the erythemal efficiency at the Central Geophysical Observatory, Belsk, have been carried out from May 1975 until now (Krzyścin et al. 2011b). Due to the length and continuity of the measurements, the Belsk's UV series is unique on a global scale. In the years 1975–1992, measurements of the erythemal radiation at Belsk were carried out using a Robertson–Berger meter, while from 1993 until present, Model 501 UV biometers have been used. Due to the use of different meters throughout the entire measurement period, the data series was homogenised for the years 1976–2008 (Krzyścin et al. 2011b). At that time, an analysis of the trend of the sums of annual erythemal daily doses was carried out. It was concluded that a statistically significant increasing trend was present throughout this period. The trend analysis was performed using a linear regression. In recent years, the database has been updated with measurements from the 2009–2014 period.

In the present chapter, data from the years 1976–2014 are analysed in order to determine the long-term variability of biologically active radiation. Data from the Belsk Observatory database, such as the daily doses of erythemal radiation, are used to calculate the monthly, annual, and April to September period (when the solar radiation strength is the greatest) summary doses.

Erythemal doses as well as the UV index were also utilised to calculate radiation doses for other biological effects – according to the methodology presented in the previous chapter. After including the data from 2009–2014, it was concluded that for the 1976–2014 series it is not possible to use linear regression to estimate the trend, and therefore it was necessary to develop a new method to determine it. An experiment based on the Monte Carlo method (Metropolis and Ulam 1949) was conducted, which consisted of creating a hypothetical data series. A detailed description of the applied method is provided below.

3.1 Method

In this part of the subchapter, the method of testing the long-term variability in the UV time series is presented. The individual stages of the method are discussed using the example of data from whole year measurements of the UV radiation with erythemal efficacy at Belsk from the years 1976–2014. Subsequently, this method is used for the data from the April–September

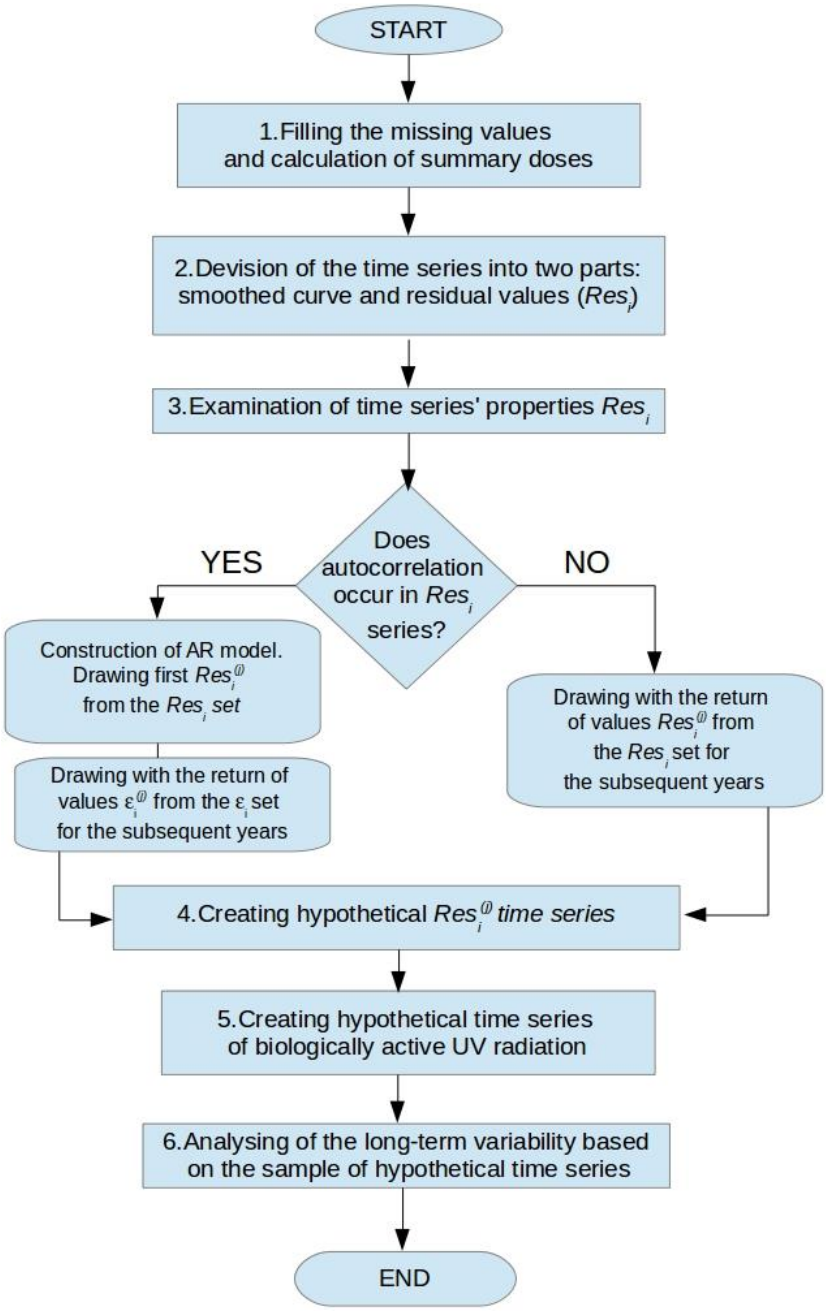

Fig. 24. The block diagram illustrating the successive stages of the long-term variability test method.

period (seasonal sum and monthly sums) as well as for the UV indexes, and for the UV radiation doses with biologically active non-erythemal efficacy, calculated according to the method presented in the previous Subchapter 2.3.

The individual stages of the method are presented in the block diagram in Fig. 24.

3.1.1 Filling of the missing values in the time series

The measurement series of erythemal daily doses from the Belsk Observatory contains 98.5% of complete data for years 1976–2014. This means that except for July 1985 and December 2014, the missing values are just several days per month. In order to calculate the annual sums from daily doses, it was necessary to fill in the missing values. Therefore, with the help of the "loess" function in the R program, the smooth curves were fitted to the monthly data from the 1976–2014 period. The "loess" function in the R program is based on the improved Lowess method (Cleveland 1979), according to Cleveland et al. (1992). The values for the missing observations in the subsequent months were interpolated from the smoothing curve using the spline function method ("spline" or "cubic" interpolation in Matlab). For July 1985 and December 2014, when the data for the whole month were missing, the values were adopted at the level of long-term monthly means from the years 1976–2014.

3.1.2 Calculation of annual doses, smoothing curve and residuals

The next step was to calculate the annual doses as the sums of daily values of erythemal doses. The results are presented in Fig. 25. In addition to the total values (points), the values (solid line) smoothed with the use of the "loess" method, calculated in the R program, are also presented. On the graph, looking at the smoothing curve, till 2005 an increase in the values of annual doses can be noted, which is followed by a slow decline. In this case, the use of linear regression for the entire measurement series seems inappropriate.

The next step was to determine residuals, i.e. deviations of the observed values from the values smoothed with the "loess" method according to Eq. (7):

$$Res_i = y_i - \langle y_i \rangle \tag{7}$$

where y_i is an annual dose from the i'th year (i = 1, 39), and $\langle y_i \rangle$ is a smoothed annual dose for the i'th year, i = 1 for the year 1976.

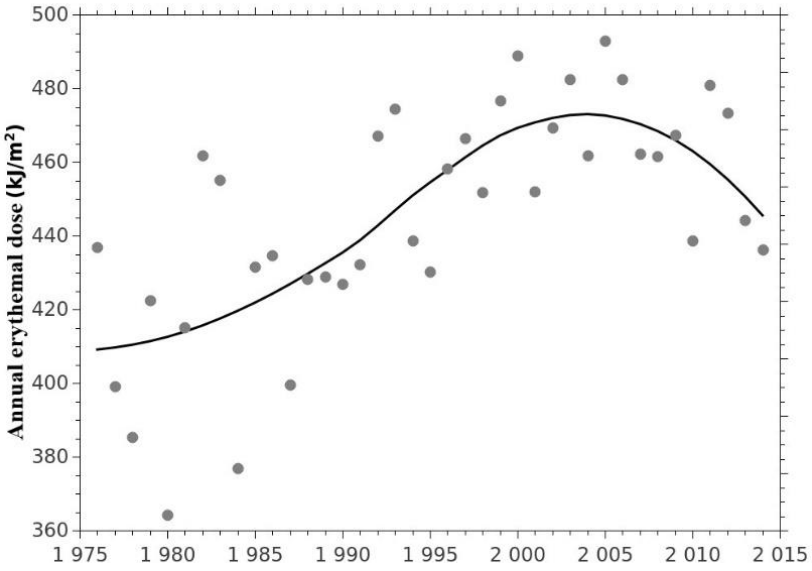

Fig. 25. Total annual erythemal doses in the years 1976–2014. The continuous curve shows the values smoothed with the "loess" function.

3.1.3 The examination of properties of the residuals time series

Subsequently, the properties of the Res_i time series were investigated. Figure 26 depicts the histogram for the Res_i values. The normality of the Res_i deviation set was investigated using the Shapiro–Wilk (S-W) test. The null hypothesis of the S-W test is that the population is normally distributed. This hypothesis can be applied when the statistic W (calculated from the population) is higher than the critical value, according to the table $W_{crit} = 0.939$ for $N = 39$ and the significance level $\alpha = 0.05$. The calculated value of statistic $W = 0.9881$. Hence, the null hypothesis cannot be rejected.

If the distribution is random, then the autocorrelation in the time series of residuals should also be below a certain critical level.

Autocorrelation for k'th degree of Res_i series, where k is a shift in years and amounts to 1, 2, ..., 10, was analysed. In order to examine the significance of the occurring correlation coefficients between the Res_i series and the Res_{i+k} series, a test based on the critical values of Pearson's correlation coefficient was applied, $r_{crit} = 2/\sqrt{N}$, where $N = 39 - k$. If the absolute value of the k'th degree correlation coefficient is higher than r_{crit} then the coefficient is statistically relevant ($\alpha = 0.05$). The calculated correlation coefficients are depicted in Fig. 27. The results of the conducted test are presented in Table 4.

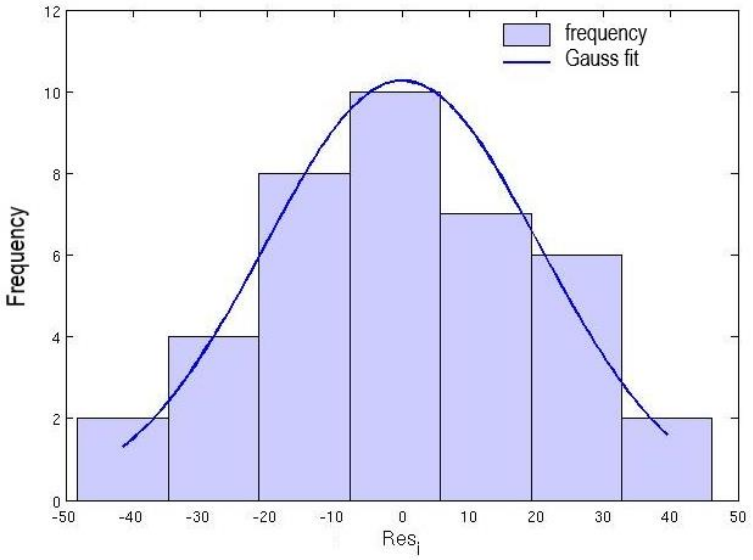

Fig. 26. Histogram for the Res_i deviations.

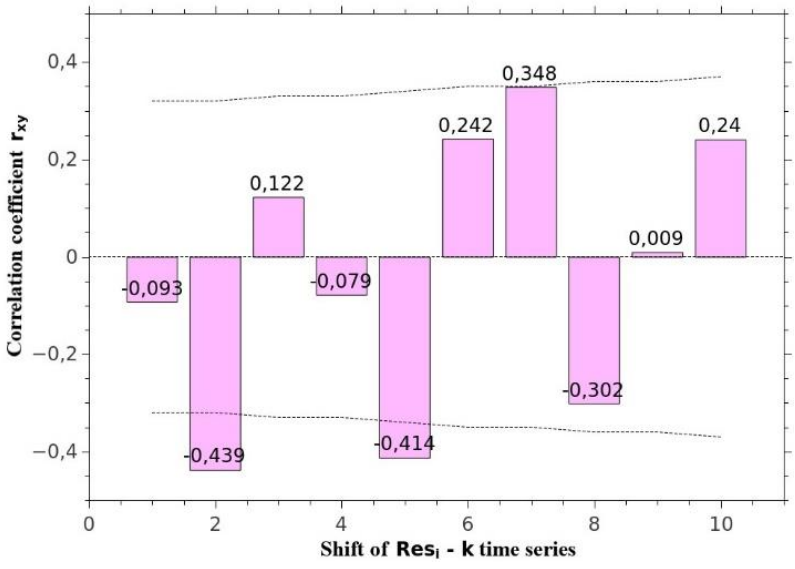

Fig. 27. The correlation coefficients for the Res_i series and the Res_{i+k} series.

Table 4

Results of the tests for the relevance of the correlation coefficient between the Res_i series and the Res_{i+k} series

k	Number of pairs	r_{xy}	r_{crit}	Relevance (+/–)
1	38	–0.093	0.32	–
2	37	–0.439	0.32	+
3	36	0.122	0.33	–
4	35	–0.079	0.33	–
5	34	–0.414	0.34	+
6	33	0.242	0.35	–
7	32	0.348	0.35	–
8	31	–0.302	0.36	–
9	30	0.009	0.36	–
10	29	0.240	0.37	–

The obtained results presented in Table 4 allow to conclude that the time series of deviations of annual doses in the period 1976–2014 from smoothed values shows autocorrelation of the second and fifth orders. It cannot be assumed that the Res_i distribution is random.

When constructing the hypothetical time series of the Res_i deviations, the properties of 2nd and 5th order correlation existence should be preserved in such time series. The Res_i values will depend on the previous Res_{i-k} values. This relation is described as an autoregressive process of order n:

$$Res_i = \varepsilon_i + \sum_{k=1}^{n} \alpha_k \, Res_{i-k} \tag{8}$$

where Res_i is a value from the considered year i, n is a model order, α_k denote coefficients, Res_{i-k} values from the previous n time steps, and ε_i is a random value.

The α_κ coefficients for the autoregression model of n'th order are calculated using the „arima()" function in the R program (Table 5). An example of the use of this function was demonstrated in Ripley (2002). With the help of the Akaike (1973) information criterion, it is concluded that the best match for the considered data would be the 5th order autoregressive model.

Table 5

5th order autoregression model coefficients, calculated utilising the "arima()" function in the R program

α_1	α_2	α_3	α_4	α_5
–0.2543	–0.5727	–0.3573	–0.3334	–0.5966

The set of the ε_i values is calculated based on Eq. (8) utilising the autoregression model coefficients from Table 5. The calculated values are depicted in Fig. 28.

Subsequently, a randomness test was carried out using a series test (http://statystyka.rezolwenta.eu.org/Materialy/Testy-los.pdf) for the set of the ε_i values. This test involves assignment of one symbol (e.g. "a") to the values smaller than the median, and the assignment of a second symbol (e.g. "b") to the values greater than the median. Values equal to the median

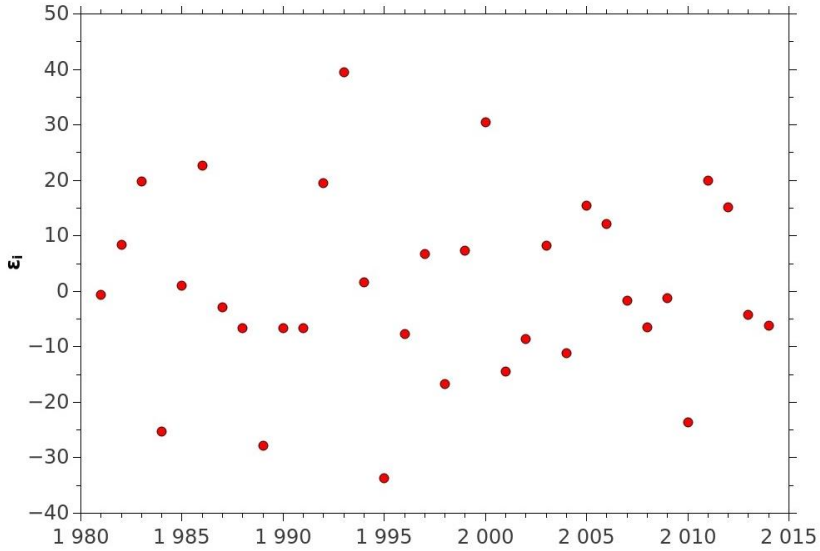

Fig. 28. The time serie of the random values ε_i.

are omitted. Then, a string of symbols resulting from the renamed string of numbers is analysed. The U_n value is a test statistic, which corresponds to the number of series of one type of symbol in a string. Critical values are taken from statistical tables, with the assumed level of confidence α and depend on the number of characters of both types. If the number of the U_n series does not belong to the critical range, it can be hypothesised that the considered values from the test are random. Because the number of series was 18 and the critical range , the number of series does not belong to the critical range. Based on the analysis of randomness of series ε_i (with the level of confidence equal to $\alpha = 0.05$) it was concluded that the series of those values is random and the "bootstrap" procedure can be applied, i.e. the hypothetical series of values ε_i can be obtained via a draw with return of all ε_i from the set.

3.1.4 Creating hypothetical time series of residuals

A generator was constructed for the determined autocorrelation and with the application of the calculated coefficients of the 5th order autoregression model (Table 5). The generator was selecting deviations $Res_i^{(j)}$ for the j'th hypothetical series of residuals, drawing with return a deviation for the first year ($i = 1$), which was obtained from a set of deviations Res_i and by selecting the next 4 successive values to the drawn deviation, i.e. Res_{i+1}, Res_{i+2}, Res_{i+3}, Res_{i+4}. The constructed generator was also drawing with the return of the ε_i values, and then calculated the subsequent $Res_i^{(j)}$ values according to Eq. (9):

$$Res_i^{(j)} = \varepsilon_i^{(j)} + \sum_{k=1}^{5} \alpha_k \, Res_{i-k}^{(j)} \tag{9}$$

The exemplary time series of deviations along with the original series are demonstrated in Fig. 29.

If no autocorrelations are found for the Res_i deviations time series, the hypothetical $Res_i^{(j)}$ series can be constructed with a method of drawing with a return of the Res_i values for subsequent years without the use of Eq. (8).

Because after conducting the randomness test of the series it was found that the residuals have a random distribution, a draw was carried out to compare the results with the return of the Res_i values also when there is an autocorrelation in the Res_i series.

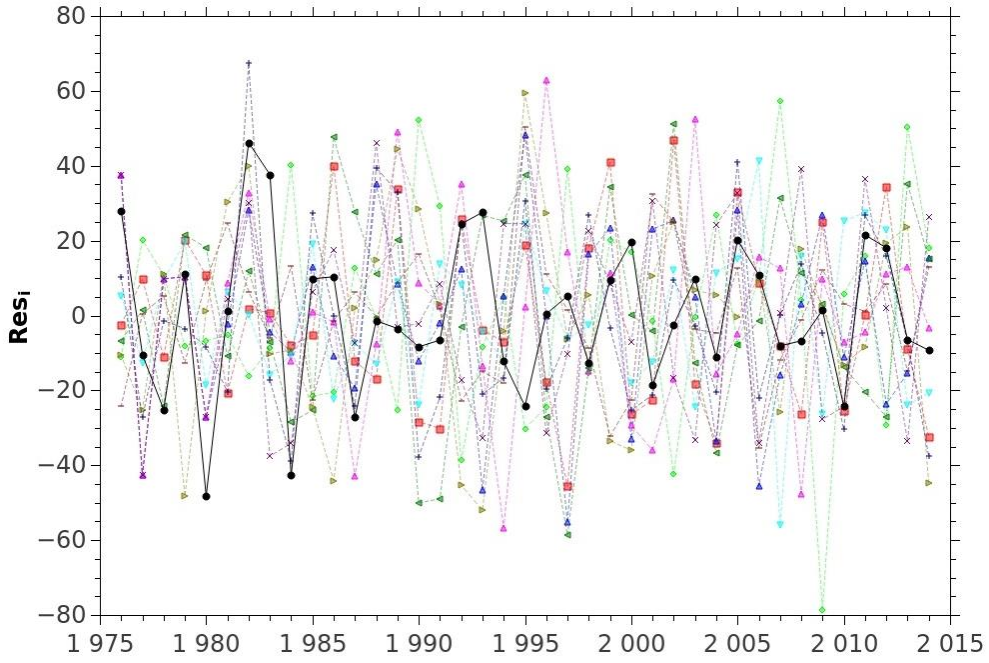

Fig. 29. Time series of residuals $Res_i^{(j)}$.

3.1.5 The construction of a hypothetical time series of biologically active UV radiation doses

According to the method presented in Subchapter 3.1.4, a hypothetical series of residuals was calculated and the hypothetical series of annual means were determined based on Eq. (10):

$$y_i^{(j)} = \langle y_i \rangle + Res_i^{(j)} \tag{10}$$

Figure 30 depicts an example of a hypothetical time series $y_i^{(j)}$ smoothed with the "loess" function and calculated using the autoregressive model.

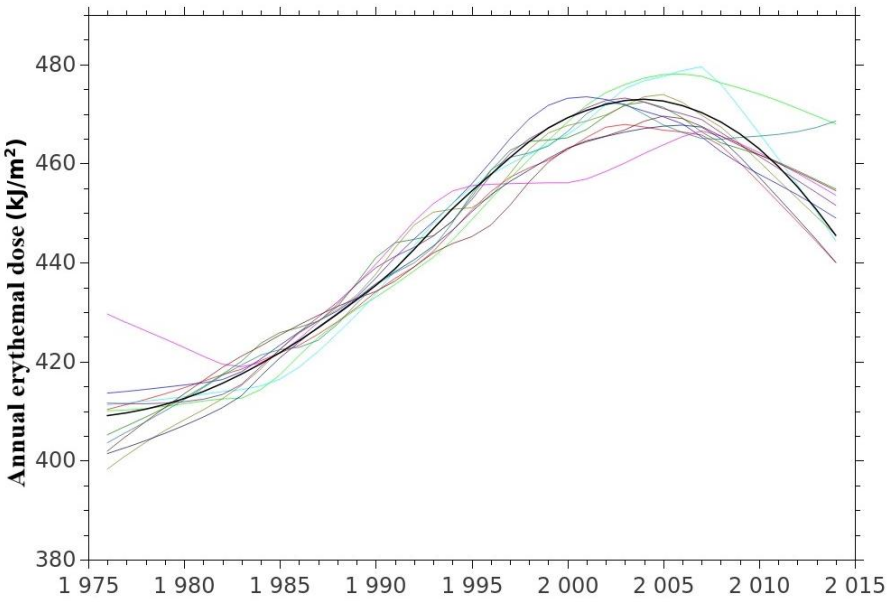

Fig. 30. Course of smoothed hypothetical time series of the erythemal annual dose.

3.1.6 Analysing of the long-term variability based on the statistical set

With the hypothetical series of annual UV values in hand, the mean values and confidence intervals of the selected statistical parameters were determined: mean UV level from the years

Table 6

Statistical values for the mean values from the 1976–1985 and 2005–2014 decades, and for trends in years 1976–2005 and 2005–2014, calculated for different number of j_{max} draws

Parameter	Median	5%	95%	Mean	Standard deviation
j_{max} = 100					
Mean values 1976–1985	413.7	408.7	418.2	413.6	2.94
Mean values 2005–2014	461.8	456.8	467.3	462.0	3.34
Trend 1976–2005	2.63	2.36	2.94	2.63	0.18
Trend 2005–2014	–3.13	–5.57	0.39	–3.00	1.69
j_{max} = 1000					
Mean values 1976–1985	414.0	409.0	419.1	414.0	2.93
Mean values 2005–2014	462.5	456.7	468.5	462.5	3.49
Trend 1976–2005	2.64	2.33	2.98	2.65	0.20
Trend 2005–2014	–3.14	–5.73	–0.27	–3.08	1.69
j_{max} = 10,000					
Mean values 1976–1985	414.0	409.2	419.2	414.0	3.00
Mean values 2005–2014	462.5	457.1	468.1	462.5	3.37
Trend 1976–2005	2.65	2.32	2.98	2.65	0.20
Trend 2005–2014	–3.02	–5.74	–0.25	–3.01	1.66
j_{max} = 50,000					
Mean values 1976–1985	414.0	409.3	419.2	414.1	2.99
Mean values 2005–2014	462.4	457.0	468.0	462.4	3.34
Trend 1976–2005	2.65	2.32	2.98	2.65	0.20
Trend 2005–2014	–3.01	–5.74	–0.27	–3.01	1.66
j_{max} = 100,000					
Mean values 1976–1985	414.0	409.2	419.1	414.1	3.00
Mean values 2005–2014	462.4	456.9	468.0	462.4	3.35
Trend 1976–2005	2.65	2.32	2.98	2.65	0.20
Trend 2005–2014	–3.02	–5.73	–0.26	–3.00	1.66

Note: Statistically significant trends are marked in bold. The mean values are expressed in kJ/m^2, and trends in kJ/(m^2 year).

1976–1985 (first decade), mean UV level from the years 2005–2014 (last decade), linear trend in the years 1976–2005 and 2005–2014. The experiment was carried out for a different number of series, where j_{max} = 100, 1000, 2000, 5000, 10,000, 20,000, 50,000 and 100,000. Statistical values such as the median, 5% and 95% percentiles, arithmetic mean and standard deviation were calculated for each j_{max}. The obtained values are presented in Table 6, where the mean values are expressed in kJ/m^2 and the trends in kJ/(m^2 year). Based on this data, it was found that the number of draws j_{max} = 100,000 is sufficient because the estimated values stabilise above j = 10,000.

Based on the conducted experiments, it is found that the mean values of annual erythemal doses from the 2005–2014 decade are higher than the mean values from the 1976–1985 decade by 11.7% ±1.1% (1 standard deviation). Based on the 5th and 95th percentiles (both positive or negative), statistically significant trends are selected: an increasing trend in years 1976–2005 (2.6 ±0.2 (1 standard deviation) kJ/m^2/year), and a decreasing one in years 2005–2014 (–3.0 ±1.66 (1 standard deviation) kJ/m^2/year). However, it should be noted that for the years 2005–2014, the ratio of standard deviation to the mean absolute value of a trend, i.e. the coefficient of variation, exceeds 55%, while for the 1976–2005 trend it does not exceed 7%.

Comparison of the obtained results using the autoregressive model and without using the autoregressive model to generate hypothetical series (Table 7) reveals that medians and arithmetic means are similar. However, the values for the 5th and 95th percentiles as well as standard deviations differ, i.e. when using the autoregressive model the standard deviations are much smaller. On this basis, it can be concluded that the analysis with a use of the autoregressive model is more accurate.

Table 7

A comparison of statistical values for the mean values from the 1976–1985 and 2005–2014 decades, and for trends in 1976–2005 and 2005–2014, calculated for j_{max} = 100,000 draws with and without the autoregressive model

Parameter	Median	5%	95%	Mean	Standard deviation
Draw without the autoregressive model					
Mean values 1976–1985	414.3	403.6	424.7	414.2	6.39
Mean values 2005–2014	462.4	451.8	472.8	462.4	6.38
Trend 1976–2005	2.63	1.94	3.34	2.64	0.43
Trend 2005–2014	–3.01	–6.65	0.66	–3.00	2.23
Draw with the autoregressive model					
Mean values 1976–1985	414.0	409.2	419.1	414.1	3.00
Mean values 2005–2014	462.4	456.9	468.0	462.4	3.35
Trend 1976–2005	2.65	2.32	2.98	2.65	0.20
Trend 2005–2014	–3.02	–5.73	–0.26	–3.00	1.66

Note: Statistically significant trends are marked in bold.

3.2 Analysis of seasonal changes in erythemal UV doses

For seasonal erythemal UV doses series, the smoothed curves were determined analogously to the method demonstrated in Subchapter 3.1 (the period from April to September collectively as well as separately for each month, see Figs. 31–33). Based on these graphs, it can be concluded that for the April–September season, a similar variability is observed as for the annual doses, i.e. in the years 1976–2005 an upward trend was observed, and in 2005–2014 probably a downward trend. For individual months, an increasing trend is observed in 1976–2005, while in 2005–2014, a clear downward trend can only be seen in May and June.

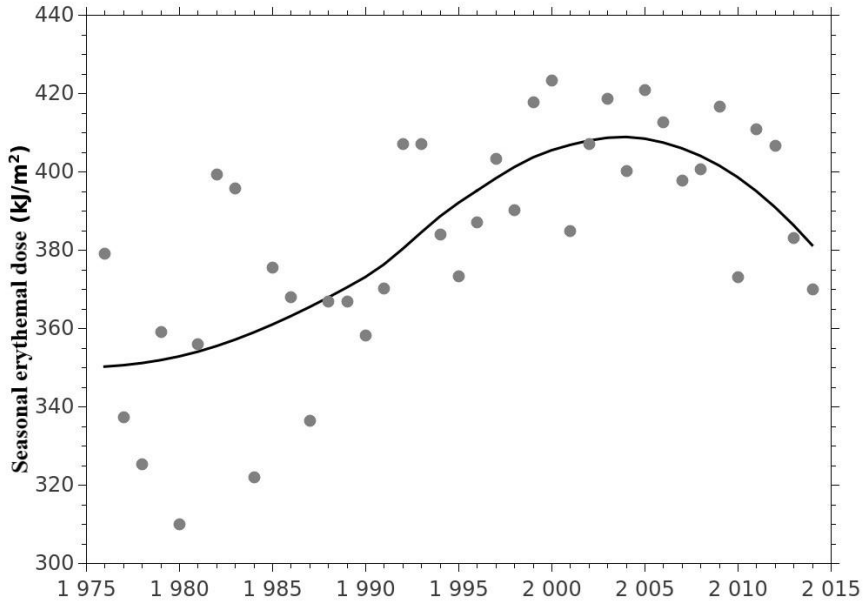

Fig. 31. Total seasonal doses (April–September) of erythemal UV radiation in the years 1976–2014. The continuous curve shows values smoothed with the "loess" function.

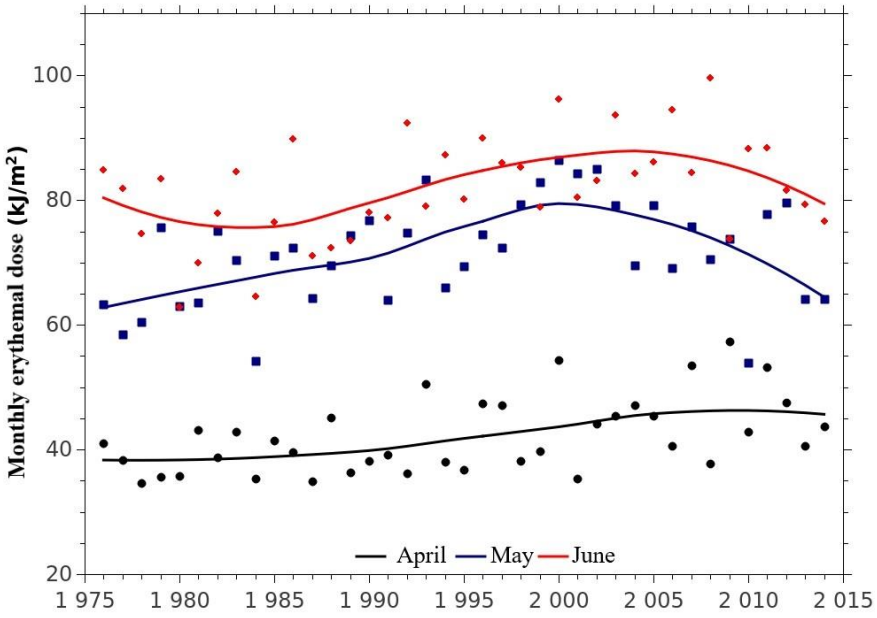

Fig. 32. Total monthly doses of erythemal radiation in the years 1976–2014 for the April–June period. Continuous curves show values smoothed with the "loess" function.

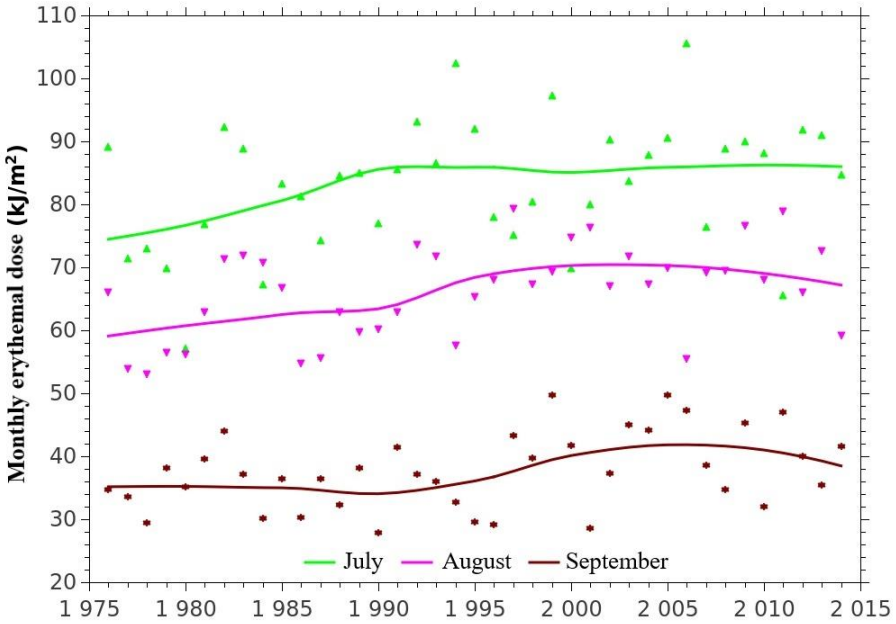

Fig. 33. Total monthly doses of the erythemal radiation in the years 1976–2014 for the July–September period. Continuous curves show values smoothed with the "loess" function.

Table 8

Results of the Shapiro–Wilk test ($W_{crit} = 0.939$ at $N = 39$ and $\alpha = 0.05$), statistically relevant autocorrelation factors and the order of the matching autoregressive model

Month	W	H_0 (+/–)	Autocorrelation factor	n
April–September	0.9924	+	$k = 2\ r_{xy} = –0.377$ $k = 5\ r_{xy} = –0.457$	5
April	0.9567	+	$k = 1\ r_{xy} = –0.509$ $k = 7\ r_{xy} = 0.446$	2
May	0.9818	+	$k = 5\ r_{xy} = –0.527$	5
June	0.9804	+	$k = 1\ r_{xy} = –0.375$	2
July	0.9862	+	–	–
August	0.9631	+	$k = 3\ r_{xy} = –0.370$ $k = 5\ r_{xy} = –0.468$ $k = 8\ r_{xy} = 0.487$	6
September	0.9846	+	$k = 4\ r_{xy} = –0.411$ $k = 6\ r_{xy} = 0.474$	6

Subsequently, an investigation of the properties of residual values time series was carried out according to the previously presented scheme (Subchapter 3.1.3), i.e. it was checked whether the $Res_{i,sea}$ residuals, calculated according to Eq. (7), for the April–September season and for individual months in the years 1976–2014, belong to the normal distribution. In addition, the correlation coefficients between the $Res_{i,sea}$ series of residuals and the $Res_{i+k,sea}$ series

Table 9

Statistical characteristics of means for decades 1976–1985 and 2005–2014 and trends for the years 1976–2005 and 2005–2014 in the period from April to September, calculated for j_{max} = 100,000 draws

Parameter	Median	5%	95%	Mean	Standard deviation
April–September					
Mean values 1976–1985	354.3	349.6	359.2	354.3	2.91
Mean values 2005–2014	398.1	392.9	403.3	398.1	3.17
Trend 1976–2005	2.46	2.12	2.78	2.45	0.20
Trend 2005–2014	–3.03	–5.61	–0.40	–3.02	1.59
April					
Mean values 1976–1985	38.4	37.0	40.0	38.4	0.91
Mean values 2005–2014	46.0	44.5	47.6	46.0	0.95
Trend 1976–2005	0.27	0.17	0.37	0.27	0.06
Trend 2005–2014	–0.02	–0.65	0.69	–0.01	0.40
May					
Mean values 1976–1985	65.5	63.4	67.5	65.5	1.24
Mean values 2005–2014	71.5	69.3	73.5	71.5	1.28
Trend 1976–2005	0.63	0.48	0.77	0.62	0.09
Trend 2005–2014	–1.39	–2.57	–0.21	–1.39	0.72
June					
Mean values 1976–1985	77.1	75.1	79.1	77.1	1.19
Mean values 2005–2014	84.6	82.7	86.6	84.6	1.20
Trend 1976–2005	0.46	0.33	0.60	0.46	0.08
Trend 2005–2014	–0.92	–1.73	–0.10	–0.92	0.49
July					
Mean values 1976–1985	77.1	72.3	81.9	77.1	2.90
Mean values 2005–2014	86.0	81.2	90.7	86.0	2.91
Trend 1976–2005	0.41	0.09	0.73	0.41	0.19
Trend 2005–2014	0.02	–1.65	1.69	0.02	1.01
August					
Mean values 1976–1985	61.0	58.9	62.9	60.9	1.22

to be continued

Table 9 contd

Mean values 2005–2014	69.2	67.0	71.2	69.2	1.28
Trend 1976–2005	0.45	0.30	0.60	0.45	0.09
Trend 2005–2014	–0.36	–1.86	1.14	–0.36	0.91
September					
Mean values 1976–1985	35.3	33.4	37.2	35.3	1.17
Mean values 2005–2014	40.9	38.7	43.1	40.9	1.33
Trend 1976–2005	0.24	0.11	0.35	0.24	0.07
Trend 2005–2014	–0.36	–1.20	0.44	–0.37	0.50

Note: Statistically significant trends are marked in bold.

shifted by $k = 1, 2, ..., 10$ years, was calculated. Significance tests were carried out for the calculated correlation coefficients. Then, according to the pattern presented in Subchapter 3.1, the hypothetical residuals series were calculated. For the April–September season and for April, May, June, August and September, the hypothetical residuals series $Res_{i,sea}^{(j)}$ were calculated using the autoregressive model, drawing from the pool with a return of values $\varepsilon_{i,sea}$. It was found that the trials $\varepsilon_{i,sea}$ are random; therefore, draw of each of the values is equally likely. For July, no autocorrelation was found in the $Res_{i,sea}$ series; hence, the hypothetical $Res_{i,sea}^{(j)}$ deviation series was calculated using a draw method with returns from the $Res_{i,sea}$ residuals pool. The results of the conducted distribution normality tests, statistically significant autocorrelation coefficients and the order of the matched autoregressive model are presented in Table 8.

The next step was to calculate a hypothetical series of data for seasonal erythemal radiation doses for $j_{max} = 100{,}000$ using Eq. (10). For each j series, mean seasonal doses for 1976–1985 and 2005–2014, as well as trends (linear slopes for $y_{i,sez}^{(j)}$) for 1976–2005 and 2005–2014 are

Table 10

Mean level of increase of mean values for the years 2005–2014 with respect to the mean values for 1976–1985 for the considered seasonal and monthly series

Period	Mean level of growth of mean values 2005–2014 with respect to mean values 1976–1985 [%]	Standard deviation [%]
April–September	12.36	1.22
April	19.8	3.75
May	9.25	2.87
June	9.77	2.30
July	11.88	5.47
August	13.52	3.15
September	15.95	5.41

Table 11

The same as Table 9 but for calculations without the use of the autoregressive model

Parameter	Median	5%	95%	Mean	Standard deviation
April–September					
Mean values 1976–1985	354.4	344.4	364.4	354.4	6.08
Mean values 2005–2014	398.0	388.1	408.1	398.1	6.07
Trend 1976–2005	2.45	1.78	3.11	2.45	0.40
Trend 2005–2014	–3.01	–6.52	0.47	–3.01	2.12
April					
Mean values 1976–1985	38.5	36.0	41.2	38.5	1.56
Mean values 2005–2014	46.1	43.6	48.8	46.1	1.57
Trend 1976–2005	0.27	0.10	0.44	0.27	0.10
Trend 2005–2014	–0.00	–0.90	0.89	–0.00	0.55
May					
Mean values 1976–1985	65.6	62.1	68.8	65.5	2.02
Mean values 2005–2014	71.5	68.1	74.7	71.5	2.03
Trend 1976–2005	0.62	0.39	0.84	0.62	0.14
Trend 2005–2014	–1.39	–2.54	–0.23	–1.39	0.70
June					
Mean values 1976–1985	76.9	73.6	80.4	77.0	2.06
Mean values 2005–2014	84.4	81.1	87.9	84.5	2.07
Trend 1976–2005	0.46	0.23	0.69	0.46	0.14
Trend 2005–2014	–0.92	–2.11	0.27	–0.92	0.72
August					
Mean values 1976–1985	60.9	57.7	64.1	60.9	1.93
Mean values 2005–2014	69.1	65.9	72.3	69.1	1.94
Trend 1976–2005	0.45	0.24	0.66	0.45	0.13
Trend 2005–2014	–0.35	–1.45	0.76	–0.35	0.67
September					
Mean values 1976–1985	35.3	32.6	38.0	35.3	1.64
Mean values 2005–2014	40.9	38.2	43.6	40.9	1.65
Trend 1976–2005	0.24	0.06	0.42	0.24	0.11
Trend 2005–2014	–0.37	–1.32	0.58	–0.37	0.57

calculated. The results of the calculations for all months are presented in Table 9, where mean values are expressed in kJ/m^2 and trends in kJ/(m^2 year).

On the basis of the analysis of the entire statistical set of hypothetical time series $y_{i,\mathrm{sez}}^{(j)}$, it was confirmed that the mean values of annual doses of UV erythemal radiation from the 1976–1985 decade are lower than the means from the 2005–2014 decade in 100% of cases for the April–September season and for April, June and August, in 99.95% of cases for May, in 98.46% of cases for July and in 99.94% of cases for September. The mean level of the increase of the mean values from the last decade, in reference to the mean values from the first decade of the series, is presented in Table 10.

For the April–September period, an increasing trend was observed for the years 1976–2005, while for 2005–2014, a decreasing trend was detected. Moreover, for the years 2005–2014, the coefficient of variation is 53%, whereas for the 1976–2005 trend it does not exceed 9%.

For all months, an increasing trend is observed in the years 1976–2005, with a coefficient of variation of approx. 15% (May, June), 20% (April, August), 30% (September), and 46% (July). In addition, for the 2005–2014 period, a decreasing trend was noted for May and June (with a coefficient of variation of approx. 50%), with the UV level higher than for the 1976–1985 period by approx. 9.5%. There is a lack of an obvious trend in the remaining months. After 2005, this level is stable in July and August and amounts to approx. 12–13% more than for the 1976–1985 period. Notably, in April and September, there is a highest increase in the level of UV radiation (20% and 16%) with regard to the 1976–1985 period.

The results of calculations without the use of the autoregressive model for $Res_{i,sea}$ in the season from April to September cumulatively and for individual months are presented in Table 11. Hypothetical series $y_i^{(j)}$ were therefore determined by drawing from the pool $Res_{i,sea}$. The table does not present the values calculated for July, which were previously calculated only with this method. The mean values are quoted in kJ/m^2 and the trends in kJ/(m^2 year).

As in the case of the annual data, it was found that the standard deviation value for the means and trends is lower than for the cases without the use of the autoregressive model. More accurate results can be obtained employing the autoregressive model. Nevertheless, the differences are much smaller for individual months than for the annual data and for the entire April–September season. The further chapter presents (for UV radiation indexes and for non-erythemal biologically effective radiation) the results of calculations using just the autoregressive model if autocorrelation occurs in a series of residuals.

3.3 Long-term changes in the UV radiation index

The Institute of Geophysics of the Polish Academy of Sciences database contains UV index values, i.e. the maximum daily intensity of UV irradiation with erythemal efficacy (DR_{ERYT}). The UV index is demonstrated as a dimensionless value (*UVI*), 1 *UVI* = 25 mW/m^2. The UV index is the basis for determining individual protection against excessive UV radiation. In the years 1976–1992, the UV index was not available, as the daily UV radiation courses were not recorded.

In line with the commonly accepted standards, depending on the level of the UV index, appropriate scenarios for outdoor stay should be applied. A table showing UV levels and the essential precautions is presented in the introduction.

In the further part of Subchapter 3.3, UV indexes were converted to DR_{ERYT} according to the following formula: $DR_{\mathrm{ERYT}} = UVI{*}25$ mW/m^2, and subsequently the long-term variability of DR_{ERYT} was determined according to the scheme presented in Subchapter 3.1.

The maximum UV index at Belsk in the measuring series (1993–2014) reach 199.3 mW/m^2, which was observed in July 1996. The time series (1993–2014) of the number of days in a year with an index equal to or higher than 6 at Belsk, i.e. one at which it is advisable to limit outdoor

stay between 10 am and 2 pm, is shown in Fig. 34. The mean value was 46.3 ±11.5 (1 standard deviation) days, and the linear trend (not statistically significant) was –0.34 days/year.

The calculated time series of the monthly DR_{ERYT} means and smoothing curves (determined according to the method from Subchapter 3.1.2) are presented in Figs. 35 and 36. Moreover, time series of residuals $Res_{i,UVI}$ were also calculated.

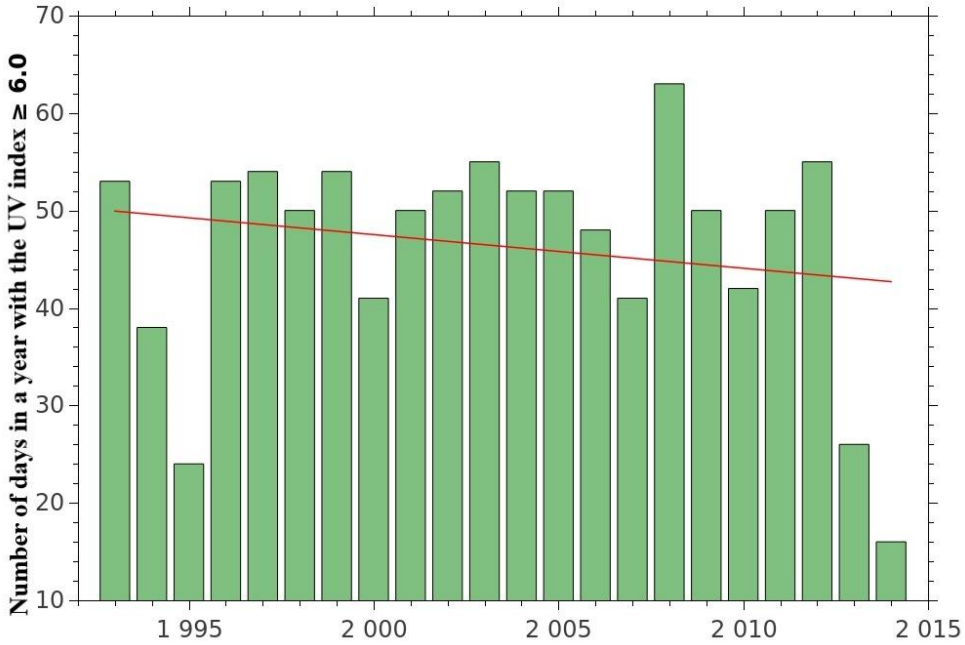

Fig. 34. Number of days per year with a UV index of 6 or higher (150 mW/m^2) at Belsk in the years 1993–2014.

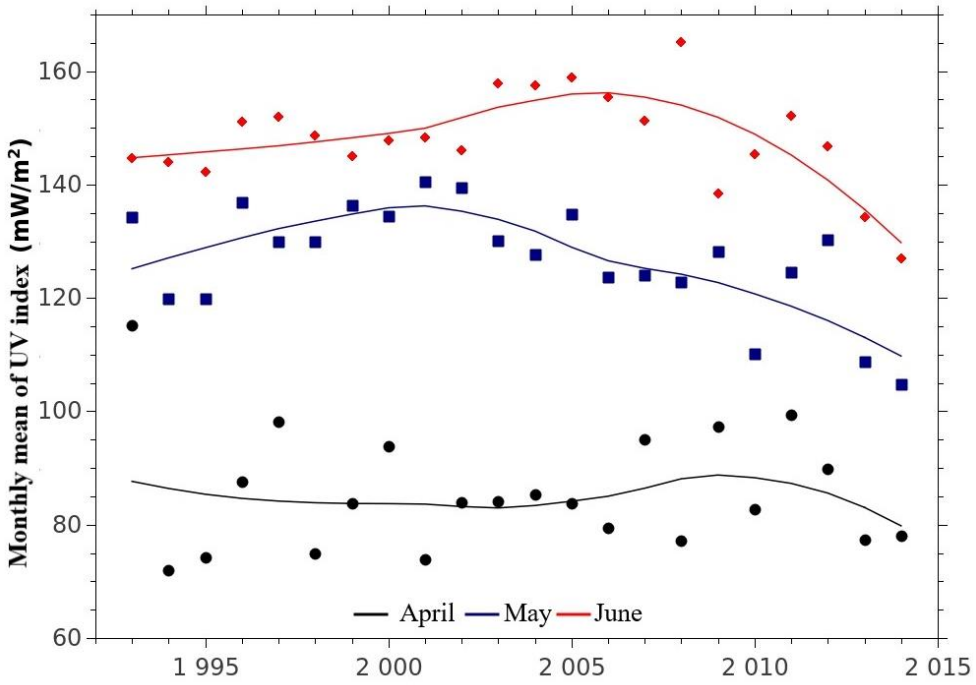

Fig. 35. Monthly mean UV index values in the years 1993–2014 for the April–June period. Continuous curves illustrate values smoothed using the “loess” function.

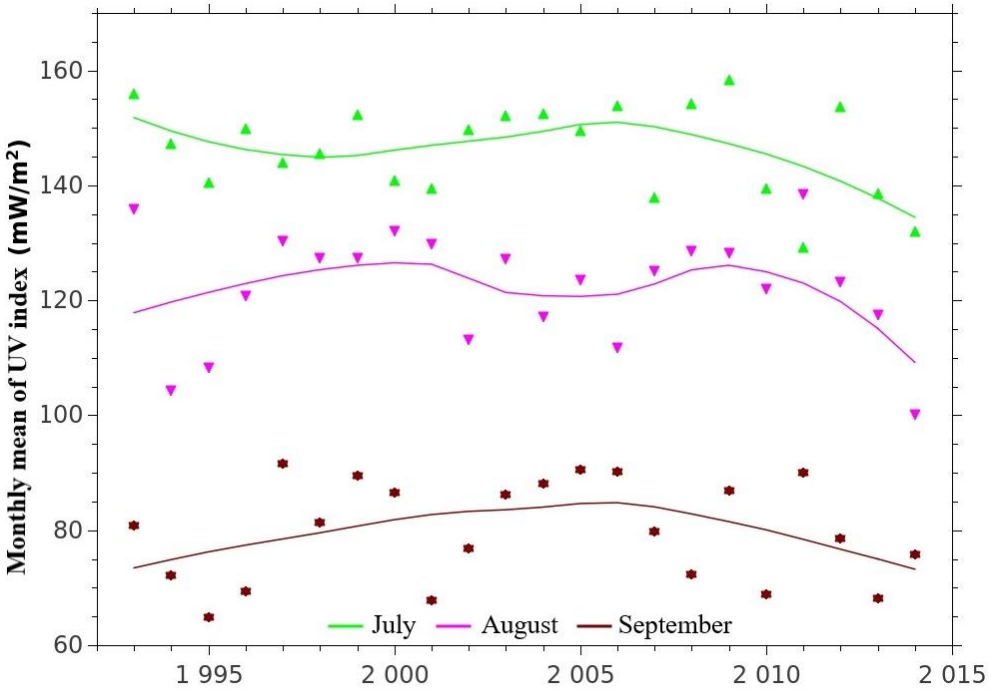

Fig. 36. Monthly mean UV index values in the years 1993–2014 for the July–September period. Continuous curves illustrate values smoothed using the "loess" function.

Basing on the graphs alone, it is difficult to clearly determine the occurrence of a significant trend in individual months. There is a clear decreasing trend in the years 2005–2014 for May, June, July and September. In the years 1993–2005, however, an increasing trend can be only seen in June and September. As in the case of the time series of daily doses, the occurrence of a statistically significant trend for the UV index will be determined by analysing the hypothetical series, calculated based on residuals $Res_{i,UVI}$.

Table 12

The Shapiro–Wilk test results ($W_{crit} = 0.911$ at $N = 22$ and $\alpha = 0.05$), statistically significant autocorrelation coefficients and the order of the fitted autoregressive model for deviations of the monthly means of the UV index from the corresponding smoothed values

Month	W	H_0 (+/–)	Autocorrelation coefficient	n
April	0.9889	+	$k = 7$ $r_{xy} = 0.61$	6
May	0.9629	+	$k = 2$ $r_{xy} = –0.53$	2
June	0.9621	+	$k = 7$ $r_{xy} = 0.56$	2
July	0.9790	+	$k = 2$ $r_{xy} = –0.56$ $k = 8$ $r_{xy} = –0.61$ $k = 10$ $r_{xy} = 0.65$	5
August	0.9388	+	$k = 9$ $r_{xy} = –0.60$	1
September	0.9488	+	$k = 6$ $r_{xy} = 0.59$	6

The properties of the time series of residual values were determined according to the methodology presented in Subchapter 3.1.3. For all months, it was found that the values belong to the normal distribution (the value of critical statistics for $N = 22$ and the significance level $\alpha = 0.05$ is $W_{crit} = 0.911$). In addition, significant autocorrelation was observed for all series; therefore, autoregressive models will be utilised for further calculations. For the residual series, a series test was also carried out for randomness. For all months, the series of residual values are random. The results of the Shapiro–Wilk test, significant autocorrelation coefficients and the rank of the autoregressive model used in further calculations are presented in Table 12.

Hypothetical series of residual values are constructed as before, i.e. autoregressive models are employed when significant autocorrelation occurred. Values $\varepsilon_{i,UVI}$ are calculated from Eq. (8) and are also put to the series test for randomness of the trial. The series test reveales that for all months, the calculated series of values of $\varepsilon_{i,UVI}$ are random. The hypothetical series deviations of $Res_{i,UVI}^{(j)}$ are calculated with the use of the autoregressive model, drawing with the return of the $\varepsilon_{i,UVI}$ values from the pool.

The next step is to determine a hypothetical series of monthly means of UV index for $j_{max} = 100{,}000$ using Eq. (10). For each j series, the mean UV index value for the years 1993–2002 and 2005–2014 as well as trends (slopes of linear regression for $y_{i,UVI}^{(j)}$) for 1993–2005 and 2005–2014 are calculated. The results of the calculations for all months are demonstrated in Table 13, where the mean values are expressed in mW/m^2 and the trends in mW/(m^2 year).

Based on the entire statistical ensemble, it is found that for all of the analysed months, the mean monthly UV index in 2005–2014 remaines at a similar level as in the 1993–2002 period, i.e. in the first decade of the UV index measurements. Similarly to Subchapter 3.2, trends are determined in periods up to 2005 and after 2005. Statistically significant decreasing trends are found in 2005–2014 for May, June, July, and September. The increasing trend in the years 1993–2005 is found in May, June, and September. The value of the standard deviation in relation to the absolute value of the mean of trends (i.e. the coefficient of variation) in the years 2005–2014 is 25% for May, 16% for June, 44% for July, and 30% for September, whereas in 1993–2005, it is 63% for May, 31% for June, and 45% for September.

The results presented in Table 13 indicate that a decreasing trend for the UV indexes is observed in the spring and summer months, when the highest UV irradiation values occur during the year (May, June, July).

Data from the years 1993–2014 demonstrate that the highest UV index values were 198 mW/m^2 in June 2005 and 199.3 mW/m^2 in July 1996. After 2009, the highest *UVI* does not exceed 190 mW/m^2 and in the last year (2014) it was 163.75 mW/m^2. For the maximum value of *UVI* = 199.3 mW/m^2, the safe tanning time, i.e. the duration of exposure needed to obtain the dose of 250 J/m^2 (MED for phototype II) was approx. 21 min, while for the maximum UV index in 2014 (163.75 mW/m^2) it was 25 min. The difference in the time of safe tanning is only 4 min, and therefore even at lower UV indexes in the spring and summer months, special care should be taken when staying in the sun. In the last two years (2013–2014), a decrease in the number of days per year with UV index greater than or equal to 150 W/m^2 was observed (Fig. 34). In the years 1996–2012, the mean number of such days was 48.85 per year. In the last two years, it decreased nearly two-fold, i.e. to the value of 26 days in 2013 and 16 days in 2014 (the lowest value in the series). In 2014, the number of days with UV index equal to or higher than 150 mW/m^2 decreased by a value larger than 2 standard deviations for the mean *UVI* in years 1993–2014. It can therefore be concluded that in the last two years, the exposure to solar radiation in the summer months is associated with a slightly lower risk of sunburn.

Table 13

Statistical characteristics of the mean *UVI* for the 1993–2002 and 2005–2014 decades and for trends in the years 1993–2005 and 2005–2014 in the period from April to September, calculated for j_{max} = 100,000 random draws

Parameter	Median	5%	95%	Mean	Standard deviation
April					
Mean values 1993–2002	84.9	82.8	86.4	84.8	1.09
Mean values 2005–2014	85.7	83.4	87.9	85.7	1.38
Trend 1993–2005	–0.24	–0.85	0.27	–0.26	0.34
Trend 2005–2014	–0.33	–1.43	0.64	–0.35	0.62
May					
Mean values 1993–2002	131.9	130.3	133.7	131.9	1.05
Mean values 2005–2014	120.5	118.8	122.4	120.5	1.09
Trend 1993–2005	0.48	0.00	0.98	0.48	0.30
Trend 2005–2014	–2.02	–2.84	–1.15	–2.01	0.51
June					
Mean values 1993–2002	147.7	145.7	149.5	147.6	1.13
Mean values 2005–2014	147.5	145.5	149.3	147.5	1.16
Trend 1993–2005	0.93	0.46	1.41	0.93	0.29
Trend 2005–2014	–2.92	–3.70	–2.15	–2.92	0.47
July					
Mean values 1993–2002	147.1	145.8	148.3	147.1	0.74
Mean values 2005–2014	145.0	143.6	146.3	144.9	0.84
Trend 1993–2005	0.03	–0.47	0.57	0.04	0.32
Trend 2005–2014	–1.84	–3.18	–0.51	–1.84	0.81
August					
Mean values 1993–2002	123.1	119.9	126.3	123.1	1.95
Mean values 2005–2014	120.5	117.2	123.6	120.4	1.92
Trend 1993–2005	0.15	–0.63	0.92	0.15	0.47
Trend 2005–2014	–1.02	–2.16	0.13	–1.02	0.69
September					
Mean values 1993–2002	78.7	76.8	81.0	78.7	1.28

to be continued

Table 13 contd

Mean values 2005–2014	80.2	78.0	82.2	80.1	1.28
Trend 1993–2005	1.03	0.23	1.64	0.99	0.45
Trend 2005–2014	–1.36	–2.06	–0.72	–1.37	0.41

Note: Statistically significant trends are marked in bold. The mean *UVI* are expressed in mW/m^2, and trends in mW/(m^2 year).

3.4 Long-term changes in UV radiation with non-erythemal biological efficacy

The time series of daily doses of UV irradiation with biological efficacy such as:

- synthesis of vitamin D_3 in the human body (VIT-D_3),
- psoriasis clearance (AP),
- destruction of the DNA structure (DNA)

could be calculated using the time series of daily doses of UV irradiation with erythemal efficacy for years 1976–2014 and the conversion factors shown in Appendix (Tables 7A–9A).

The period from April to September is considered, when the intensity of the UV radiation is the highest in the year. Subsequently, according to the algorithm presented in Subchapter 3.1, the seasonal doses (in total) as well as doses for individual months were calculated as sums of daily doses for biological effects of VIT-D_3, AP, and DNA.

3.4.1 UV radiation with vitaminal efficacy

Figures 37–39 demonstrate the time series of seasonal sums of vitaminal daily doses (for the April–September period) and for each month separately, as well as the appropriate smoothed values.

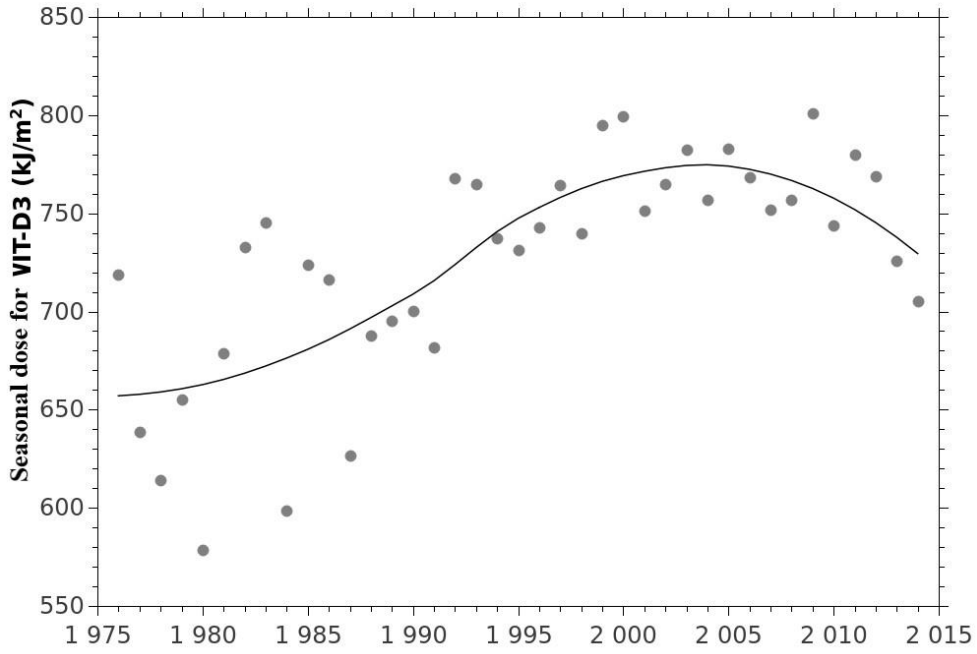

Fig. 37. Total seasonal doses (April–September) of VIT-D_3 radiation in the years 1976–2014. The continuous curve shows values smoothed with the "loess" function.

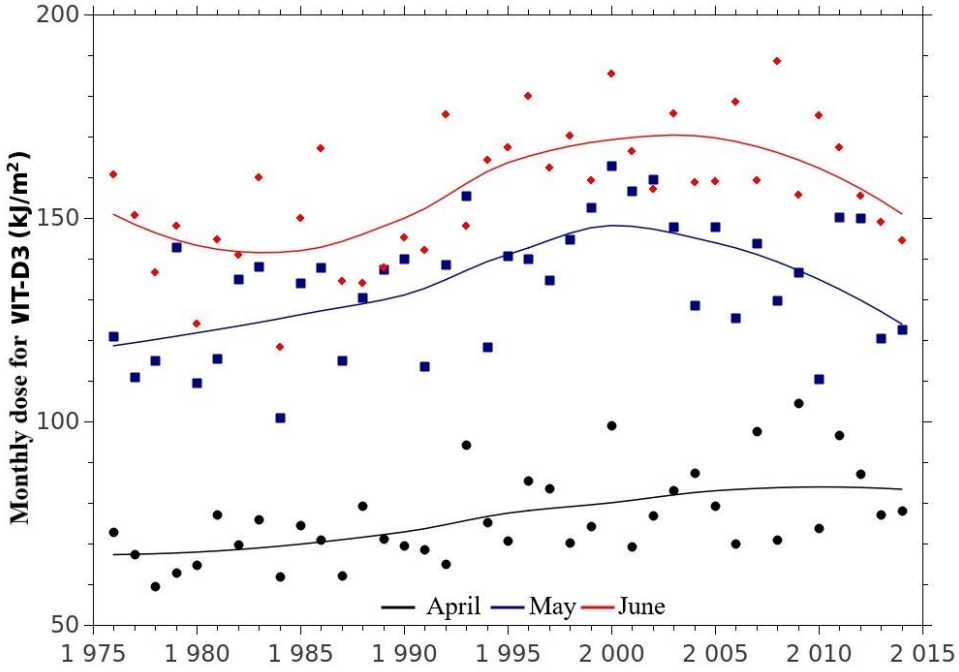

Fig. 38. Total monthly doses of VIT-D_3 radiation in the years 1976–2014 for April, May and June. Continuous curves illustrate values smoothed using the "loess" function.

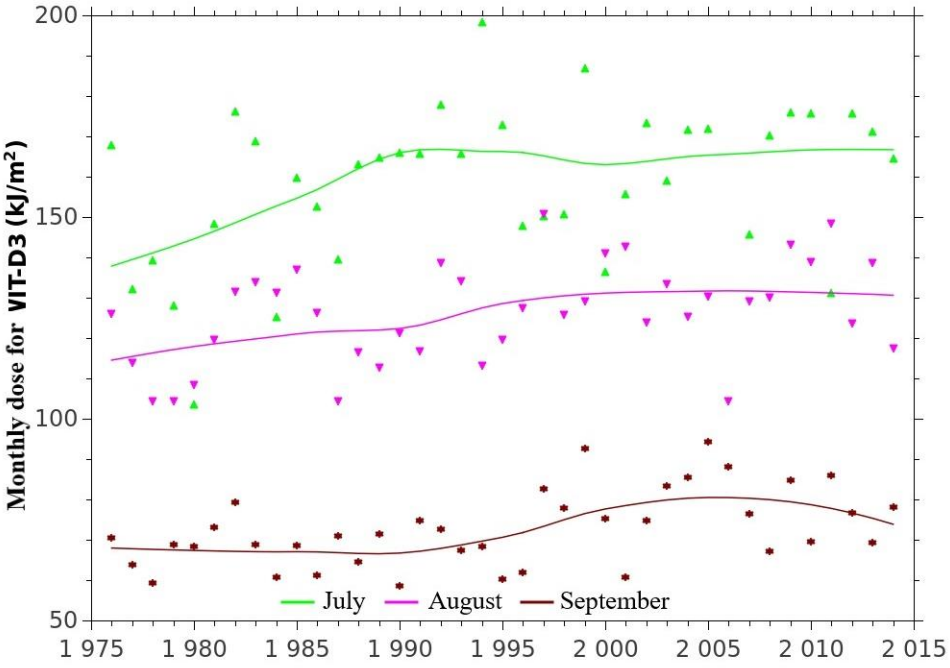

Fig. 39. Total monthly doses of VIT-D_3 radiation in the years 1976–2014 for July, August, and September. Continuous curves illustrate values smoothed using the "loess" function.

Preliminary analysis of the course of the graphs leads to the conclusion that the long-term variability of vitaminal doses is similar to the variability of erythemal doses. For the April–September season, an increasing trend is observed in 1976–2005, and in 2005–2014, probably a decreasing trend exists. For individual months, an increasing trend is observed in the years 1976–2005, while in 2005–2014, a clear decreasing trend can only be seen in May and June.

The next step is to examine the residual series and to determine the autoregressive models (according to the method presented in Subchapter 3.1). It is stated, with the help of the series randomness test, that all tested time series (1976–2014) of residual values $Res_{i,\text{VIT-D3}}$, as well as the $\varepsilon_{i,\text{VIT-D3}}$ values are random. The results of the distribution normality tests, statically significant autocorrelation coefficients and the order of the matched autoregressive model are presented in Table 14.

Table 14

The results of the Shapiro–Wilk test ($W_{crit} = 0.939$ with $N = 39$ and $\alpha = 0.05$), statistically significant autocorrelation coefficients and the order of the fitted autoregressive model for deviations of values of seasonal and monthly doses from the corresponding smoothed values (the VIT-D_3 radiation)

Month	W	H_0 (+/–)	Autocorrelation coefficient	n
April–September	0.9650	+	$k = 5\ r_{xy} = –0.45$ $k = 7\ r_{xy} = –0.44$	8
April	0.9444	+	$k = 1\ r_{xy} = –0.47$ $k = 7\ r_{xy} = 0.42$	6
May	0.9753	+	$k = 5\ r_{xy} = –0.45$ $k = 7\ r_{xy} = 0.35$ $k = 8\ r_{xy} = –0.39$ $k = 10\ r_{xy} = 0.41$	6
June	0.9633	+	$k = 1\ r_{xy} = –0.33$	1
July	0.9774	+	–	–
August	0.9733	+	$k = 5\ r_{xy} = –0.5$	5
September	0.9914	+	$k = 3\ r_{xy} = –0.39$ $k = 4\ r_{xy} = –0.47$ $k = 6\ r_{xy} = 0.44$	5

As in the previous subchapters, the hypothetical series $Res_{i,\text{VIT-D3}}^{(j)}$ are determined using the autoregressive model and drawing with the return of the values $\varepsilon_{i,\text{VIT-D3}}$ or $Res_{i,\text{VIT-D3}}$ with the lack of autocorrelation and determined randomness of the series of residual values.

Subsequently, the hypothetical time series of mean seasonal and monthly vitamin doses for $j_{max} = 100{,}000$ are determined using Eq. (10) and the course of the long-term variability is analysed (Table 15). For each j series, the mean seasonal doses are calculated for the 1976–1985 and 2005–2014 periods. Furthermore, linear trends are calculated for the years 1976–2005 and 2005–2014. The mean values are expressed in kJ/m^2 and the trends in kJ/(m^2 year).

Based on the analysis of the entire statistical ensemble of hypothetical time series $y_{i,\text{VIT-D3}}^{(j)}$, it is found that the mean values of annual doses of the vitaminal irradiation from the 1976–1985 decade are lower than the means from the 2005–2014 decade in 100% of cases for the April–September season and for April, May, June, and September, in 99.99% of cases for August and in 99.56% of cases for July. The mean level of growth is determined by comparing the mean values from the last decade with the mean values in the first decade (Table 16).

Table 15

VIT-D_3 means for the 1976–1985 and 2005–2014 decades and trends in the years 1976–2005 and 2005–2014 in the period from April to September, calculated for j_{max} = 100,000 draws

Parameter	Median	5%	95%	Mean	Standard deviation
April-September					
Mean values 1976–1985	665.9	660.0	671.7	665.9	3.56
Mean values 2005–2014	756.9	750.9	762.6	756.9	3.54
Trend 1976–2005	4.98	4.49	5.46	4.98	0.29
Trend 2005–2014	–5.03	–9.92	–0.23	–5.04	2.95
April					
Mean values 1976–1985	68.2	66.4	70.7	68.3	1.32
Mean values 2005–2014	83.6	81.2	86.2	83.6	1.51
Trend 1976–2005	0.60	0.45	0.75	0.60	0.09
Trend 2005–2014	0.02	–1.27	1.44	0.04	0.82
May					
Mean values 1976–1985	122.0	118.6	125.3	122.0	2.05
Mean values 2005–2014	135.2	131.6	138.6	135.2	2.12
Trend 1976–2005	1.17	0.92	1.41	1.17	0.15
Trend 2005–2014	–2.22	–4.53	0.06	–2.23	1.39
June					
Mean values 1976–1985	144.0	139.4	148.9	144.0	2.87
Mean values 2005–2014	161.8	157.2	166.7	161.9	2.89
Trend 1976–2005	1.16	0.84	1.47	1.16	0.19
Trend 2005–2014	–2.08	–3.83	–0.27	–2.07	1.07
July					
Mean values 1976–1985	145.7	136.5	154.7	145.7	5.54
Mean values 2005–2014	166.1	157.0	175.1	166.1	5.52
Trend 1976–2005	0.93	0.32	1.53	0.93	0.37
Trend 2005–2014	0.15	–3.02	3.34	0.16	1.93
August					
Mean values 1976–1985	118.4	114.2	122.4	118.4	2.50

to be continued

Table 15 contd

Mean values 2005–2014	131.7	127.3	135.8	131.6	2.58
Trend 1976–2005	0.63	0.33	0.93	0.63	0.18
Trend 2005–2014	–0.13	–2.79	2.54	–0.13	1.62
September					
Mean values 1976–1985	67.4	65.0	70.0	67.5	1.54
Mean values 2005–2014	78.5	75.5	81.4	78.4	1.79
Trend 1976–2005	0.49	0.33	0.64	0.49	0.09
Trend 2005–2014	–0.73	–1.87	0.39	–0.73	0.69

Note: Statistically significant trends are marked in bold.

Table 16

Growth of the mean VIT-D_3 values in the years 2005–2014 with respect to the means in 1976–1985 for the considered seasonal and monthly series for VIT-D_3 irradiation

Period	Growth of the mean values 2005–2014 with respect to the mean values 1976–1985 [%]	Standard deviation [%]
April–September	13.66	0.83
April	22.41	3.24
May	10.85	2.53
June	12.45	3.00
July	14.24	5.7
August	16.34	3.79
September	15.95	5.41

For the April–September period, an increasing trend is observed in the years 1976–2005, whereas in 2005–2014, a decreasing trend was detected. For 1976–2005, the coefficient of variation is approx. 6%, while for 2005–2014 it is 58%.

For all months in the years 1976–2005, an increasing trend is observed, with the coefficient of variation of approx. 13–18% (April, May, June, September), 29% (August), and 40% (July). In the years 2005–2014, a statistically significant decreasing trend is noted only in June (with a coefficient of variation of approx. 50%), with the level of VIT-D_3 radiation higher than in 1976–1985 by approx. 12%. There is a lack of a clear trend direction in the remaining months. After 2005, the level of VIT-D_3 radiation in July and August remains trendless, which is approx. 14–16% higher than in years 1976–1985. The highest increase in the level of VIT-D_3 radiation (i.e. 22% and 16%) in 2005–2014, in relation to the 1976–1985 period, is observed for April and September, and the lowest for May (11%).

3.4.2 Irradiation with anti-psoriatic efficacy

Figures 40–42 show the time series of monthly and seasonal sums of the anti-psoriatic irradiation (for the April–September period) as well as the corresponding smoothed values for these series.

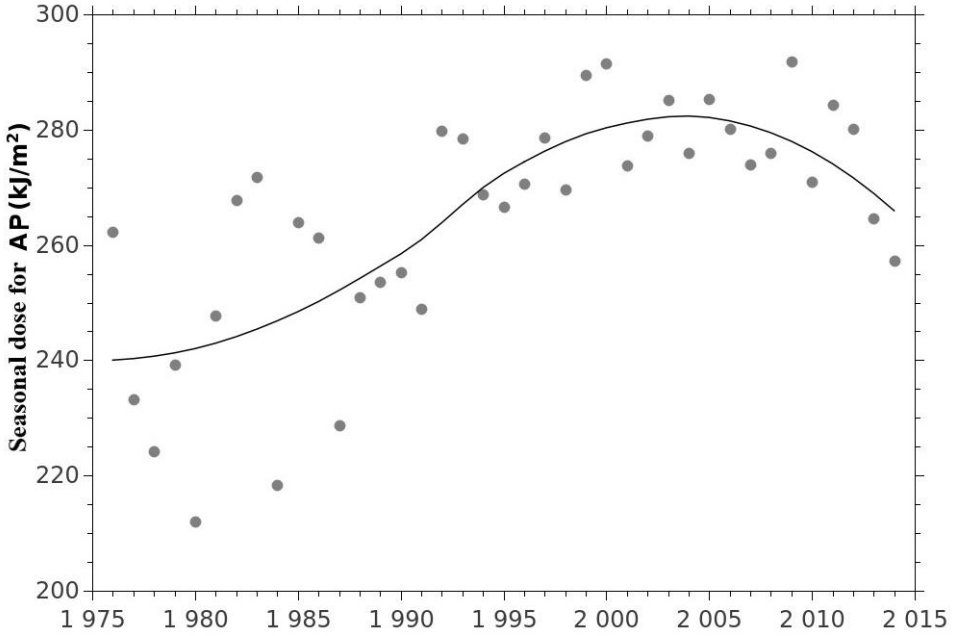

Fig. 40. Total seasonal doses (April–September) of the AP radiation in the years 1976–2014. The continuous curve shows values smoothed with the "loess" function.

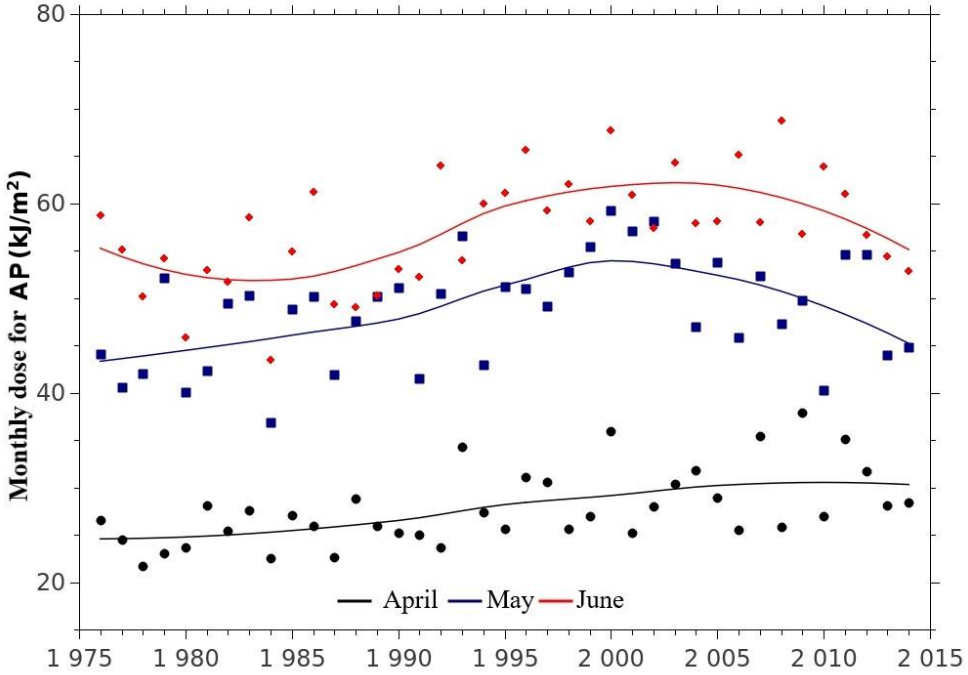

Fig. 41. Total monthly doses of the AP radiation in the years 1976–2014 for April, May, and June. Continuous curves illustrate values smoothed using the "loess" function.

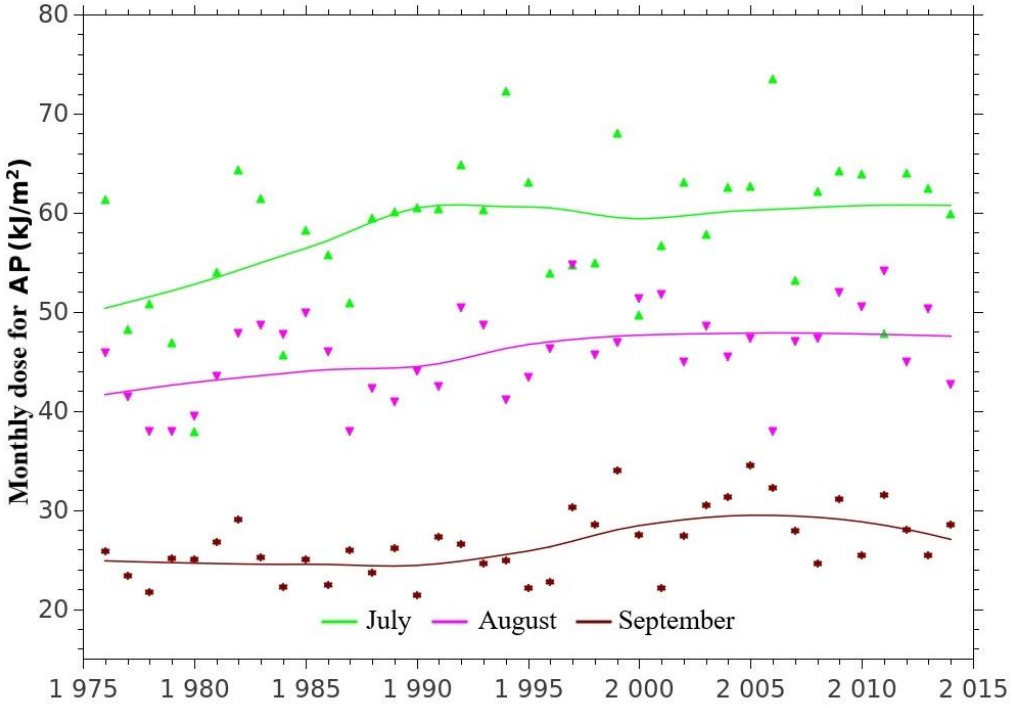

Fig. 42. Total monthly doses of the AP radiation in the years 1976–2014 for July, August, and September. Continuous curves illustrate values smoothed using the "loess" function.

By analysing the course of the graphs, it can be stated that the long-term variability of the AP doses is similar to that for erythemal and VIT-D_3 radiation, i.e. for the April–September season in 1976–2005 an increasing trend is observed, while in 2005–2014 probably a decreasing trend or no trend exists. For individual months, an increasing trend is observed in the years 1976–2005, while in 2005–2014, a clear decreasing trend can only be seen in May and June.

The next step is to examine the residual series and to determine the autoregressive models (according to the method presented in Subchapter 3.1). Moreover, with the help of the series randomness test, it is concluded that all tested time series (1976–2014) of residual values $Res_{i,AP}$, as well as $\varepsilon_{i,AP}$ values are random. The results of the conducted normality test, statically significant autocorrelation coefficients, and the order of the fitted autoregressive model are presented in Table 17.

Similarly to previous subchapters, the hypothetical series $Res_{i,AP}^{(j)}$ are determined using the autoregressive model and drawing with the return of $\varepsilon_{i,AP}$ values or $Res_{i,AP}$ with the lack of autocorrelation in series of residual values with determined randomness.

Subsequently, the hypothetical time series of mean seasonal and monthly doses with antipsoriatic efficacy for $j_{max} = 100{,}000$ are determined utilising Eq. (10) and the course of the long-term variability is analysed. For each j series, mean seasonal doses are calculated for the years 1976–1985 and 2005–2014. In addition, linear trends were calculated for 1976–2005 and 2005–2014. The mean values (Table 18) are expressed in kJ/m^2 and the trends in kJ/(m^2 year).

Based on the analysis of the entire statistical ensemble of hypothetical time series $y_{i,AP}^{(j)}$, it is found that the mean values of annual doses of the AP from the 1976–1985 decade are lower than the means from the 2005–2014 decade in 100% of cases for the April–September season and for April, May, June, and September, in 99.99% of cases for August and in 99.48% of cases for July. The mean level of growth is determined by comparing the means from the last and first decade of the $y_{i,AP}^{(j)}$ series (Table 19).

Table 17

The results of the Shapiro–Wilk test ($W_{crit} = 0.939$ with $N = 39$ and $\alpha = 0.05$), statistically significant autocorrelation coefficients and the order of the fitted autoregressive model for deviations of values of seasonal and monthly doses from the corresponding smoothed values (the AP radiation)

Month	W	H_0 (+/–)	Autocorrelation coefficient	n
April–September	0.9646	+	$k = 5\ r_{xy} = –0.45$ $k = 7\ r_{xy} = 0.44$	8
April	0.9463	+	$k = 1\ r_{xy} = –0.47$ $k = 7\ r_{xy} = 0.42$	6
May	0.9757	+	$k = 5\ r_{xy} = –0.45$ $k = 7\ r_{xy} = 0.35$ $k = 8\ r_{xy} = –0.39$ $k = 10\ r_{xy} = 0.41$	6
June	0.9632	+	$k = 1\ r_{xy} = –0.33$	1
July	0.9774	+	–	–
August	0.9733	+	$k = 5\ r_{xy} = –0.5$	5
September	0.9917	+	$k = 3\ r_{xy} = –0.39$ $k = 4\ r_{xy} = –0.47$ $k = 6\ r_{xy} = 0.44$	5

Table 18

AP means for the 1976–1985 and 2005–2014 decades and trends in the years 1976–2005 and 2005–2014 in the period from April to September, calculated for $j_{max} = 100{,}000$ draws

Parameter	Median	5%	95%	Mean	Standard deviation
April-September					
Mean values 1976–1985	243.1	241.0	245.2	243.1	1.28
Mean values 2005–2014	275.9	273.7	278.0	275.9	1.28
Trend 1976–2005	1.79	1.61	1.96	1.79	0.11
Trend 2005–2014	–1.84	–3.62	–0.10	–1.84	1.07
April					
Mean values 1976–1985	24.9	24.2	25.8	24.9	0.47
Mean values 2005–2014	30.4	29.6	31.4	30.4	0.54
Trend 1976–2005	0.21	0.16	0.27	0.22	0.03
Trend 2005–2014	0.00	–0.46	0.52	0.01	0.30

to be continued

Table 18 contd

May					
Mean values 1976–1985	44.6	43.3	45.8	44.6	0.74
Mean values 2005–2014	49.3	48.0	50.5	49.3	0.77
Trend 1976–2005	0.42	0.33	0.51	0.42	0.05
Trend 2005–2014	–0.80	–1.63	0.03	–0.80	0.51
June					
Mean values 1976–1985	52.8	51.1	54.5	52.8	1.04
Mean values 2005–2014	59.1	57.4	60.9	59.1	1.04
Trend 1976–2005	0.41	0.30	0.53	0.41	0.07
Trend 2005–2014	-0.76	-1.39	-0.12	-0.76	0.39
July					
Mean values 1976–1985	53.2	49.8	56.4	53.2	2.01
Mean values 2005–2014	60.5	57.2	63.8	60.5	2.01
Trend 1976–2005	0.33	0.11	0.56	0.33	0.13
Trend 2005–2014	0.06	–1.09	1.21	0.06	0.70
August					
Mean values 1976–1985	43.0	41.5	44.5	43.0	0.91
Mean values 2005–2014	47.9	46.3	49.4	47.9	0.94
Trend 1976–2005	0.23	0.12	0.34	0.23	0.07
Trend 2005–2014	–0.04	–1.02	0.94	–0.04	0.59
September					
Mean values 1976–1985	24.7	23.8	25.6	24.7	0.56
Mean values 2005–2014	28.7	27.6	29.8	28.7	0.66
Trend 1976–2005	0.18	0.12	0.24	0.18	0.03
Trend 2005–2014	–0.27	–0.69	0.14	–0.27	0.25

Note: Statistically significant trends are marked in bold.

For the April–September period, an increasing trend is observed in the years 1976–2005, while for 2005–2014, a decreasing trend exists. For the years 1976–2005, the coefficient of variation is approx. 6%, and for 2005–2014 it is 58%.

For all months, an increasing trend is noted in the years 1976–2005, with the coefficient of variation of approx. 12–17% (April, May, June, September), 30% (August), and 39% (July). In the years 2005–2014, the statistically significant decreasing trend is detected in June (with the

Table 19
Growth of the mean values in the years 2005–2014 in relation to the means in 1976–1985 for the considered seasonal and monthly series for AP irradiation

Period	Growth of the mean values 2005–2014 with respect to the mean values 1976–1985 [%]	Standard deviation [%]
April–September	13.47	0.82
April	22.14	3.19
May	10.58	2.52
June	12.00	2.96
July	14.07	5.65
August	11.26	3.26
September	16.39	3.79

coefficient of variation of approx. 50%), with the AP irradiation higher by approx. 12% than in 1976–1985. There are no clear trends in the remaining months. After 2005, the AP irradiation in July and August remains trendless, which is approx. 11–14% higher than in 1976–1985. The highest increase of the AP irradiation (22% and 16%) in 2005–2014, in relation to the 1976–1985 period, is observed in April and September, and the lowest in May (below 11%).

3.4.3 Irradiation with the DNA structure destruction efficacy

Figures 43–45 show the time series of seasonal irradiation totals (for the April–September period) and separately for each month, as well as the appropriate smoothed values of these series.

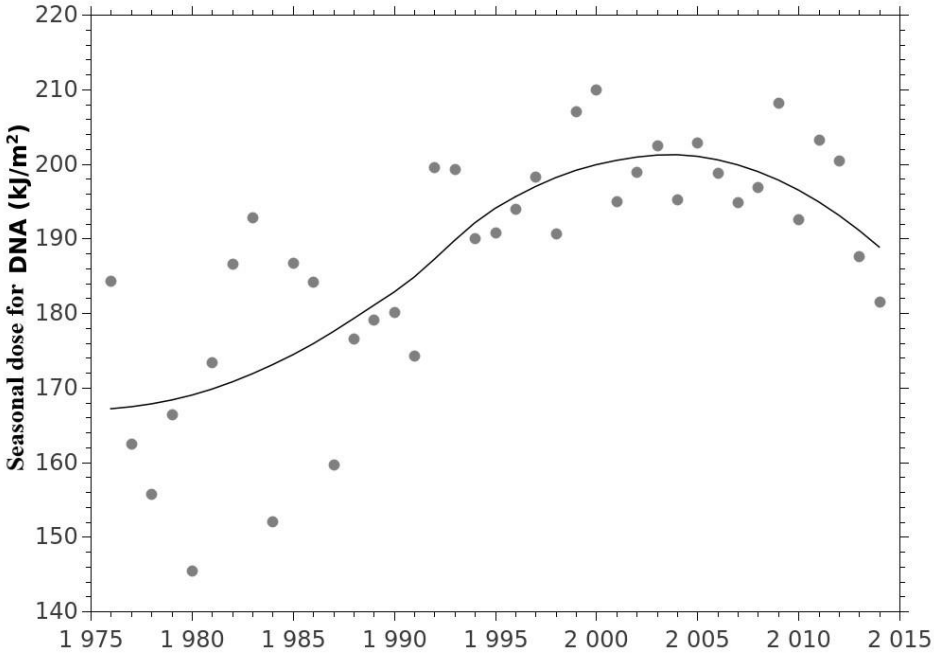

Fig. 43. Total seasonal DNA doses (April–September) in the years 1976–2014. The continuous curve shows values smoothed with the “loess” function.

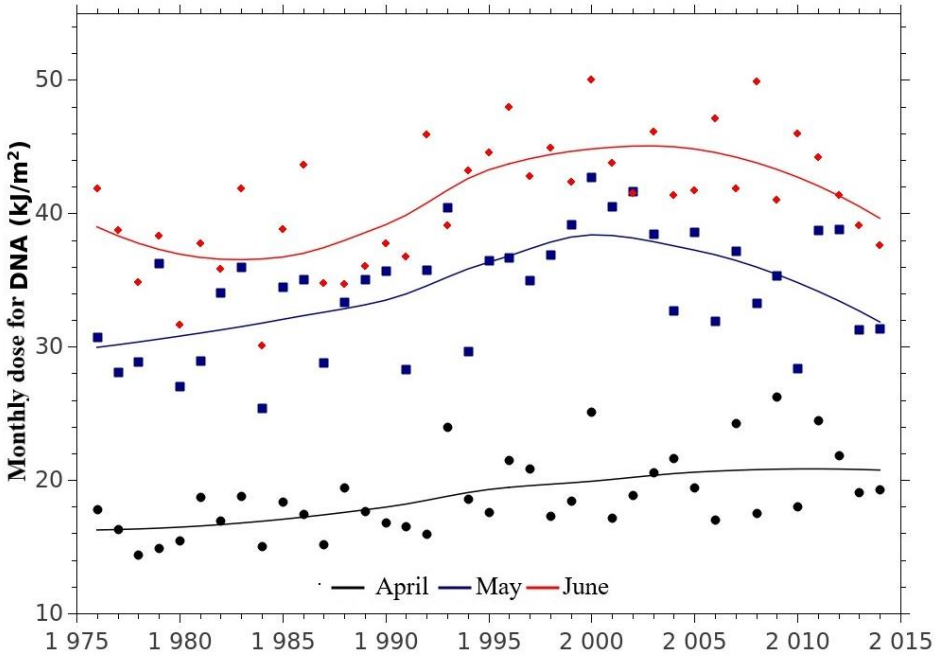

Fig. 44. Total monthly DNA doses in the years 1976–2014 for April, May, and June. Continuous curves show values smoothed with the "loess" function.

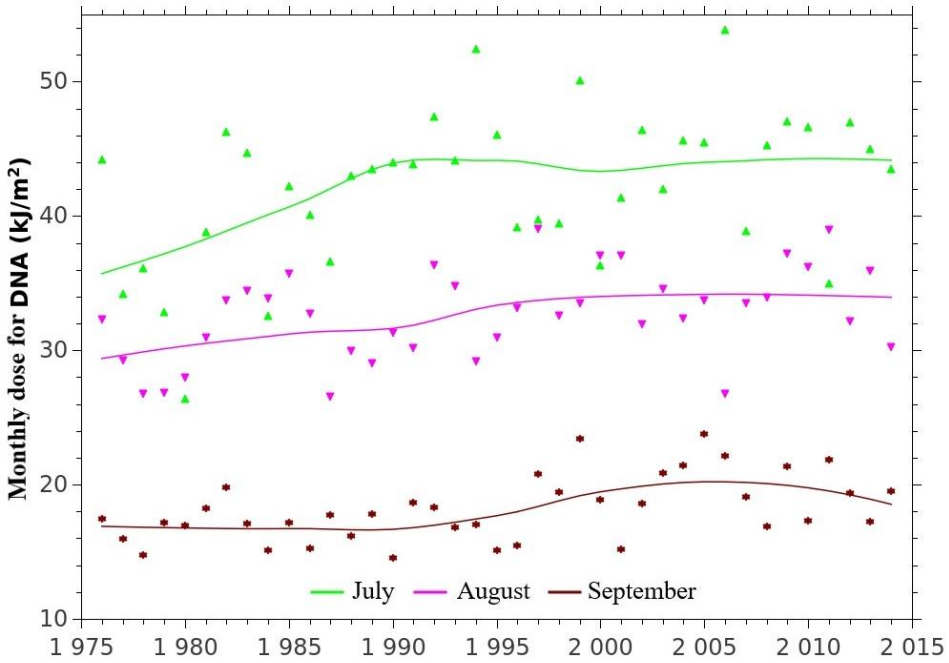

Fig. 45. Total monthly DNA doses in the years 1976–2014 for July, August, and September. Continuous curves show values smoothed with the "loess" function.

Initially, it can be concluded from the course of the graphs that the long-term variability of the anti-DNA irradiation is similar to the erythemal, vitaminal and anti-psoriatic data, i.e. for the April–September season in the years 1976–2005, an increasing trend is observed, whereas in 2005–2014, probably a decreasing trend occurs. For individual months, an increasing trend is observed in the years 1976–2005, while in 2005–2014, a clear decreasing trend can only be seen in May and June.

The next step is to examine the residual series and to determine the autoregressive models. With the help of the series randomness test, it is found that all tested time series (1976–2014) of residual values of $Res_{i,\mathrm{DNA}}$, as well as $\varepsilon_{i,\mathrm{DNA}}$ values are random. The results of the conducted distribution normality tests, statically significant autocorrelation coefficients and the order of the fitted autoregressive model are presented in Table 20.

Table 20

The results of the Shapiro–Wilk test ($W_{\mathrm{crit}} = 0.939$ with $N = 39$ and $\alpha = 0.05$), statistically significant autocorrelation coefficients and the order of the fitted autoregressive model for deviations of values of seasonal and monthly doses from the corresponding smoothed values (the anti-DNA radiation)

Month	W	H_0 (+/–)	Autocorrelation coefficient	n
April–September	0.9676	+	$k = 5\ r_{xy} = -0.46$ $k = 7\ r_{xy} = 0.45$	6
April	0.9355	–	$k = 1\ r_{xy} = -0.44$ $k = 7\ r_{xy} = 0.41$	6
May	0.9634	+	$k = 5\ r_{xy} = -0.42$ $k = 7\ r_{xy} = 0.36$ $k = 8\ r_{xy} = -0.40$ $k = 10\ r_{xy} = 0.43$	6
June	0.9615	+	$k = 1\ r_{xy} = -0.32$	1
July	0.9797	+	–	–
August	0.9725	+	$k = 5\ r_{xy} = -0.50$ $k = 8\ r_{xy} = 0.36$	6
September	0.9921	+	$k = 3\ r_{xy} = -0.38$ $k = 4\ r_{xy} = -0.47$ $k = 6\ r_{xy} = 0.46$	5

Similarly to the previous subchapters, the hypothetical series $Res_{i,\mathrm{DNA}}^{(j)}$ are built using the autoregressive model and drawing with return of values $\varepsilon_{i,\mathrm{DNA}}$ or $Res_{i,\mathrm{DNA}}$ with a lack of autocorrelation in the series of the residual values with the determined randomness.

Subsequently, the hypothetical time series of mean seasonal and monthly doses with DNA destruction efficacy for $j_{\max} = 100{,}000$ are determined using Eq. (10). The course of the long-term variability is analysed. For each j series, the mean seasonal doses are calculated for the years 1976–1985 and 2005–2014. In addition, linear trends for the 1976–2005 and 2005–2014 periods are also calculated (Table 21). The mean values are expressed in kJ/m^2 and the trends in kJ/(m^2 year).

Based on the analysis of the entire statistical ensemble of hypothetical time series $y_{i,\mathrm{DNA}}^{(j)}$, it is found that the mean annual DNA doses in the 1976–1985 decade are lower than the means in the 2005–2014 decade in 100% of cases for the April–September season, and for April, May, June, August, and September and in 99.80% of cases for July. The mean level of increase of the mean values in the last decade in relation to the mean values in the first decade of the series is presented in Table 22.

Table 21

DNA means for the 1976–1985 and 2005–2014 decades and trends in the years 1976–2005 and 2005–2014 in the period from April to September, calculated for j_{max} = 100,000 draws

Parameter	Median	5%	95%	Mean	Standard deviation
April-September					
Mean values 1976–1985	170.0	167.5	172.2	169.9	1.41
Mean values 2005–2014	196.4	193.5	199.0	196.4	1.66
Trend 1976–2005	1.45	1.27	1.61	1.44	0.10
Trend 2005–2014	–1.33	–2.98	0.21	–1.35	0.97
April					
Mean values 1976–1985	16.6	16.0	17.2	16.6	0.36
Mean values 2005–2014	20.8	20.1	21.5	20.8	0.41
Trend 1976–2005	0.17	0.13	0.21	0.17	0.02
Trend 2005–2014	0.01	–0.35	0.40	0.02	0.23
May					
Mean values 1976–1985	30.9	29.9	31.8	30.9	0.56
Mean values 2005–2014	34.9	33.9	35.8	34.9	0.58
Trend 1976–2005	0.34	0.27	0.40	0.34	0.04
Trend 2005–2014	–0.60	–1.21	0.01	–0.60	0.37
June					
Mean values 1976–1985	37.1	35.9	38.5	37.2	0.80
Mean values 2005–2014	42.6	41.3	44.0	42.6	0.80
Trend 1976–2005	0.35	0.26	0.44	0.35	0.05
Trend 2005–2014	–0.58	–1.07	–0.08	–0.58	0.30
July					
Mean values 1976–1985	38.0	35.5	40.5	38.0	1.50
Mean values 2005–2014	44.1	41.6	46.6	44.1	1.50
Trend 1976–2005	0.28	0.12	0.45	0.28	0.10
Trend 2005–2014	0.02	–0.85	0.88	0.02	0.53
August					
Mean values 1976–1985	30.4	29.4	31.4	30.4	0.59

to be continued

Table 21 contd

Mean values 2005–2014	34.2	33.1	35.2	34.1	0.62
Trend 1976–2005	0.18	0.10	0.25	0.18	0.05
Trend 2005–2014	–0.03	–0.82	0.75	–0.03	0.48
September					
Mean values 1976–1985	16.8	16.2	17.5	16.8	0.39
Mean values 2005–2014	19.7	18.9	20.4	19.7	0.46
Trend 1976–2005	0.13	0.09	0.17	0.13	0.02
Trend 2005–2014	–0.18	–0.48	0.10	–0.18	0.18

Note: Statistically significant trends are marked in bold.

Table 22

Growth of the mean values in the years 2005–2014 in relation to the means in 1976–1985 for the considered seasonal series for anti-DNA data

Period	Growth of the mean values 2005–2014 with respect to the mean values 1976–1985 [%]	Standard deviation [%]
April–September	15.56	1.42
April	25.30	3.72
May	13.07	2.80
June	14.74	3.28
July	16.23	6.02
August	12.36	3.06
September	17.28	3.93

For the April–September period, an increasing trend in the years 1976–2005, with the coefficient of variation of approx. 7% is observed.

For all months, an increasing trend is noted in the years 1976–2005, with the coefficient of variation of approx. 12–15% (April, May, June, September), 28% (August), and 36% (July). In the years 2005–2014, the statistically significant decreasing trend is noted in June (with a coefficient of variation of approx. 50%), with the anti-DNA irradiation approx. 15% higher than in 1976–1985. There is no clear trend in the remaining months. After 2005, the level of the anti-DNA irradiation in July and August remains stable, which is approx. 12–16% higher than in 1976–1985. The highest growth of the level of the anti-DNA radiation in the years 2005–2014 (25% and 17%), in relation to the 1976–1985 period, is observed for April and September. For May, this growth is approx. 13%.

3.5 Summary

Based on the study of statistical ensembles of biologically active irradiation doses, it can be concluded that for irradiation with erythemal, vitamin, anti-psoriatic and anti-DNA efficacy, a higher level of biologically active radiation is observed in the years 2005–2014 than in 1976–1985. In addition, a statistically significant increasing trend is detected in the years 1976–2005. This tendency is noticed both for the seasonal data in the April–September period (Fig. 46) and for individual months (Fig. 47). The percentage trends in the seasonal sums of erythemal, vita-

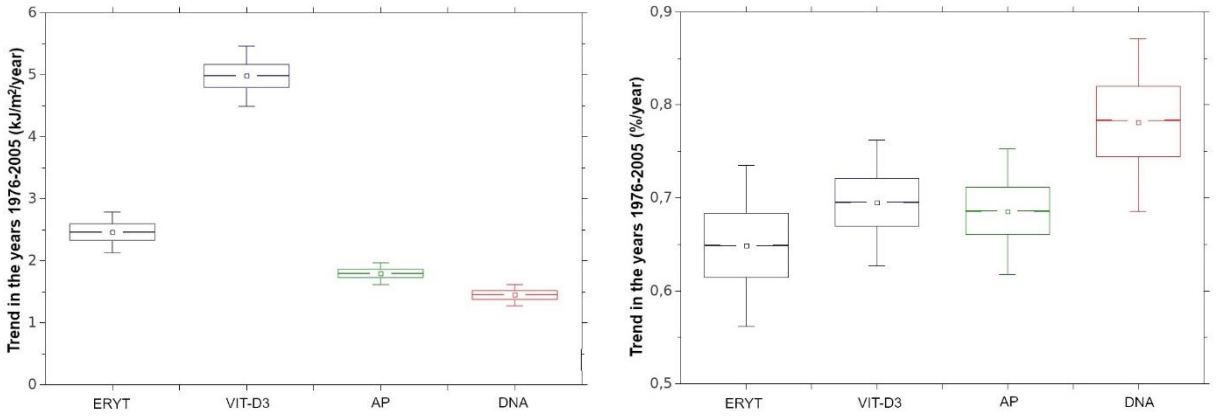

Fig. 46. The trend in the years 1976–2005 for the seasonal sums of biologically active irradiation doses (April–September). The edges of the rectangle mark the standard deviation, the horizontal line inside – the median, the point – the mean, the whiskers – the 5% and 95% percentile. In the left figure trends are in $kJ_{BIOL}/(m^2\ year)$, on the right figure in %/year.

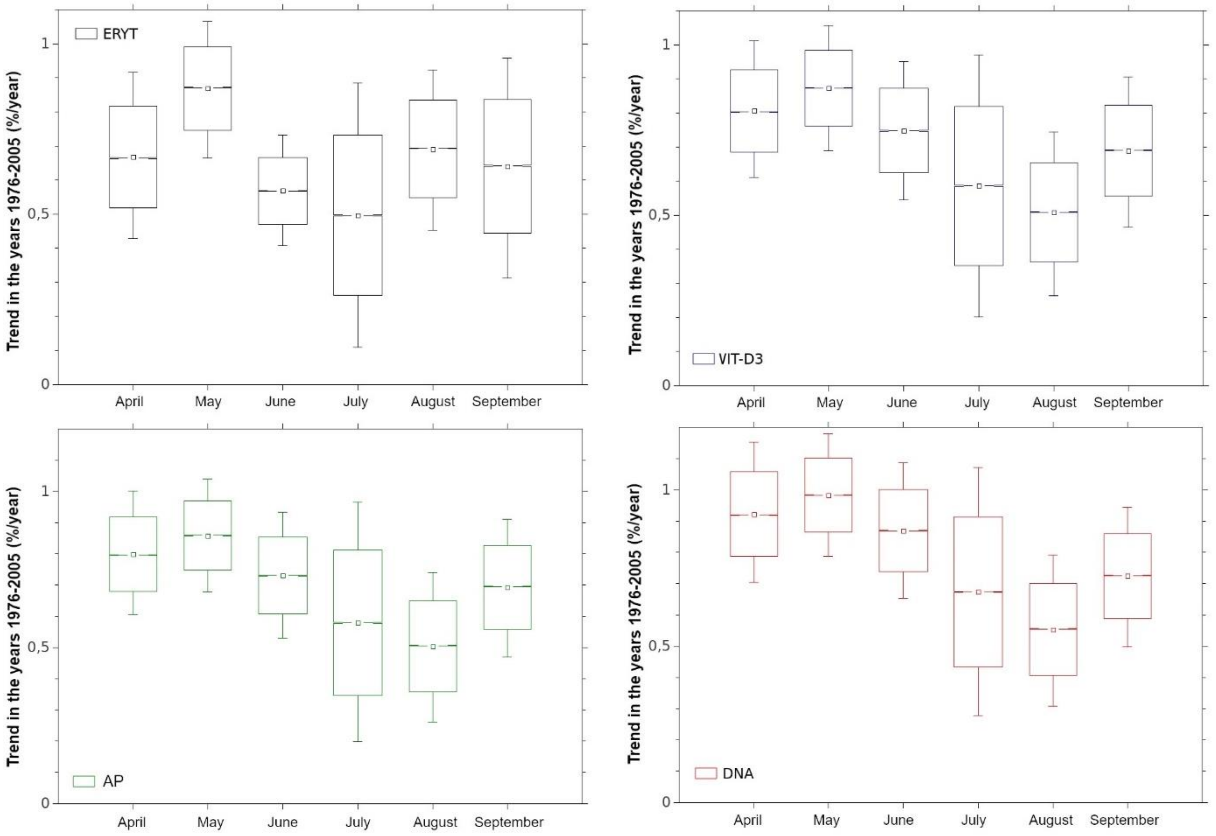

Fig. 47. Trend in the years 1976–2005 for the monthly totals of biologically active irradiation doses. The edges of the rectangle mark the standard deviation, the horizontal line inside – the median, the point – the mean, the whiskers – the 5% and 95% percentile.

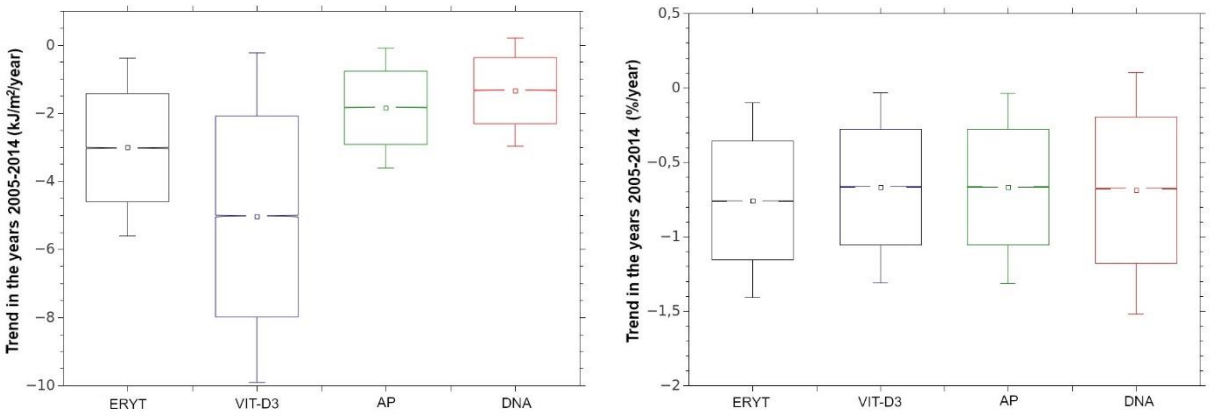

Fig. 48. Markings as in Fig. 46 but trends are for the period 2005–2014.

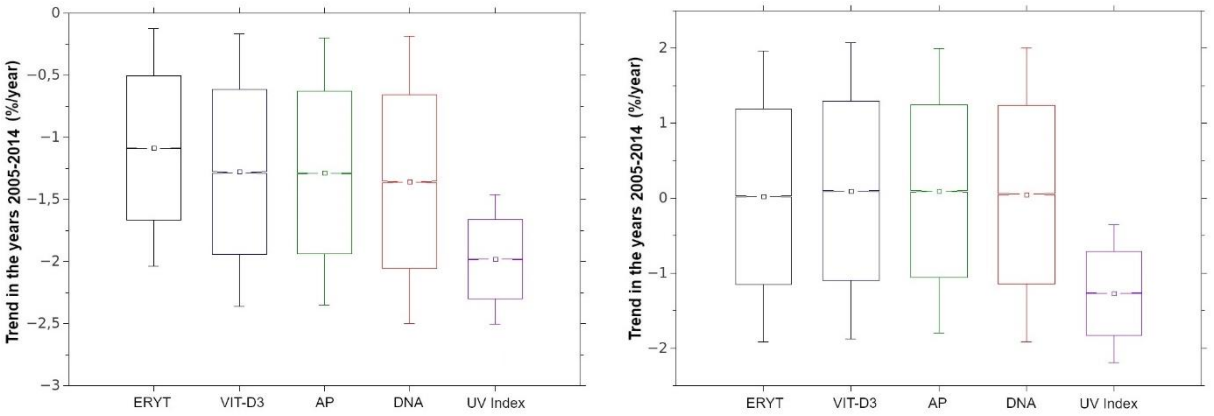

Fig. 49. Trends in 2005–2014 in June (left panel) and July (right panel). Markings as in Fig. 46.

min and anti-psoriatic radiation are at a similar level (~0.7%/year). The seasonal trend in anti-DNA irradiation is slightly higher (~0.8%/year). For all considered biological effects, the highest percentage trend (~1%/year) is observed in May. On the other hand, the smallest percentage trend (~0.5%/year) was found in August for vitaminal, anti-psoriatic and anti-DNA irradiation. For the erythemal irradiation, the smallest percentage trend (~0.5%/year) was determined in July.

In the years 2005–2014, a statistically significant decreasing trend for seasonal doses (annual and seasonal together) of the erythemal, vitamin and anti-psoriatic irradiation is detected (Fig. 48). The level of the trend remains at a similar level for all biological effects. However, for the anti-DNA irradiation, the trend is statistically insignificant (values for the 5% and 95% percentiles have different signs).

For monthly doses, the decreasing trend in these years is detected in May (only erythemal data) and in June (all considered biological effects and the UV index; Fig. 49). The trends in June (%/year) are similar for all analysed biological effects. In the remaining months in the years 2005–2014, the trends are not statistically significant. It should be noted that the decreasing trends observed in June are of particular importance due to the fact that the highest UV radiation values of the year are observed in this month.

In the last 10 years, the statistically significant decreasing trend of UV index is found in June and July (Fig. 49).

In summary, it can be concluded that around 2005, there is a change in the trend direction in the biologically active radiation at Belsk. The clear increasing trend in the years 1976–2005 in the seasonal and monthly sums is replaced by a decreasing trend in 2005–2014, which is best shown in the seasonal sums. These trends are less visible in the monthly totals.

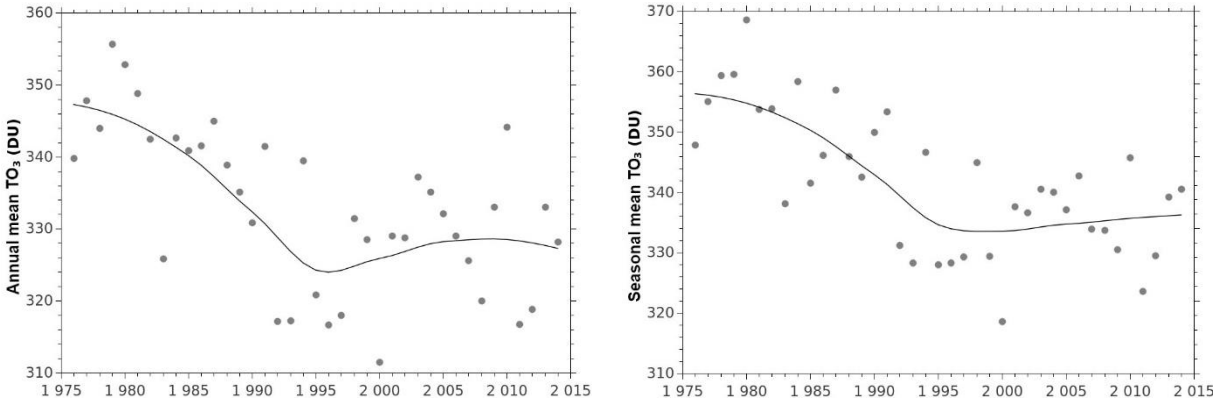

Fig. 50. Annual (left panel) and seasonal mean from April to September (right panel) of total ozone in the years 1976–2014 from the measurements by the Dobson spectrophotometer at Belsk. Continuous curves show the values smoothed by the "loess" function.

The factors that affect the level of UV radiation are: total ozone, cloudiness, and aerosol content in the atmosphere. With the monthly means of TO_3 measured using the Dobson spectrophotometer in 1976–2014, it was possible to check whether the detected change in the trend direction could be explained by the changes in TO_3. Figure 50 illustrates the time series of the annual and seasonal means of TO_3.

Based only on the comparison of Fig. 50 with Figs. 25 and 31, it can be concluded that the change in the biologically active radiation trend in 2005 cannot be explained by the trend in total ozone. Figure 50 indicates that the change in the trend of total ozone was in 1995.

It will be assessed, how the percentage change in TO_3 transforms into a change (in %) of the erythemal irradiation to determine the impact of ozone changes on the level of erythemal irradiation in individual months.

For example, the procedure is shown for April. The observed percentage differences of TO_3 in subsequent years from the long-term mean value (1976–2014) for April are determined:

$$\Delta \mathrm{TO}_3(i) = \frac{\mathrm{TO}_3(i) - \overline{\mathrm{TO}_{3,1976-2014}}}{\overline{\mathrm{TO}_{3,1976-2014}}} \cdot 100\% \tag{11}$$

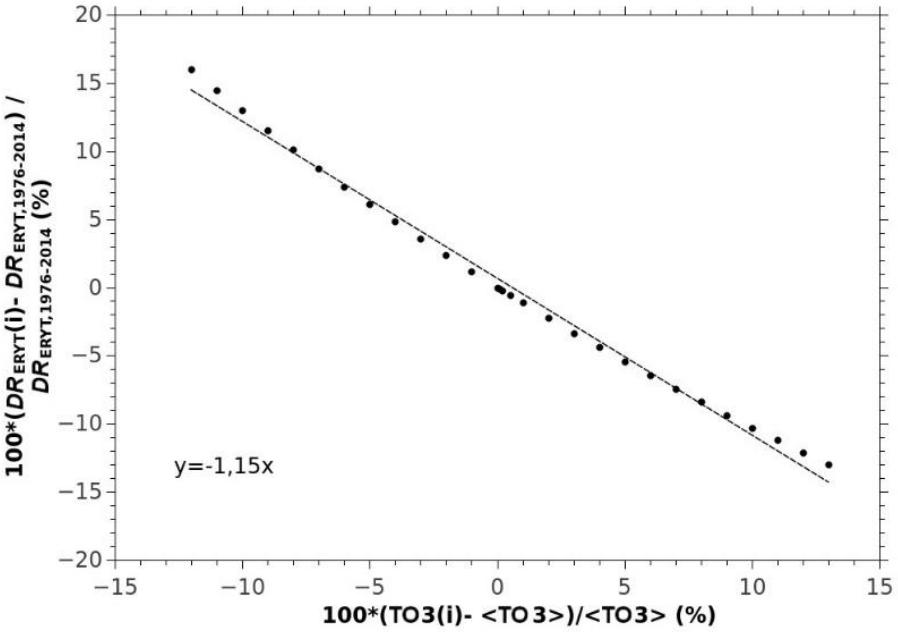

Fig. 51. The modelled change (in %) of the erythemal irradiation as a function of total ozone change (in %) for 15 April.

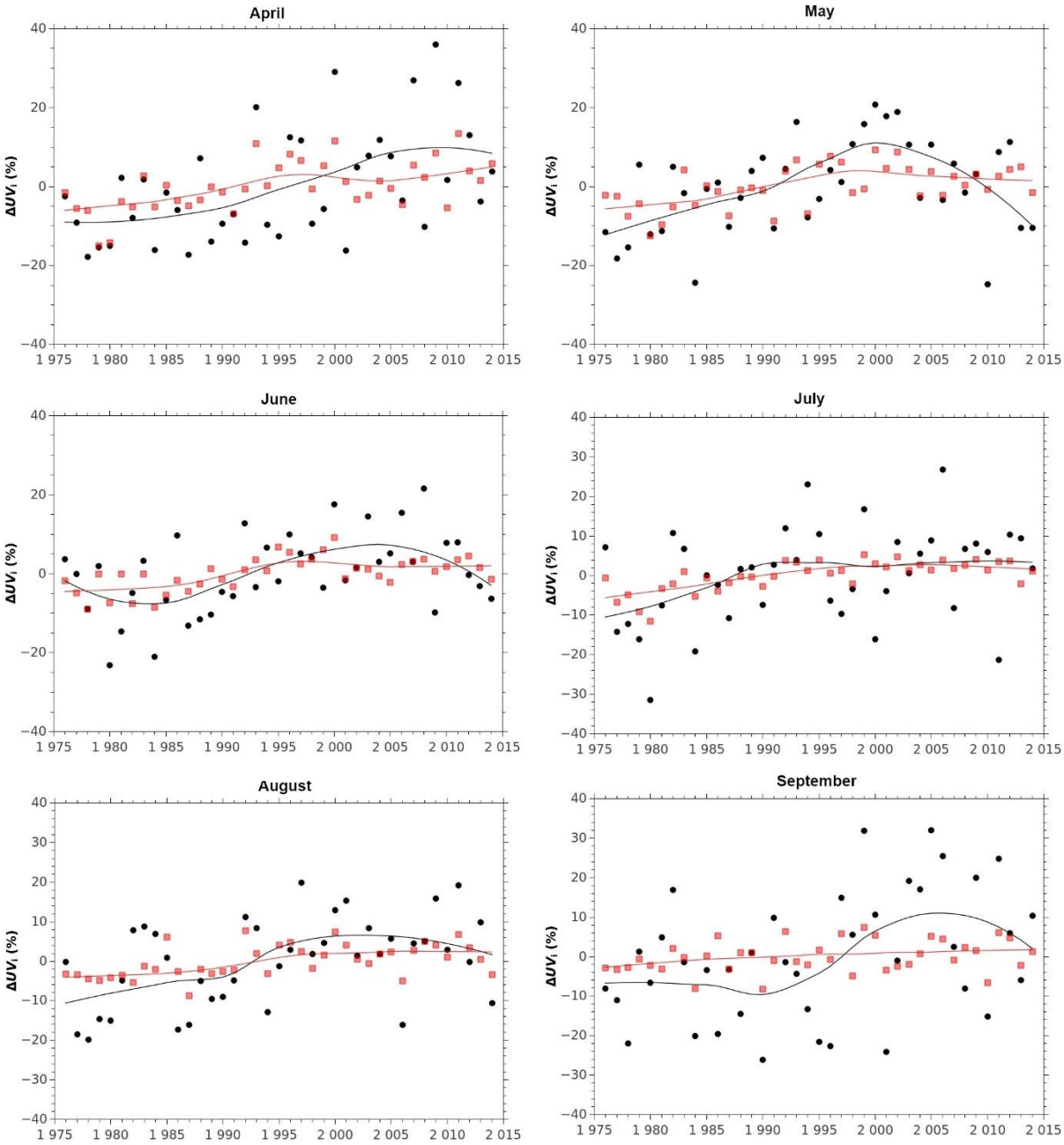

Fig. 52. Time series (1976–2005) of the monthly deviations of erythemal irradiation from the long-term mean monthly doses from the April–September period. The values from observations at Belsk are marked in black, while the values modelled on the basis of the observed changes in the total content of ozone are marked in red. Continuous curves determine the values smoothed by the "loess" function.

Next, the percentage difference of the modelled clear-sky erythemal dose rate at local noon corresponding to the percentage differences of TO_3 are determined:

$$\Delta DR(i) = \frac{DR_{\mathrm{ERYT}}(i) - \overline{DR_{\mathrm{ERYT},1976-2014}}}{\overline{DR_{\mathrm{ERYT},1976-2014}}} \cdot 100\% \tag{12}$$

The FastRT radiative transfer model is used (Engelsen and Kylling 2005), which is described in Chapter 4. The input parameters are TO_3 and the noon SZA for 15 April. Subsequently, a line was fitted to the data using the standard least square linear regression (Fig. 51).

The slope of the regression line (the so-called erythemal irradiation strengthening coefficient – EISC) is:

$$\mathrm{EISC}_4 = -1.15\left[\frac{\Delta DR_{\mathrm{ERYT}}(\%)}{\Delta \mathrm{TO}_3(\%)}\right] \tag{13}$$

where "4" denotes the value for April.

The procedure is repeated for the subsequent months in the April–September period, obtaining the following EISC_m: –1.15, –1.16, –1.11, –1.13, and –1.17 for May, June, July, August, and September, respectively.

Using the aforementioned EISC_m values and the observed deviations of TO_3 from the long-term mean ($\Delta \mathrm{TO}_{3i,\mathrm{obs}}$), the percentage differences of the monthly means of irradiation, $\Delta \mathrm{UV}_{i,\mathrm{model}}$, induced by ozone changes, are determined according to Eq. (14):

$$\Delta \mathrm{UV}_{i,\mathrm{model}} = \mathrm{EISC}_m \cdot \Delta \mathrm{TO}_{3i,\mathrm{obs}} \tag{14}$$

where *m* is the calendar month corresponding to the value of *i*, which is the subsequent number of the month counted from the beginning of the series i = (year-1976) × 12 + m.

Figure 52 shows the modelled and observed values of the percent deviations of monthly erythemal doses from long-term mean doses for 1976–2014. The best agreement is observed in July, and the worst in September. In May and June, when a significant decreasing trend in monthly doses of the biologically active radiation is detected in the years 2005–2014, no similar relationship is observed for the modelled values. The figure shows that in the first period, changes in TO_3 lead to an increase of the erythemal irradiation doses in the series of monthly measurements. On the other hand, changes in TO_3 in 2005–2014 are trendless and do not lead to the decreasing trend in the erythemal irradiation. The possible reason for the change of the UV trend in 2005 is the increase in the attenuation of solar radiation reaching the ground by clouds (greater cloudiness or optical thickness of clouds) or aerosols (the increase in radiation extinction). Only in July, in both the modelled and observed data, a similar course of long-term changes can be observed, i.e. an increase in the initial period (to approximately 1990), afterwards followed by a constant level of erythemal irradiation.

4. SHORT-TERM CHANGES IN THE BIOLOGICALLY ACTIVE IRRADIATION – THE BALTIC 2014 MEASUREMENT CAMPAIGN

During an over two week stay (16 days) at the Baltic Sea, the measurement campaign on the intensity of the erythemal irradiation, was carried out, using low-cost personal hand-held *UVI* meters, available in supermarkets. The aim of the study was to check the relationship between the modelled *UVI* with the use of the radiative transfer model, and *UVI* measured by the aforementioned meters. The *UVI* values obtained by the selected meters correspond to the *UVI* measured by the professional devices (Krzyścin et al. 2014). In the current chapter, by comparing the results of the FastRT model with *UVI* observations by hand-held meters, the availability of such measurements during holidays (for example in the summer by the Baltic Sea) has been studied. The meters, pre-calibrated prior the field measurements, were used to monitor the UV intensity during the Baltic 2014 measurement campaign. The usefulness of the personal hand-held *UVI* meters for conducting individual heliotherapy is discussed.

Furthermore, the *UVI* measurements are utilised to calculate the erythemal, vitaminal and anti-psoriatic doses using the model presented in Subchapter 2.1. The calculations will help to answer the question whether a person, during a typical stay on the beach, using a sunscreen with SPF 30 (following the dermatologists' recommendations), is able to obtain an adequate dose of vitamin D_3, i.e. equivalent to 1000 international units (IU) taken orally. The methodology presented in the work by Sobolewski et al. (2014) is employed herein. These calculations

will also help to establish whether the minimum erythemal dose is exceeded and whether during a beach stay, the dose of solar radiation would be sufficient to cure psoriatic lesions.

4.1 Characteristics of the measurements

4.1.1 Measurement location

The measurements have been carried out in July in Kąty Rybackie. It is a small, tourist resort by the Baltic Sea (Gdańsk Bay), located on the Vistula Spit (longitude 54.3°N, latitude 19.2°E) (Figs. 53 and 54).

The UV index was registered at two measurement points:

- a garden next to a residential property, approx. 1.3 km from the sea,
- beach.

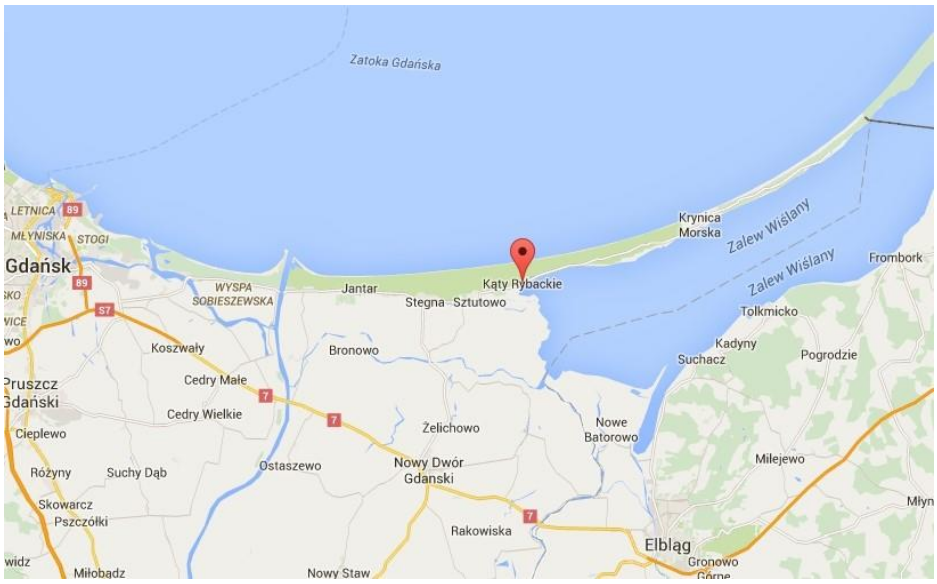

Fig. 53. Geographical location of Kąty Rybackie (source: maps.google.com).

Fig. 54. Measurement point – beach (photo by the author).

4.1.2 Instruments

The following instruments were used for the measurements (Fig. 55):

- Oregon Scientific model EB612/UV888 (measurement scale ± 1 *UVI*),
- Silver Crest UV Meter model H14338A/H14338B (measurement scale ± 0.5 *UVI*).

Fig. 55. Meters used for the measurements. Oregon Scientific – left, Silver Crest UV Meter – right (photos by the author).

In 2013, *UVI* values obtained from the aforementioned meters were compared with values indicated by the Davis meteorological station, equipped with the broad-band *UVI* meter, located on the roof of the main building of the Institute of Geophysics of the Polish Academy of Sciences in Warsaw (Krzyścin et al. 2014).

4.1.3 The time of measurements and the measurement series

The measurements were carried out from the 7 July to the 22 July 2014, from 9 am to 3 pm local time (time interval between the single measurements varied from 15 to 60 minutes). Both meters were used, and for the second device (Silver Crest) the measurements were taken in a horizontal position and perpendicular to the solar rays (the maximum *UVI* reading). Though, three measurement series were obtained during this campaign: "Observation 1", "Observation 2_hor" and "Observation 2_max". On the 12, 13, and 20 July, the measurements were not carried out (due to the heavy overcast). Moreover, on the 14, 16, and 17 July, the measurements were conducted under partially clouded sky.

4.2 FastRT model

The FastRT model used for further calculations (http://nadir.nilu.no/~olaeng/fastrt/fastrt.html) allows fast and accurate calculation of the spectral irradiance in the UV range from 290 to 400 nm with a resolution of 0.05 nm (Engelsen and Kylling 2005). The input parameters of the model are: SZA, TO_3, optical thickness of the clouds and aerosol, Ångström exponent for aerosol, the type/albedo of the ground, altitude and the type of cloudiness.

The *UVI* values are taken from look-up table algorithm using the input parameters defined by the user. Despite the simple design of the FastRT model, the accuracy of the calculations is comparable to the accuracy obtained by solving the radiative transfer equation, using the LibRadtran model (Mayer and Kylling 2005). The biggest errors were noted for wavelengths less than 300 nm and in the presence of clouds.

4.3 Discussion of results

The results of the measurements are compared with the forecast of the maximum *UVI* and the values calculated on the basis of the FastRT model. It uses SZA as one of the input parameters, not the time and geographical coordinates. Therefore, the function calculating SZA for a selected location, date and time is added. The constant values used in the model are visibility (23 km) and altitude above mean sea level (0.001 km).

TO_3 values, used as one of the input parameters, are selected as follows:

- by utilising the 24 hour forecast of the global ozone distribution according to the Global Forecast System (GFS) model,
- from measurements obtained using an Ozone Monitor Instrument (OMI) spectrophotometer, located on the Aura satellite platform.

Data from the GFS prognostic model have been available for each day at hourly intervals (for full hours). TO_3 values for measurements time are calculated using the linear interpolation. For one day (19 July 2014), the predicted daily ozone value from the prognostic model available at http://www.temis.nl/uvradiation/nrt/uvindex.php is used.

The satellite data are available with a resolution of $0.25° \times 0.25°$. For the considered location, TO_3 is determined based on the value from the nearest grid point. For 9 July 2014, the nearest point for which TO_3 is determined is more than 1° away from Kąty Rybackie; therefore, it is not taken into consideration. The satellite data are obtained from a single measurement around noon. Thus, constant TO_3 value is assumed for the whole day.

It should also be noted that for the first two days of the measurements (7 and 8 July 2014), it was noticed that the values recorded with the Silver Crest meter are considerably smaller than those recorded with the Oregon Scientific meter. On the 8 July, the battery was replaced in the above-mentioned instrument. It is also possible that the sensor was soiled with sunscreen, which could have affected the measurement result.

4.3.1 Cloudless sky

Figures 56 and 57 show the worst and the best fit of the UV index measurements to the model values during the Baltic 2014 campaign, respectively. On 8 July 2014, after 1 pm local time, it was observed that the measured UV index is lower than the forecast value by 1.5 units at most.

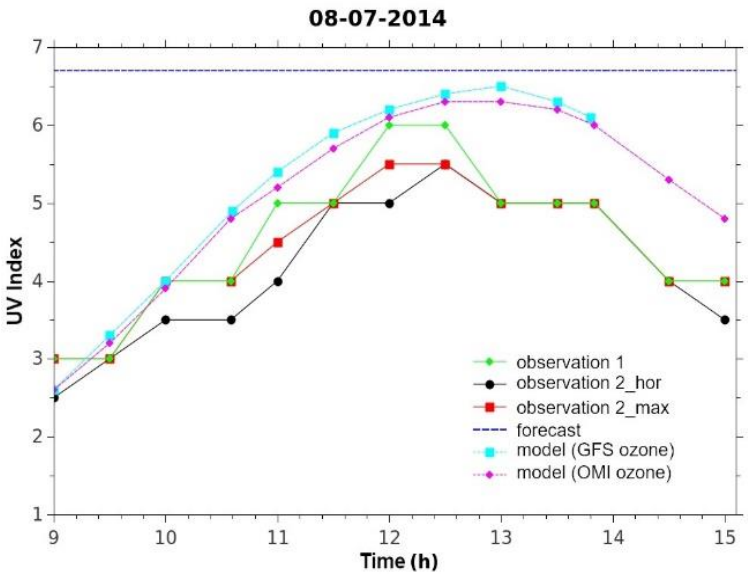

Fig. 56. Results of *UVI* measurements for 8 July 2014 (worst fit), local time. Observation 1 means measurement with the Oregon Scientific sensor; Observation 2_hor and Observation 2_max indicate measurements with the Silver Crest UV Meter in the horizontal position and perpendicular to the sun rays. Forecast means the maximum predicted UV index on a given day based on the data from http:// www.temis.nl/uvradiation/nrt/uvindex. php. Model (GFS ozone) and model (OMI ozone) indicate the UV index calculations with the FastRT model using the total ozone data obtained from the GFS model and the data from the OMI satellite measurements, respectively.

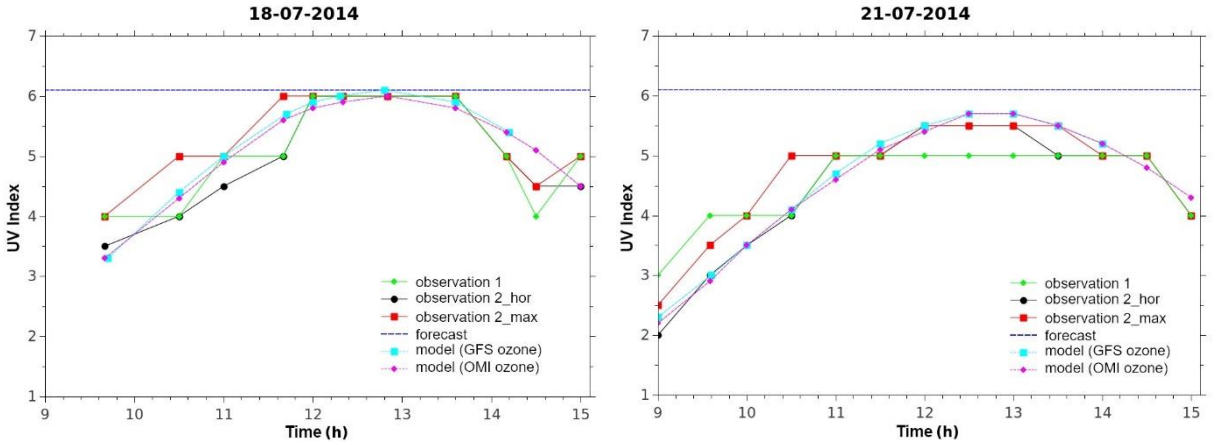

Fig. 57. Markings as in Fig. 56, for the best fit (18 and 21 July 2014).

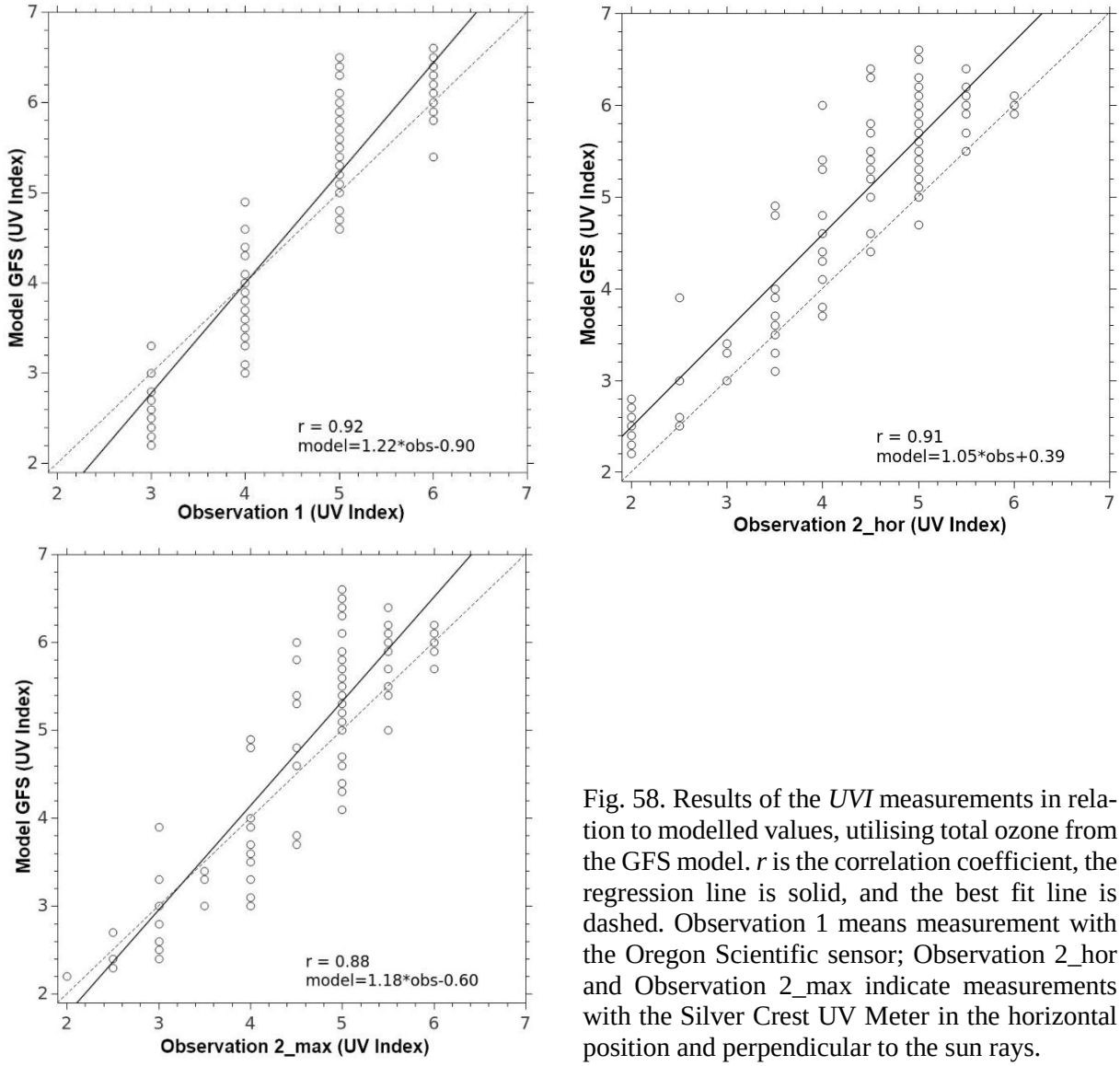

Fig. 58. Results of the *UVI* measurements in relation to modelled values, utilising total ozone from the GFS model. *r* is the correlation coefficient, the regression line is solid, and the best fit line is dashed. Observation 1 means measurement with the Oregon Scientific sensor; Observation 2_hor and Observation 2_max indicate measurements with the Silver Crest UV Meter in the horizontal position and perpendicular to the sun rays.

Figures 58 and 59 demonstrate the relationships between the observed and modelled *UVI* (using ozone data from GFS and OMI). The correlation coefficients, as well as the regression lines ($f(x) = a*x + b$) and the best fit line ($f(x) = x$, diagonal of the square) are also shown.

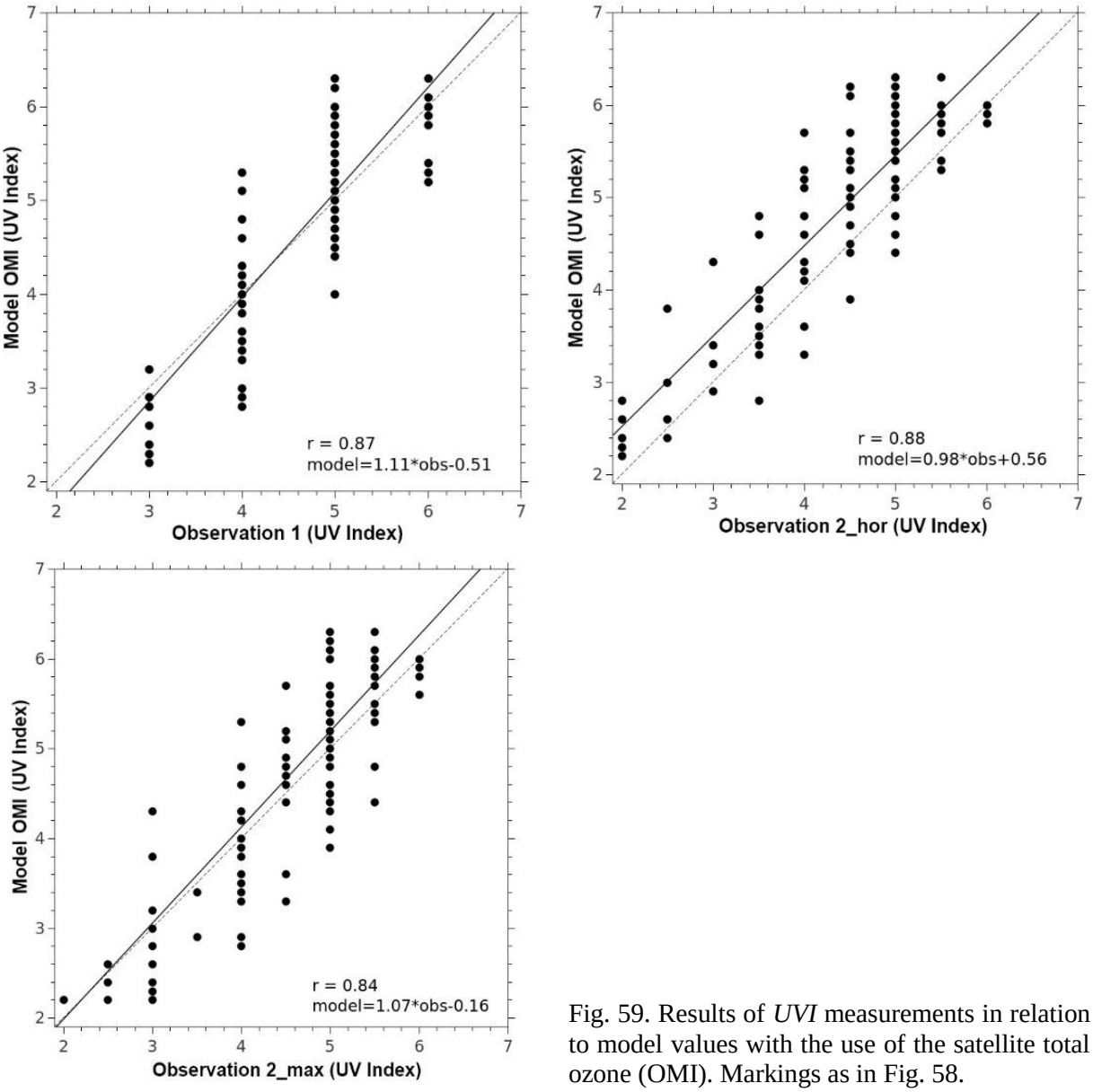

Fig. 59. Results of *UVI* measurements in relation to model values with the use of the satellite total ozone (OMI). Markings as in Fig. 58.

High values of correlation coefficients (~0.9) indicate a good fit with the results of the GFS model, particularly for observation 1, where *UVI* usually reaches higher values than in other observations. For observation 2_hor (horizontal position of the meter), the regression coefficient *a* is close to one, and coefficient *b* is the closest to zero (in comparison to other observations), which indicates a dependence similar to the perfect dependence.

Comparing the observed with the modelled *UVI* based on the total ozone from OMI, the highest correlation coefficient is found for 2_hor observations. Moreover, for this observation the slope coefficient *a* is also close to one. For the remaining observations, there is a good agreement between the measured and the modelled values.

Table 23 shows the percentage of cases for which the model did not differ from observations by more than 0.5 *UVI* (for the Silver Crest meter) and 1.0 *UVI* (for the Silver Crest and Oregon meters). Approximately 80–95% of the measurement results are within the range, modelled value ±1.0 *UVI*, while ~50% within ±0.5 *UVI*. The best fit during the Baltic 2014 measurement campaign is achived for the Oregon meter, and marginally worse for the Silver Crest meter, measuring in the horizontal position. It can be initially estimated that under the conditions of

the Baltic 2014 experiment, the measurement accuracy of the index is within ±1.0 *UVI*, which is not surprising in the case of the Oregon meter, indicating only integer values.

Table 23

Comparison of the UV index measured with the personal meters with modelled values (total ozone from the GFS model or from the OMI observations)

	The percentage of cases $\lvert UVI_{model} - UVI_{obs} \rvert \leq 0.5$ [%]	The percentage of cases $\lvert UVI_{model} - UVI_{obs} \rvert \leq 1.0$ [%]
Cloudless sky (model based on the data from GFS)		
Observation 1	–	95.37
Observation 2_hor	50.00	79.63
Observation 2_max	55.56	90.74
Cloudless sky (model based on the data from OMI)		
Observation 1	–	93.58
Observation 2_hor	58.72	81.65
Observation 2_max	56.88	85.32

Note: Percentage of cases for clear-sky conditions, where the UV index difference between the model and observation does not exceed 0.5 or 1.

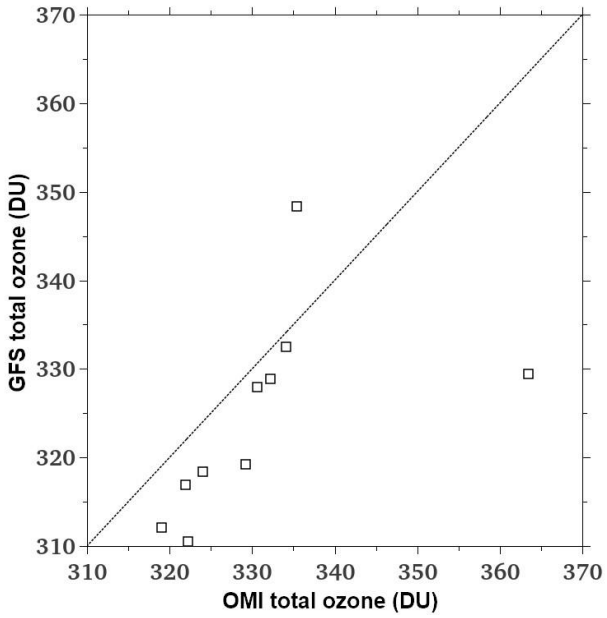

Fig. 60. Comparison of total ozone from the 24-hour GFS forecast with the OMI satellite observations.

In Fig. 60, TO_3 from the 24-hour forecast using the GFS model is compared with the corresponding satellite data from OMI measurements interpolated to the location of Kąty Rybackie for days with *UVI* observations have been carried out. On the basis of the figure, it can be concluded that in most cases (except for one day), the OMI TO_3 was greater than the data calculated with the GFS model. Therefore, the modelled *UVI* based on the observations taken from OMI will be smaller. Nevertheless, the difference between the modelled UV indexes, calculated using GFS and OMI, is small (Figs. 56 and 57).

4.3.2 Partly cloudy skies

Figure 61 illustrates the results of the UV index measurements for three measurement series taken in the partly clouded sky days as well as the corresponding model values for cloudless sky with GFS and OMI total ozone. The measured values are lower than the forecasted ones. The models significantly overestimated the index values over this period, not taking into account the attenuation of solar radiation caused by clouds.

On 14 July 2014, the weather rapidly changed after 12:30 pm local time. After 1:30 pm, the sky was so cloudy that no further measurements have been possible. On 16 July, the cloudiness was variable. A significant decrease in *UVI* value was observed at 10 am and 11 am when the meters indicated 0 *UVI* due to heavy clouds. On 17 July, after 10 am local time, the measured *UVI* was lower than the modelled values – the cloudiness persisted until the afternoon.

Personal hand-held meters work well in any conditions, allowing the assessment of UV intensity directly at the user's location. In this regard, *UVI* obtained from personal meter are better than the modelled values, especially in cloudy sky conditions.

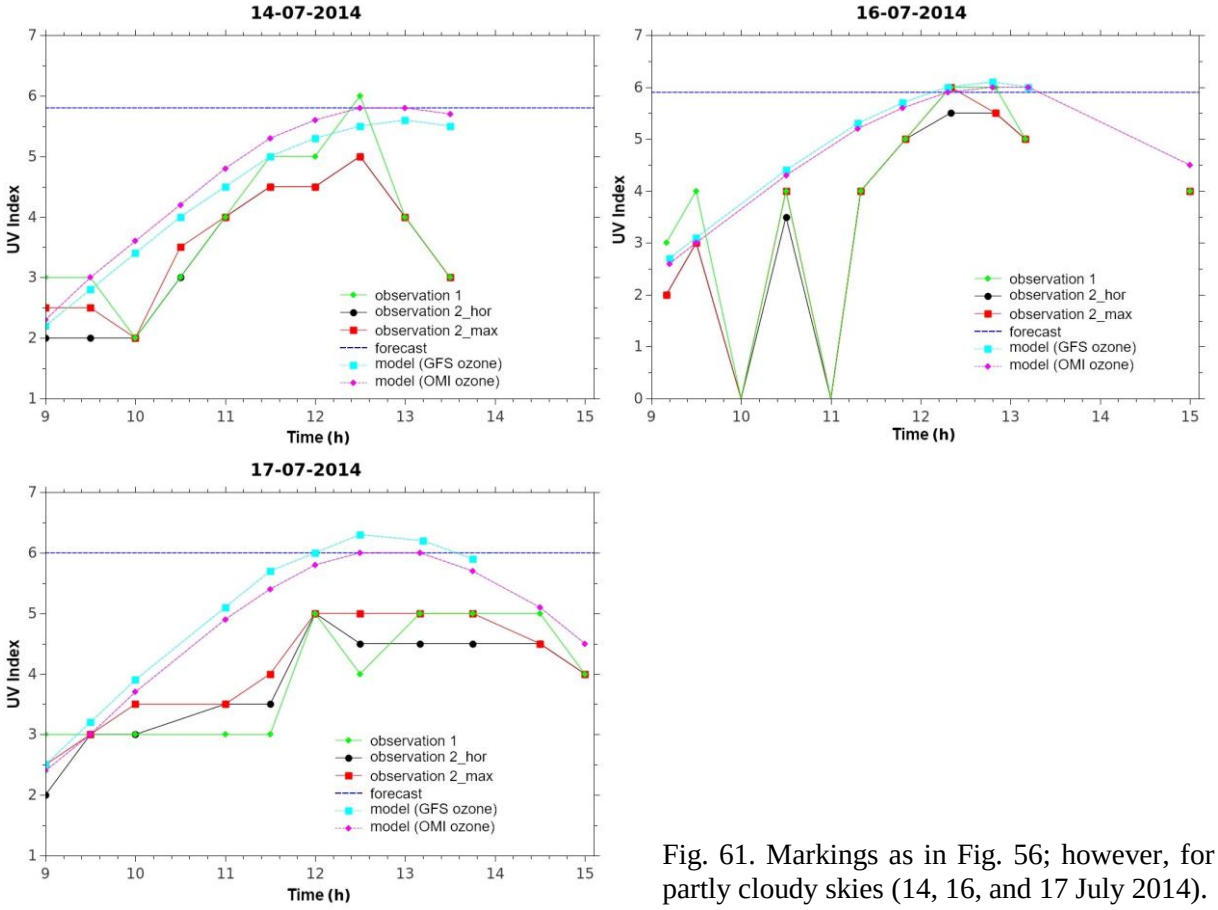

Fig. 61. Markings as in Fig. 56; however, for partly cloudy skies (14, 16, and 17 July 2014).

4.4 Erythemal, vitaminal and anti-psoriatic doses

This part of the subchapter presents the calculation results of erythemal, vitamin and anti-psoriatic doses obtained during a stay on the beach on cloudless and partly cloudy days during the Baltic campaign.

In order to calculate erythemal doses, the irradiance intensity (DR_{ERYT}) is determined from the UV index values measured with the Silver Crest UV Meter set in the position directly "to the Sun" (Observation 2_max). *UVI* is converted to DR_{ERYT} according to the following formula: $DR_{ERYT} = UVI*25$ [mW/m^2].

Subsequently, $DR_{\text{VIT-D3}}$ and DR_{AP} are calculated using the model presented in Subchapter 2.1, according to Eq. (2), using the currently measured TO_3 (from OMI observations) and SZA, corresponding to the moment of the *UVI* measurement.

The next step is to determine the doses of biologically active UV radiation during the actual stay on the beach. The doses for the periods between successive measurements, i.e. between t_1 and t_2 moments, are determined according to Eq. (15):

$$D_{\text{BIOL}}(t_1, t_2) = 0{,}5 \cdot (DR_{\text{BIOL}}(t = t_1) + DR_{\text{BIOL}}(t = t_2)) \cdot (t_2 - t_1) \tag{15}$$

where the dose of the biologically active radiation, D_{BIOL}, is expressed in J/m^2.

To calculate the personal dose of vitamin radiation $Person\_D_{\text{VIT-D3}}(t_1, t_2)$, the formula described by Sobolewski et al. (2014) is employed:

$$Person\_D_{\text{VIT-D3}}(t_1, t_2) = D_{\text{VIT-D3}}(t_1, t_2) \times FR_{\text{AREA}} \times FR_{\text{POSTURE}} \tag{16}$$

FR_{POSTURE} is a coefficient dependent on the position of the body with respect to the position of the Sun. The value of 0.5 is assumed for sunbathing in a vertical position with randomly oriented face towards the Sun. FR_{AREA} is a coefficient dependent on the area of the exposed skin, determined using Lund and Browder' chart (http://www.emed.ie/Trauma/Wounds/Burns.php). This diagram was initially used to determine the burnt body surface area, e.g. during a fire. Then it was adapted by dermatologists to determine the exposed body surface area in percent of the whole skin.

The FR_{AREA} coefficient is calculated for an average adult wearing a one-piece swimsuit, according to Fig. 62.

When determining anti-psoriatic doses, it is assumed that small psoriasis lesions located on one side of the body are irradiated, and this part of the body is maximally exposed and oriented directly to the sun. Therefore, the doses are calculated excluding the FR_{AREA} and FR_{POSTURE} coefficients.

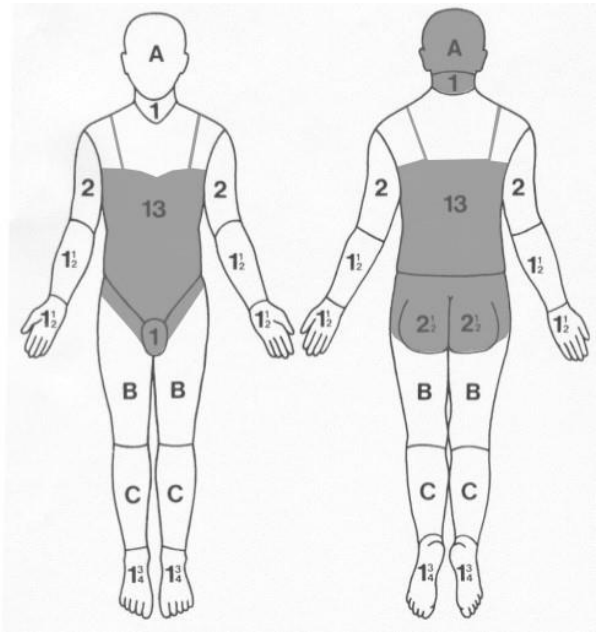

Fig. 62. The Lund and Browder chart with indication of the body surface area covered with swimsuit and headwear (headscarf). According to the diagram for an adult, area A indicates 3.5%, area B – 4.75%, and area C – 3.5% of the body surface area.

The doses are determined for the actual time of staying on the beach for three sunny and three cloudy days. For two cloudy days, the hypothetical tanning time is assumed. During those days, measurements were taken only at the first site (the garden next to the residential property).

Subsequently, the calculated erythemal doses are compared to the critical erythemal dose, causing skin redness, i.e. MED = 250 J/m^2 for skin phototype II. Vitaminal doses will be compared to the minimum dose necessary for the skin synthesis of vitamin D_3 corresponding to the daily intake of 1000 IU, i.e. 1 MVD$_3$D = 100 J/m^2 (Krzyścin et al. 2011a). Anti-psoriatic doses will be compared with the minimum dose, corresponding to the dose obtained in the dermatological cabin during exposure to the TL-01 fluorescent lamps, i.e. 1 MAPD = 317.9 J/m^2 (Krzyścin et al. 2014).

The doses are calculated assuming the following options for sunbathing: no sunscreen, sunscreen used only after a short (~30 min) sunbathing time without UV protection, sunscreen with SPF 30 used all the time (the option recommended by dermatologists).

4.4.1 Cloudless sky

Figure 63 shows the maximum duration of the sunbathing without sunburn depending on the skin phototype and the UV index (for the most common skin phototypes in Poland). The duration of the safe exposure for a person with skin phototype II to get the dose of 1 MED, is up to 33 min for *UVI* = 5. On 18 and 21 July, when arriving at the beach, the UV index was ~6 and the safe tanning time was 28 min (Fig. 63). Thus, in-situ readings of *UVI* from the personal hand-held meter can provide information to optimise the sunbathing duration.

Figure 64 demonstrates the results for erythemal and vitaminal doses on 8, 18, and 21 July. The measured *UVI*s in those days have been shown in Figs. 56 and 57. Based on Fig. 64, it can be concluded that the maximum dose for the entire stay on the beach (for all days), when using SPF 30 sunscreen, does not exceed the dose of 1 MED and 1 MVD$_3$D. Without photoprotection, MVD$_3$D would be reached faster than the MED.

Further in this chapter, pro-healthy scenarios of staying on the beach to obtain the adequate dose of vitamin D_3 as a result of sunbathing (the vitaminal dose > 1 MVD$_3$D) while avoiding sunburn (erythemal dose < 1 MED) are presented. The following pro-healthy scenario is ex-

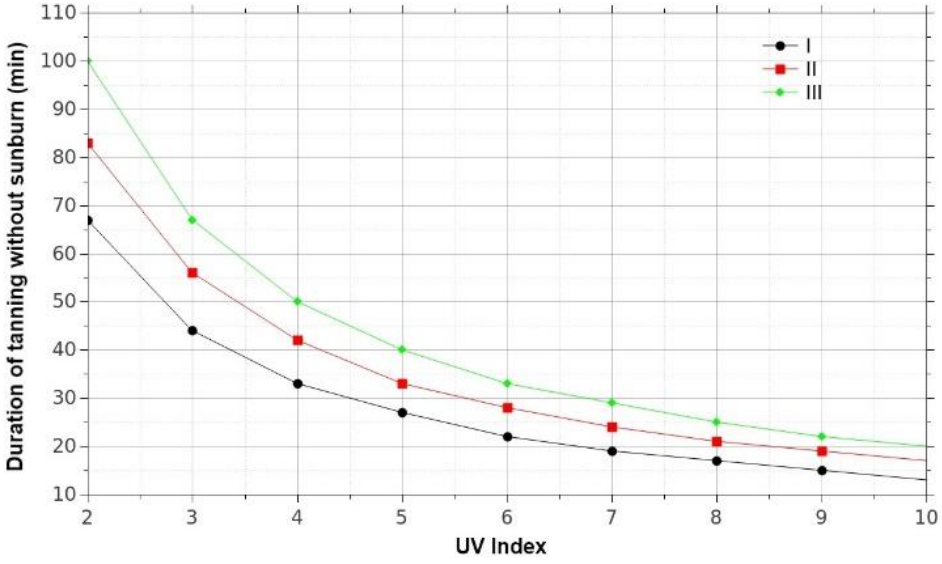

Fig. 63. Maximum duration of safe tanning (without sunburn) depending on the UV index and skin phototypes (most commonly occurring in Poland). Black line – phototype I, red line – phototype II, green line – phototype III.

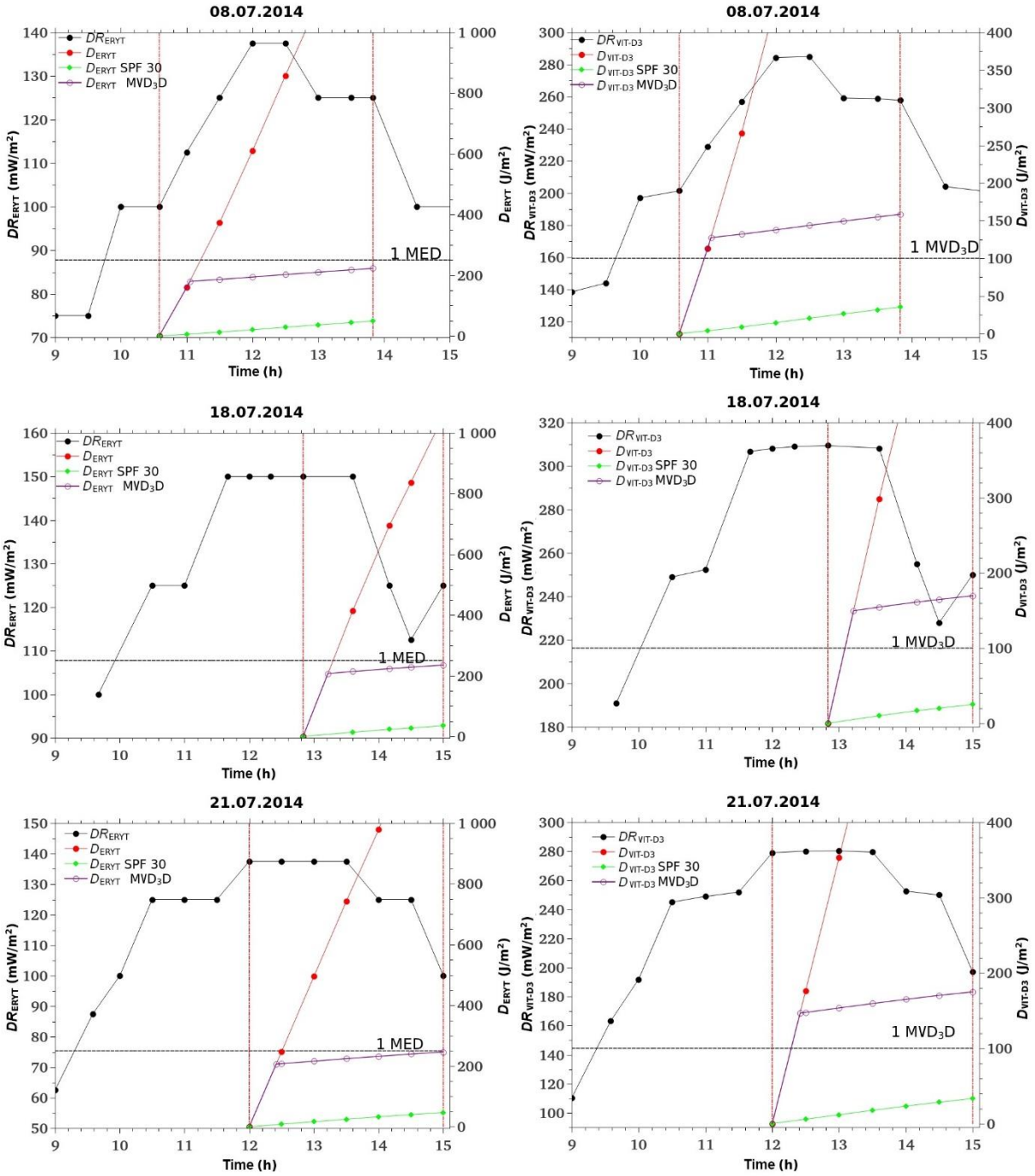

Fig. 64. Dose rates and ERYT (left panels) and VIT-D_3 (right panels) doses on 8, 18, and 21 July 2014. Red vertical lines indicate the time spent on the beach, black horizontal dashed lines indicate the minimum doses needed to achieve a given biological effect. Solid black lines indicate the intensity of UV radiation [mW/m^2] determined from *UVI* measured by the Silver Crest meter. The remaining lines indicate the doses obtained during the stay on the beach: red – without using photoprotection, green – using SPF 30, purple – 20–30 min without photoprotection, and then applying SPF 30.

amined: do not use a sunscreen for the first 20–30 min of being on the beach, afterwards apply a cream with SPF 30. The erythemal and vitaminal doses obtained by the person based on this scheme are shown in Fig. 64 (purple line). The duration of short sun exposure without photoprotection for this scenario is determined from the UV index adding 1 to the personal meter

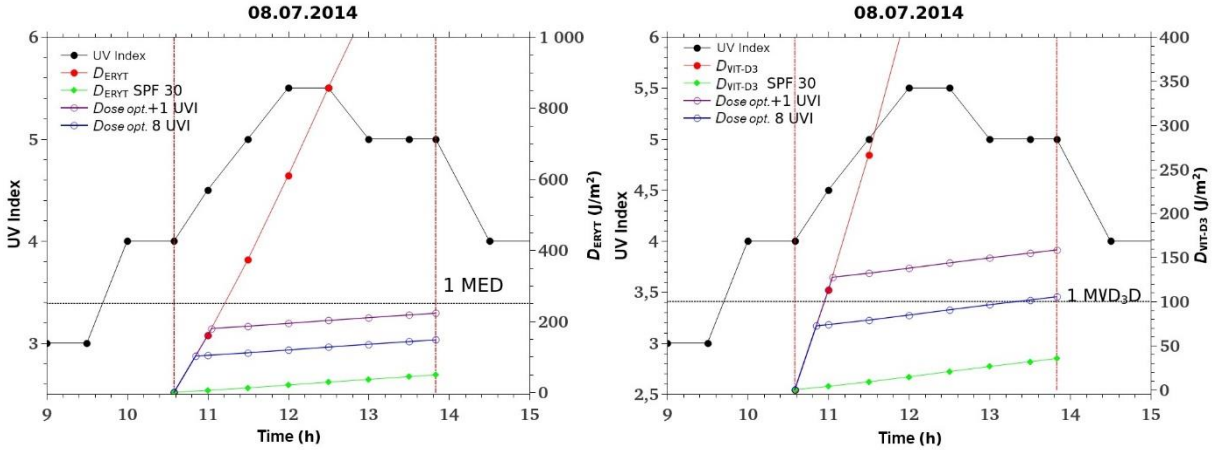

Fig. 65. UV index measured with Silver Crest on 8 July 2014 – solid black line. The blue line indicates the combined dose obtained when applying the scenario without personal meter readings (for a maximum *UVI* = 8). Doses are demonstrated for ERYT (left panel) and VIT-D_3 effects (right panel). Other markings as in Fig. 64.

reading at the moment of arriving at the beach in the morning hours (due to the fact that in the summer, between 9 am and 12 pm, *UVI* increases rapidly). When arriving at the beach around noon, it is assumed that the measured *UVI* represents its later values. In both cases, 5 min is included for the sunscreen's application. For example, on 7 July 2014, the measured *UVI* at the moment of arriving at the beach (at 10:35 pm) was 4 (Fig. 64). Subsequently, 1 *UVI* is added to this value, and finally, 33 min duration of safe sunbathing is determined for phototype II (Fig. 63). On 18 July 2014, when arriving at the beach (at 12:50 pm), the UV index was 6. Hence, 28 min duration of safe tanning is determined.

If personal hand-held meter is not at the disposal, the duration of safe tanning can be determined based on the maximum UV index recorded in central Poland (8 *UVI* at Belsk, July 1996). Hypothetical doses, calculated using Eqs. (15) and (16), are illustrated for 8 July 2014 (Fig. 65). This figure shows the erythemal and vitaminal doses for exposures without the sunscreen, with the use of SPF 30 during the whole stay, and doses according to the aforementioned pro-healthy scenario – short time without photoprotection, next application of SPF 30. The duration of safe tanning is determined for the measured *UVI* + 1 (purple line) or the *UVI* = 8 (blue line). Figure 65 demonstrates that even without knowing the current value of *UVI*, the recommended dose of vitamin D_3 (1000 IU) can be obtained by assuming 21 min of safe tanning (for skin phototype II) for *UVI* = 8 (when going to the beach in the morning and following the previously proposed scenario). Similarly to the previous case, 5 min is reserved for the application of the sunscreen. The duration of exposure, needed to obtain 1 MVD$_3$D, since arriving at the beach, would be approximately 3 hours.

When applying SPF 30 sunscreen before arriving at the beach (as recommended by dermatologists), the required dose of 1 MVD$_3$D will not be obtained, even after several hours. It is calculated that even with the application of SPF 10, MVD$_3$D would not be obtained.

In Poland over 90% of people have vitamin D_3 deficiency (Płudowski et al. 2014). Vitamin D_3 deficiency can result in not only incorrect bone mineralisation, but also muscle pain and atrophy, cardiovascular and autoimmune diseases, and lowering the body's immunity. Moreover, it can adversely affect the nervous system and contribute to the occurrence of depression (Holick and Chen 2008). The presented results indicate that the vitamin D_3 deficiency cannot be filled by sunbathing using the sunscreen with high SPF all the time. Hence, one should sunbath without photoprotection for a short time (~30 min), and then apply sunscreen.

4.4.2 Partly cloudy skies

Figures 66 and 67 present the results of calculations for erythemal and vitaminal doses for 14, 16, and 17 July 2014. The purple line indicates the dose of biologically active UV radiation, corresponding to the scenario of safely (without erythema) reaching 1 MVD_3D (described in the previous chapter).

On these days, partly cloudy skies were observed: on 14 July there was a sudden change of weather after 12:30 pm, on 16 July, the cloud cover was variable with sunny moments, while on 17 July the cloudiness was almost constant throughout the day. The actual time spent on the beach is presented for 14 July. On 16 and 17 July, measurements were conducted only at the first site (the garden near residential house), thus hypothetical duration of sunbathing at the beach is assumed. For 16 July, at 10 am and 11 am, the UV radiation was significantly attenuated by clouds (the meter indicated "0").

Combined doses (allowing to achieve 1 MVD_3D without sunburn) are calculated according to the pro-healthy scenario proposed for the cloudless sky, i.e. after a short time (20–30 min) without photoprotection, the SPF 30 sunscreen is applied (purple line on Figs. 66 and 67). The duration of safe tanning is determined based on the personal meter measurement. The calculation procedure for such doses is presented in Subchapter 4.4.1. For 17 July, two hypothetical beach stay periods were considered, from 9.30 am to 1.10 pm and from 12.00 pm to 3.00 pm. Results for 17 July are presented in Fig. 67.

The pro-healthy tanning scenario, which allows to obtain 1 MVD_3D without sunburn, presented for cloudless sky conditions, also works in the case of cloudy sky, which slightly atten-

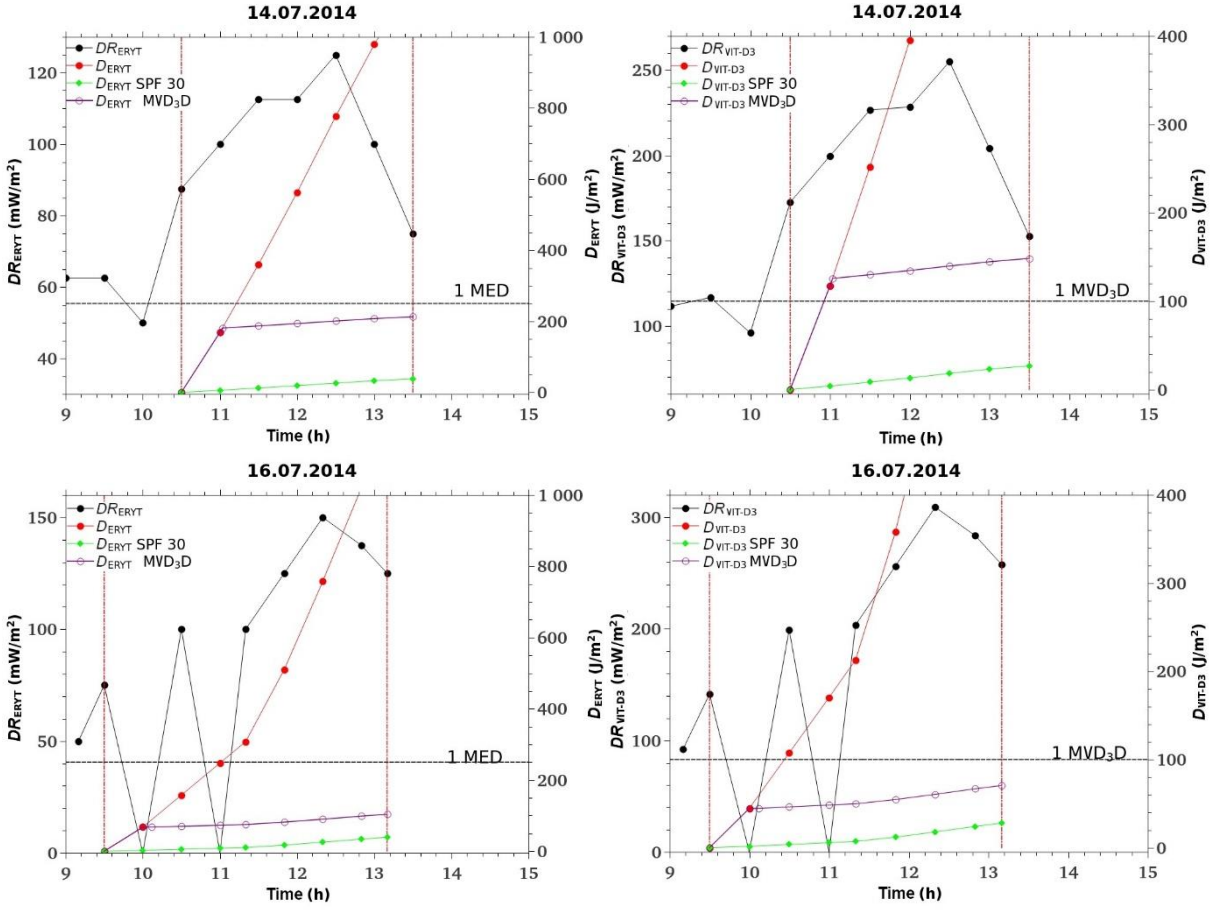

Fig. 66. Dose rates and ERYT (left panels) and VIT-D_3 (right panels) doses on 14 and 16 July 2014. Other markings as in Fig. 64.

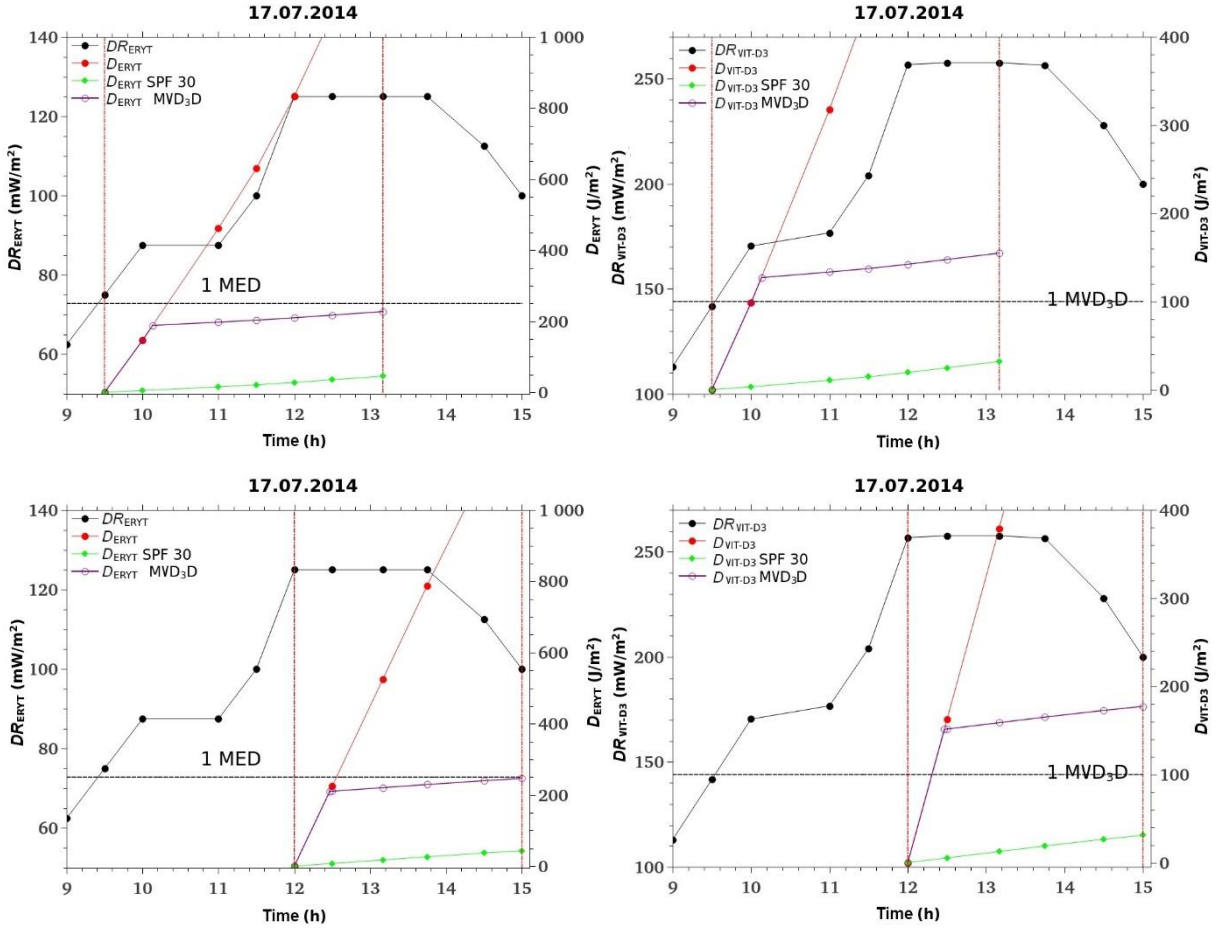

Fig. 67. Dose rates and ERYT (left panels) and VIT-D_3 (right panels) doses on 17 July 2014. Other markings as in Fig. 64.

uates the solar radiation intensity (14 and 17 July). In the case of variable cloudiness with sunny moments (such as 16 July), when the clouds temporarily block the solar radiation (the meter indicates "0"), it would not be possible to obtain 1 MVD_3D using the proposed scenario. Calculation of the exact time needed to obtain 1 MVD_3D without photoprotection, taking into account the low *UVI* due to with heavy clouds, would be impossible during a recreational stay on the beach from a technical point of view (no computer). However, it is assumed that in such situation, staying on the beach would be significantly shortened anyway due to bad weather.

4.4.3 Anti-psoriasis heliotherapy

This subchapter describes whether anti-psoriasis heliotherapy could be conducted by the Baltic Sea in the summer of 2014. For the purpose of heliotherapy it is assumed that the exposure goes over 1 MED, thus the skin must be prepared to high UV intensity. Therefore, it is necessary to carry out initial pre-tanning with increasing UV doses to adapt to high UV doses, the so-called skin photoadaptation. Anti-psoriasis heliotherapy was performed in just a few places, e.g. in Israel by the Dead Sea (Cohen et al. 2008), as well as on the Canary Islands (Nilsen et al. 2009). In both cases, heliotherapy was conducted after one-week photoadaptation of the psoriatic patients.

In an experiment carried out by the Dead Sea, photoadaptation consisted of skin exposure to solar radiation for 15 minutes on the first day, and then in the following days, the duration has been gradually increased up to 3 hours. For people with skin phototype III and IV, the

adaptation time was 5 days, and for people with phototype II, the adaptation time was 6 days. The assumption of the experiment was that patients' exposure should not exceed in total 3 hours per day (divided into morning and afternoon sunbathing), because according to Cohen et al. (2008), a longer stay in the sun could lead to harmful unnecessary effects. In the experiment on the Canary Islands, the process of photoadaptation looked different. On the first day, between 11 am and 1 pm local time, the patient was supposed to expose the front of the body for 30 min, the back for 30 min, and then each side for 15 min in a horizontal position. In the afternoon, patients could stay in the sun using the sunscreen with SPF 25. On the following days, this period has been gradually increased to 3 hours. Some of the exposure took place before noon and some in the afternoon. At this time, the patients were not allowed to use sunscreen, except on parts of the body that are very sensitive to sunburn. After 10 days, the patients could stay in the sun without any restrictions, except for cases of sunburn. In both situations, the photoadaptation process was conducted under medical supervision. In this subchapter, calculations of the duration of anti-psoriatic heliotherapy refer to people after photoadaptation, i.e. those prepared for high erythemal doses.

A heliotherapy scenario is proposed, according to which the patient would stay in the sun without photoprotection until she/he obtains a dose of 1 MAPD = 317.9 J/m^2, i.e. the dose received in a dermatological cabin, while being irradiated the artificial light (TL-01 fluorescent lamp; Krzyścin et al. 2014). Next, the patient should apply a cream with an SPF 30 filter to avoid fourther exposure to the UV radiation. The time needed to get 1 MAPD is determined on the basis of the *UVI* measurements with a personal hand-held meter and the corresponding duration of the tanning taken from Fig. 68. The figure shows the relationship of the duration of the tanning which is needed to obtain 1 MAPD, on the *UVI*. The conversion ratio of the ERYT to AP is calculated according to Table 2A (Appendix), assuming the mean values of SZA = 42.6° and SZA = 33.9° at 9 am – 12 pm and 12 pm – 2 pm local time, respectively, and TO_3 = 330 DU (mean value from 7–22 July 2014).

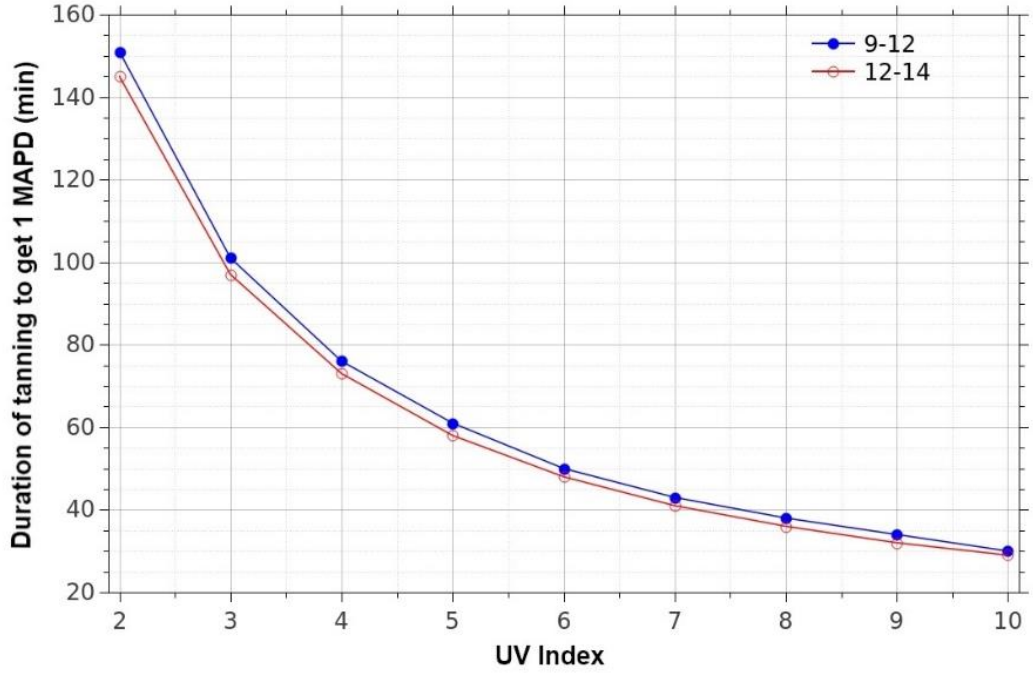

Fig. 68. Duration of tanning to get 1 MAPD by the Baltic Sea (by a person with skin phototype II) as a function of the UV index. The blue line refers to the doses achievable between 9 am – 12 pm, the red line refers to 12 pm – 2 pm, TO_3 = 330 DU.

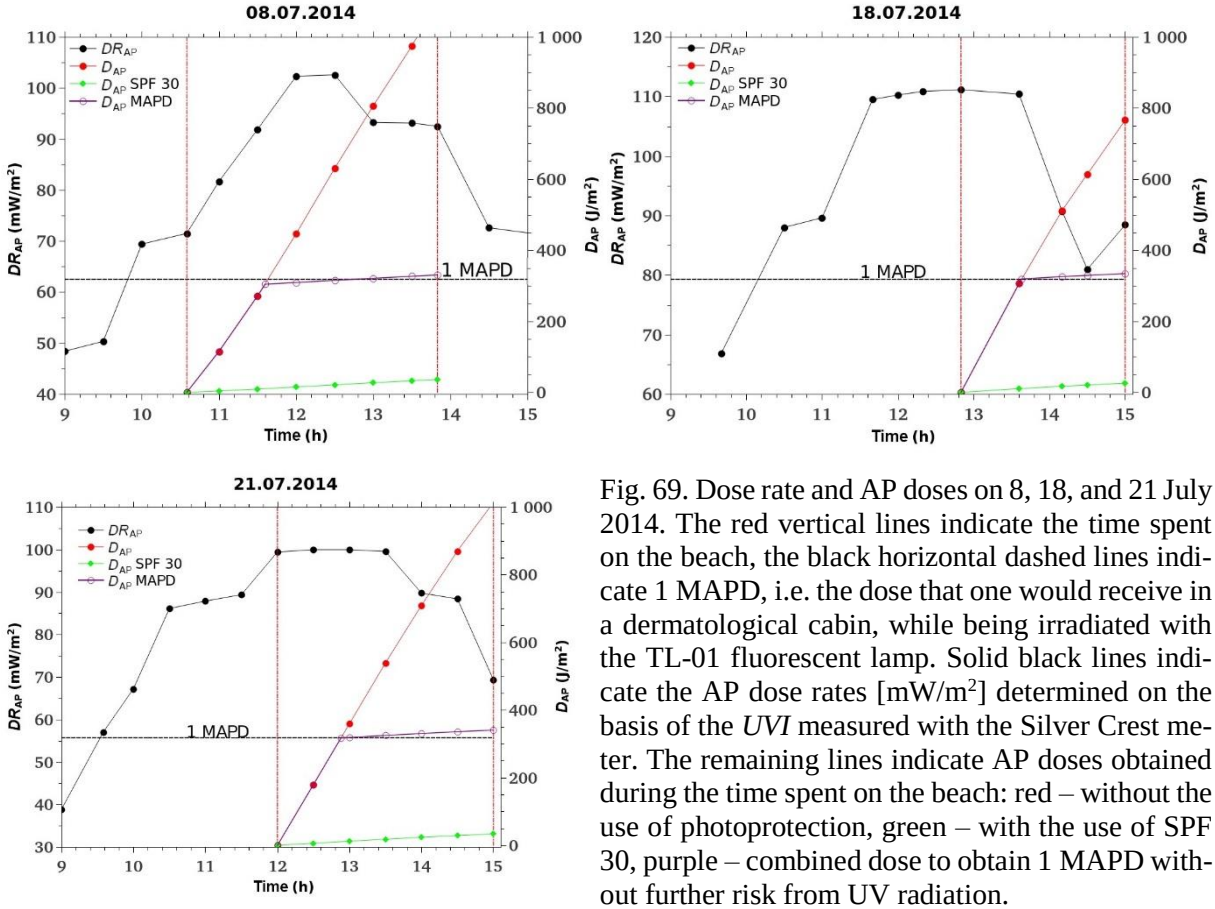

Fig. 69. Dose rate and AP doses on 8, 18, and 21 July 2014. The red vertical lines indicate the time spent on the beach, the black horizontal dashed lines indicate 1 MAPD, i.e. the dose that one would receive in a dermatological cabin, while being irradiated with the TL-01 fluorescent lamp. Solid black lines indicate the AP dose rates [mW/m^2] determined on the basis of the *UVI* measured with the Silver Crest meter. The remaining lines indicate AP doses obtained during the time spent on the beach: red – without the use of photoprotection, green – with the use of SPF 30, purple – combined dose to obtain 1 MAPD without further risk from UV radiation.

Figure 69 demonstrates the anti-psoriatic doses (purple line) calculated for 8, 18, and 21 July 2014 based on the following scenario. At the moment of arriving at the beach before noon, the personal meter reading is increased by 1 *UVI*. Thus, for 8 July, based on Fig. 68, 60 min of tanning to get 1 MAPD is determined (blue line). For 18 and 21 July (going to the beach in the afternoon), the duration of tanning time to get 1 MAPD is determined on the basis of the first measured *UVI*, i.e. for 18 July the measured *UVI* at the moment of arriving at the beach was 6, thus the duration of tanning to gain 1 MAPD is 43 min (red line on Fig. 68).

Analysis of Fig. 69 reveals that the duration of tanning to get 1 MAPD was correctly determined using Fig. 68 and aforementioned heliotherapy scenario. The results indicate that anti-psoriatic heliotherapy is possible by the Baltic Sea in the summer.

When conducting anti-psoriatic heliotherapy by the Baltic Sea during a stay on the beach, even in the case of cloudy skies, it is possible to achieve 1 MAPD (Fig. 70). As a result of attenuation of the radiation due to clouds, according to our estimates, the time needed to reach the dose of 1 MAPD may be approximately 3 hours. The scenario of self-controled heliotherapy would only work for 17 July 2014 and partly for 14 July 2014, when the obtained dose was ~1 MAPD. For 16 July, the dose would be much smaller than 1 MAPD. When conducting professional anti-psoriasis heliotherapy, a qualified person who continuously monitors the ultraviolet radiation is required. Measurements with the personal meter on days with variable cloudiness are insufficient to precisely determine the exposure duration to get the dose equal to 1 MAPD. It is possible to create a scenario, involving entering the measured *UVI* into a smartphone and summing up the irradiation doses obtained in the periods between the *UVI* measurements by an appropriate application (created for the needs of heliotherapy). Then, during the stay on the beach, in variable cloudiness, the duration of tanning to get 1 MAPD could be precisely determined.

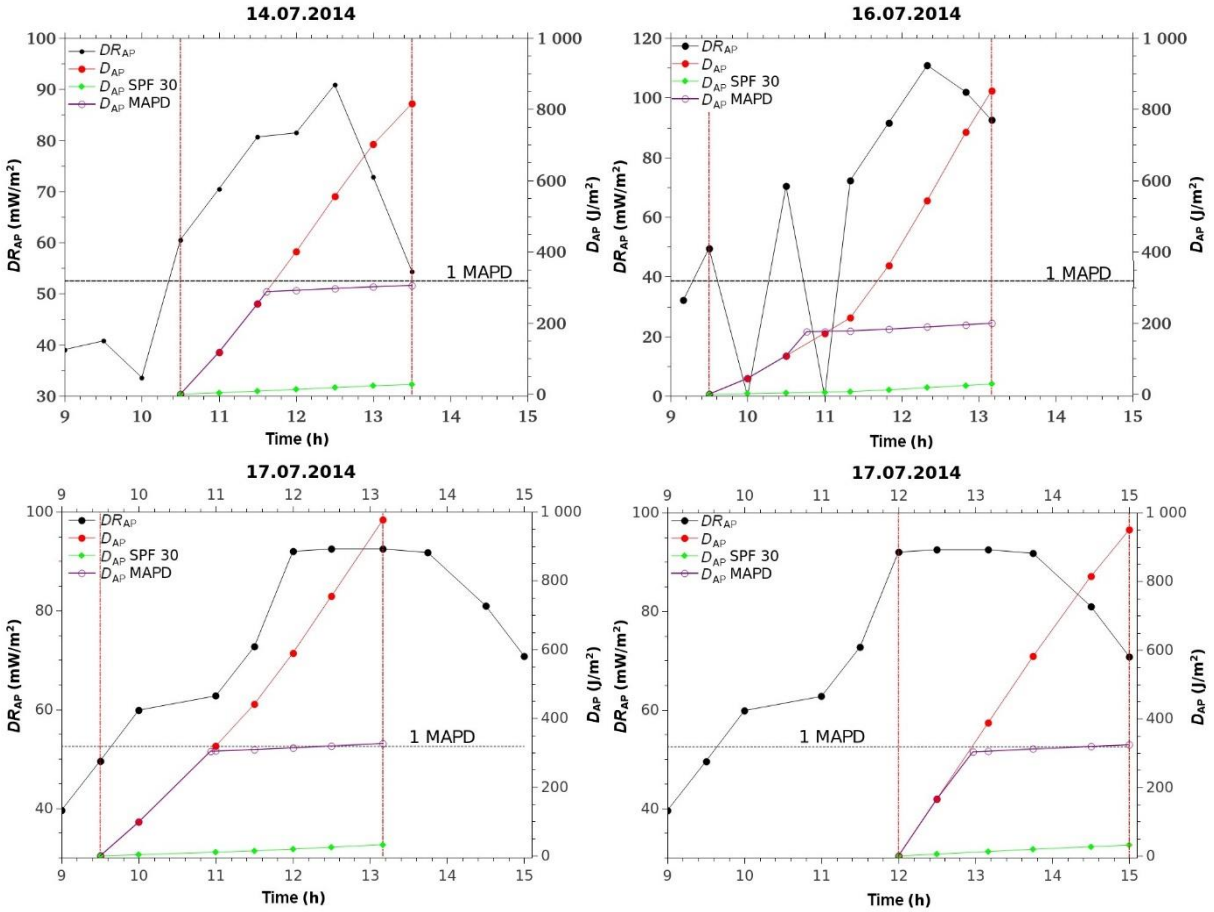

Fig. 70. Dose rate and AP doses on 14, 16, and 17 July 2014. Other markings as in Fig. 69.

4.5 Summary

In summary, it can be concluded that:

- when the sky is cloudless, the results of the *UVI* measurements obtained using low-cost hand-held personal meters are consistent with the modelled values of *UVI* obtained from the radiative transfer model;
- in cloudy skies conditions, personal meters can be used to assess in-situ the conditions for pro-healthy tanning;
- when using the SPF 30 sunscreen during the entire sun exposure, it is not possible to reach a VIT-D_3 dose corresponding to the required vitamin D daily dose taken orally;
- anti-psoriasis heliotherapy could be conducted by the Baltic Sea coast in the summer.

A pro-healthy scenario is proposed to safely obtain a vitamin D dose from the skin synthesis, which is equal to 1000 IU vitamin D_3 taken orally (recommended dose). For this purpose, photoprotection should not be used for a short period (20–30 min), afterwards a cream with SPF 30 should be applied. The time without photoprotection for a selected skin phototype can be determined on the basis of the *UVI* measured with the personal meter and a diagram (Fig. 63). When staying on the beach in the morning, the increase in the observed UV index should be taken into consideration, and 1 should be added to the *UVI* value. Without any measurements, *UVI* = 8 (maximum value, recorded in CGO at Belsk in 1993–2014) can be assumed for the calculations. However, by measuring *UVI*, the optimal scenario of obtaining the adequate dose of vitamin D_3 can be determined. Some types of personal meters show the duration of safe tanning after imputing skin phototype data into the device. A sound signal informs us about exceeding the safe tanning duration.

During a stay on the beach, even on a cloudy day, anti-psoriatic heliotherapy can be carried out, as it is possible to achieve 1 MAPD in 2–3 hours. The duration of heliotherapy needed to achieve the 1 MAPD = 317.9 J/m^2 (i.e. the standard dose that a patient would receive in a dermatological cabin, being irradiated by the TL-01 fluorescent lamp) can be determined using the *UVI* measurements and the diagram presented in Fig. 68. In the future, it is possible to introduce a smartphone application that would significantly simplify the conducting of anti-psoriatic heliotherapy.

5. THE IMPACT OF A CITY ON THE BIOLOGICALLY ACTIVE SOLAR RADIATION REACHING THE EARTH'S SURFACE

The atmosphere over Poland is one of the most polluted by dust in Europe. This is particularly true for industrial regions such as Silesia, Cracow, but also Warsaw, where the dust concentration in the air with a diameter smaller than 10 and 2.5 μm (PM10 and PM2.5) is exceeded repeatedly during the year (WIOŚ 2015) according to the Regulation from the 24 August 2012 by the Minister of the Environment considering the levels of selected substances in the air (Ministerstwo Środowiska 2012). This chapter presents to what extent the Warsaw urban agglomeration influences ultraviolet radiation with erythemal efficacy reaching the Earth's surface. The difference in UV radiation level between Warsaw and the less polluted rural area, Belsk, is determined on the basis of the measurement data obtained from the Brewer spectrophotometers operating simultaneously in these sites. This will allow to assess whether the conditions in Warsaw are adequate for conducting heliotherapy and the synthesis of vitamin D_3 in human skin.

Zawadzka et al. (2013) confirmed on the basis of observations using simple spectrophotometers such as Microtops II and a CIMEL Electronique 318A solar photometer (installed in CGO Belsk) that the difference in the atmospheric optical depth (AOD) for the wavelength of 500 nm between Belsk and Warsaw was ≤ 2% (up to 4% at higher wind speeds). This difference was ~5% in relation to the satellite observations from the MODIS spectroradiometer on the Aqua and Terra satellite platforms. The authors did not demonstrate a significant difference in the value of the Angstrom coefficient for aerosols present in the considered sites.

Studies on the effects of atmospheric aerosol on the ultraviolet solar radiation have been previously conducted by Papayannis et al. (1998). Measurements taken in the suburbs and the centre of Athens, where a higher concentration of the atmospheric aerosols was observed, were analysed. However, the measurements were not carried out at the same time. The group found that for similar total ozone and for greater AOD, erythemal UV in the centre of Athens was approx. 30% smaller. Similar changes in the strength of the UV radiation were found on the basis of numerical simulations of the intensity of UV-B, using AOD and TO_3 measurements in the suburbs of Athens. Papayannis et al. (1998) concluded that differences in AOD in these locations lead to an increase in UV level in the suburbs.

Similar observations were made in Mexico from September 1994 to 1995 (Acosta and Evans 2000) in the city centre and in the suburbs. During winter, the intensity of erythemal UV radiation was 9% higher in the suburbs than in the city, while in the summer this difference reached 43% (on average 21% in the period considered). Considering the scale of dust pollution observed in Mexico and the specific location of the city, a similar attenuation of UV radiation in Polish cities cannot be expected.

The Institute of Geophysics of the Polish Academy of Sciences has two Brewer spectrophotometers. Brewer 064 has been operating at the CGO Belsk since 1992, while Brewer 207 has been operating on the roof of the IG PAS main building in Warsaw since 2013. Using measurements from the Brewer spectrophotometers in 2013–2014, the comparison of the erythemal UV radiation in Warsaw and at the CGO Belsk is shown in this chapter. Calculations are made for cloudless sky and for all-sky conditions. Previously, to assess the difference associated with

technical parameters of the spectrophotometers, the results of the UV measurements from the period 2010–2013 (when the instruments worked simultaneously at Belsk) are compared. The Brewer 064 spectrophotometer (operating at the CGO at Belsk) is an older generation Mark II type instrument, which is equipped with a single monochromator. The accuracy of the measurements using this type of instrument decreases with increasing proportion of the scattered radiation in total radiation, i.e. in case of large AOD and SZA. In addition, the instrument is not equipped with a ventilation system. Brewer 064 output is in the spectral range from 290 to 325 nm. The Brewer 207 spectrophotometer, Mark III, is a newer generation instrument type. It is equipped with a double monochromator, which significantly reduces the measurement error associated with the instrument's straylight. Moreover, Brewer 207 is also equipped with a ventilation system, which protects the instrument from the overheating on hot days. Mark III spectral range is 290–365 nm. Both instruments are regularly calibrated using a set of calibration lamps. The UV radiation measurement accuracy for both instruments is approx. 5% (Jarosławski 2015). Reconstruction of the UV spectrum in the spectral range up to 400 nm is performed using the SHICRivm method. The SHICRivm method of reconstructing Brewer spectra to the full UV range (290–400 nm) was proposed by Slaper et al. (1995) and Slaper (2002). For selected days for which the total ozone measurements were available, numerical simulation results are also presented to estimate the geographical location influence on the Warsaw–Belsk's UV difference.

5.1 Comparison of the instruments

The Brewer spectrophotometers, used to monitor UV radiation, located on the roof of the Institute of Geophysics of the Polish Academy of Sciences main building in Warsaw and at the CGO Belsk (Fig. 71), have been operating simultaneously at these locations since 2013. In the years 2010–2013, both instruments were installed at Belsk. For this period, the values of UV dose rate with erythemal efficacy DR_{ERYT} (t) are calculated according to Eq. (1) from Chapter 2. Then, the near-noon doses are calculated for a period of ±3 hours from the solar noon (t_{NOON}), determined according to astronomical formulas for a given day of the year. D_{ERYT} (t_1,t_2) values are determined according to Eq. (5), where instead of the sunrise and sunset hours, $t_1 = t_{NOON} - 3$ h and $t_2 = t_{NOON} + 3$ h are inserted, respectively. The values of $DR_{ERYT}(t_1)$ and $DR_{ERYT}(t_2)$ in the absence of measurements are interpolated from the nearest observations. The doses are cal-

Fig. 71. Brewer 064 spectrophotometer – left and Brewer 207 – right (photo by Izabela Pawlak and the author).

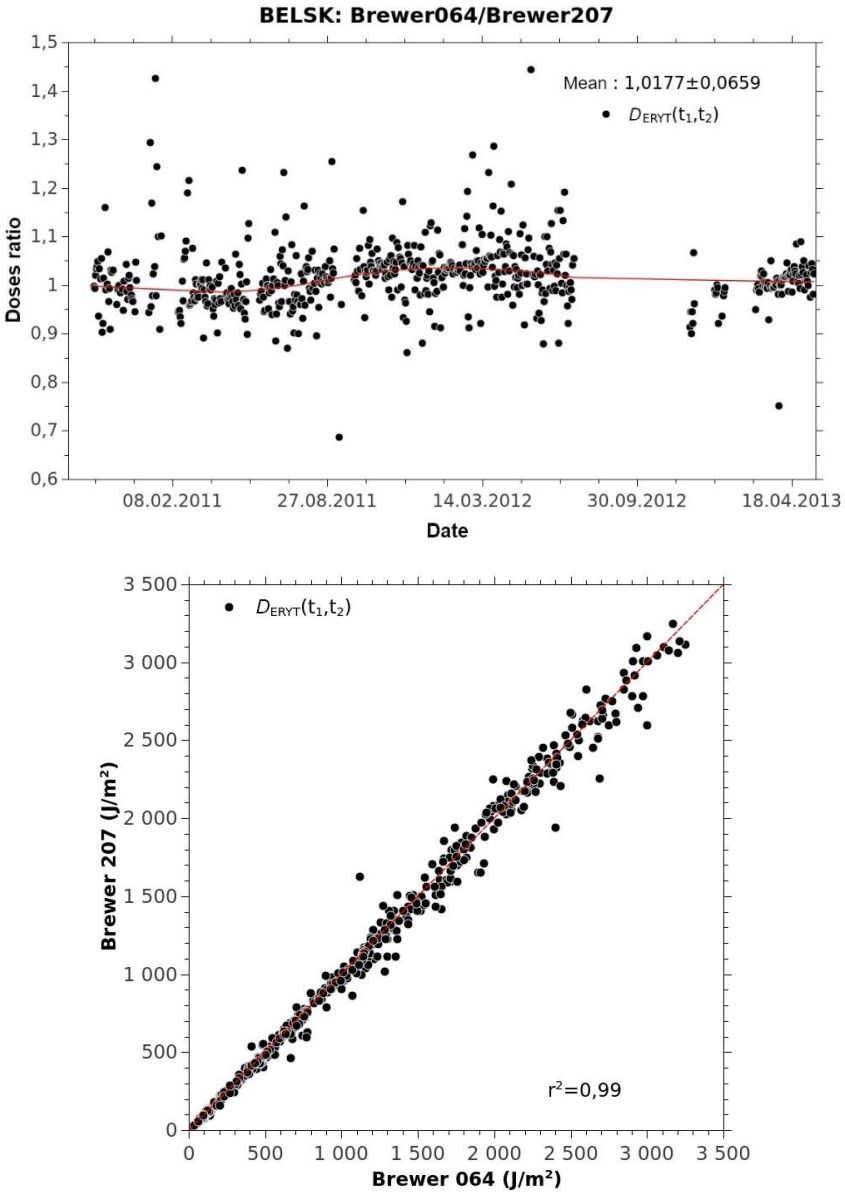

Fig. 72. Comparison of near-noon doses of the erythemal radiation measured by the Brewer spectrophotometers no. 064 and 207 in all-sky conditions. The solid red line indicates a curve smoothed using the lowess function.

culated for all-sky and separately for cloudless conditions. The cloudless days are identified according to the following algorithm: by the time of solar noon, when the radiation is strongest, each subsequent measurement should be higher than the previous one. Further, after the solar noon, the criterion that each subsequent measurement is lower than the previous one was employed. Using this approach, the situations when the sky was partly cloudy or overcasted during the measurement are eliminated.

Figure 72 presents a comparison of daily doses for all-sky conditions when both instruments operated at Belsk. The figure shows that the near-noon doses measured at Belsk by both instruments were practically the same. The coefficient of determination is 0.99 and the mean difference between the measurements obtained from Brewer 064 and Brewer 207 for all-sky conditions is approx. 2%, with the coefficient of variation not exceeding 7%. Larger differences between doses (above 2%) are due to the fact that measurements were not always taken simultaneously, and therefore the effect of variable cloudiness should be taken into account.

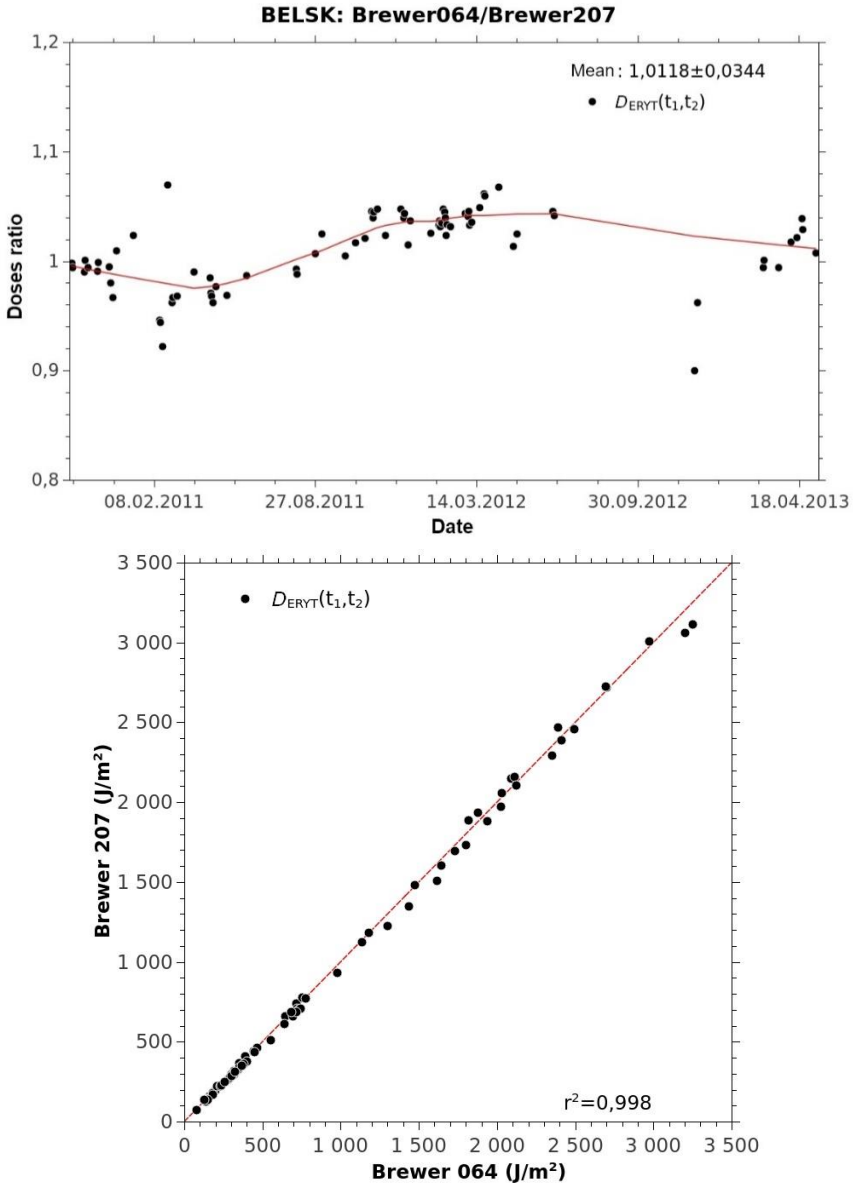

Fig. 73. Markings as in Fig. 72 but doses are for cloudless conditions.

Figure 73 presents a comparison of near-noon doses for cloudless days. The agreement between erythemal doses from both instruments is even better when the sky is cloudless. The coefficient of determination is 0.998 and the mean difference between the measurements obtained using Brewer 064 and Brewer 207 is approx. 1%, with the coefficient of variation not exceeding 3.5%.

Figure 73 (top) shows (smoothed curve) that in the colder period, Brewer 064 indicates higher values than Brewer 207. The opposite situation is observed in the warm period of the year. For the Brewer spectrophotometers, the temperature effect has been set. An increase in temperature inside the device by 4°C relative to the reference temperature (20°C) results in a decrease in the instrument by 1%, which means that the measured UV radiation values are lower than in reality. When comparing Mark II and Mark III type Brewer spectrophotometers, it is necessary to consider the significant temperature difference inside the instruments, resulting from the ventilation system and forced air circulation in the Mark III device (Jarosławski

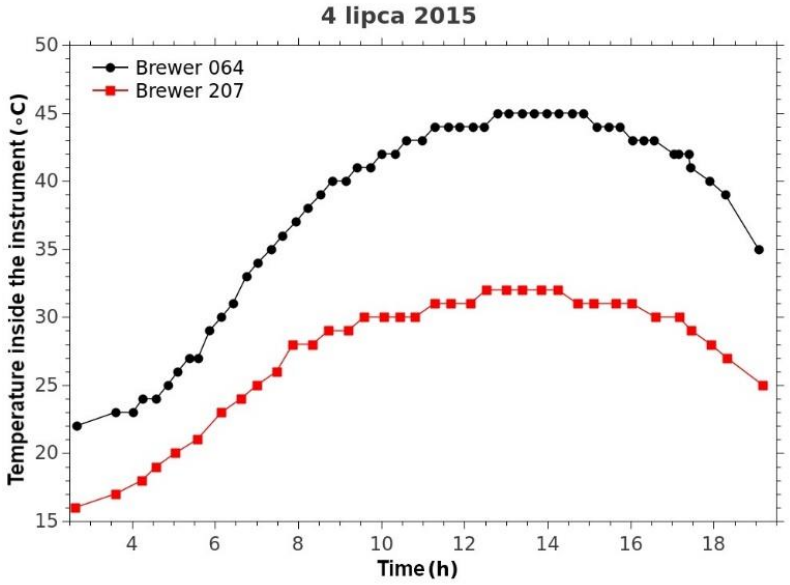

Fig. 74. The temperature difference inside Brewer 064 (black line) and Brewer 207 (red line) spectrophotometers.

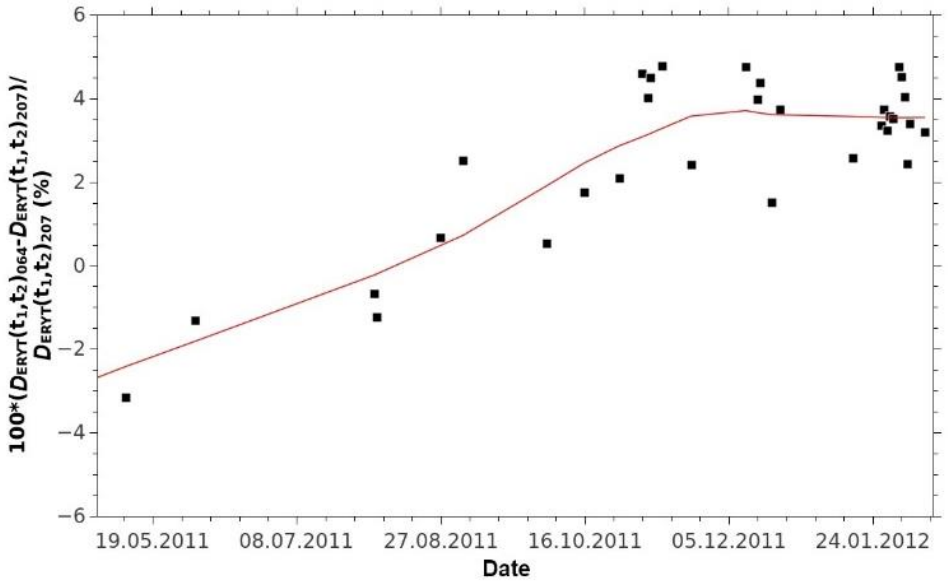

Fig. 75. The daily dose percentage deviations between Brewer 064 and Brewer 207 spectrophotometers on the dates indicated. The solid red line indicates a curve smoothed using the lowess function.

2015). During a hot day, the inside temperature difference between the instruments can be ~13°C.

Figure 74 shows the temperature inside Brewer 064 and 207 spectrophotometers for 4 July 2015, when the air temperature was above 30°C.

In this case, observations from one instrument in relation to the other differed by approx. 3% due to the strong heating of the Brewer 064 spectrophotometer.

The thermal effect is the cause of seasonal differences in the readings of both spectrophotometers observed in the spring/summer 2011 – winter 2011/2012 period (Fig. 73). For this period, Fig. 75 presents the time series of the instruments' relative differences [%]. The difference between the measurements is larger by approx. 5% in the winter comparing to the summer one.

The accuracy of the measurement depends not only on the temperature inside the instrument, but also on the individual characteristics, e.g. the geometry of optical parts. For the Brewer spectrophotometers, a decrease in the measurement accuracy is also observed with the increase of SZA. However, this decrease is an individual characteristic of each instrument.

Based on the presented comparison of the measurements at Belsk, after eliminating the cloud factors and temperature effect (it does not occur in the winter, because both instruments are heated to a temperature of ~10°C), it can be concluded that in the winter Brewer 064, indicates on average 3% higher values than Brewer 207. In the summer, Brewer 207 indicates more erythemal UV radiation (2%), which is a consequence of the lack of air circulation inside the Mark II spectrophotometer. Averaging the measurements of both instruments in the whole period considered, Brewer 064 indicates values by 1% higher than Brewer 207 in cloudless conditions (Fig. 73).

5.2 Comparison of the modelled values – the impact of geographical location

Numerical simulations are carried out for the days on which both spectrophotometers operated simultaneously in Warsaw and Belsk. The simulations are conducted using the FastRT model, which was also used for the calculations presented in Chapter 4. The geographical location,

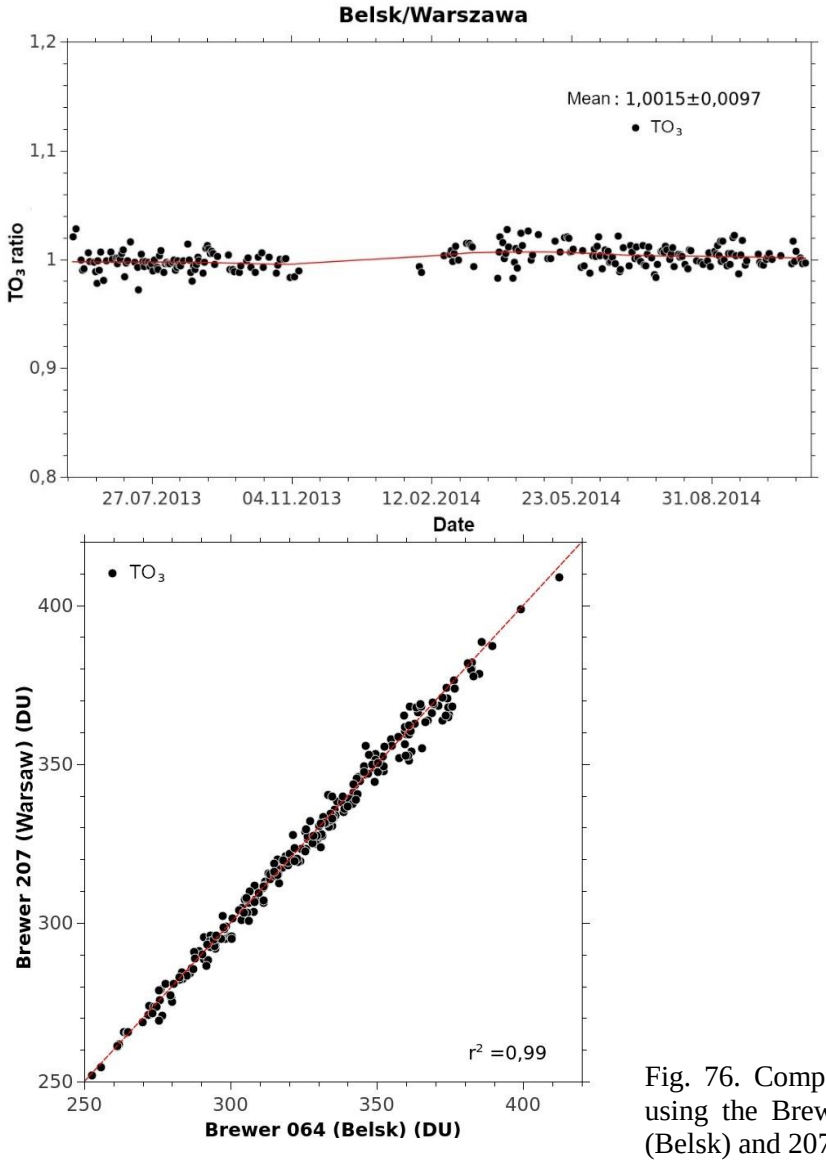

Fig. 76. Comparison of total ozone measured using the Brewer spectrophotometers no. 064 (Belsk) and 207 (Warsaw).

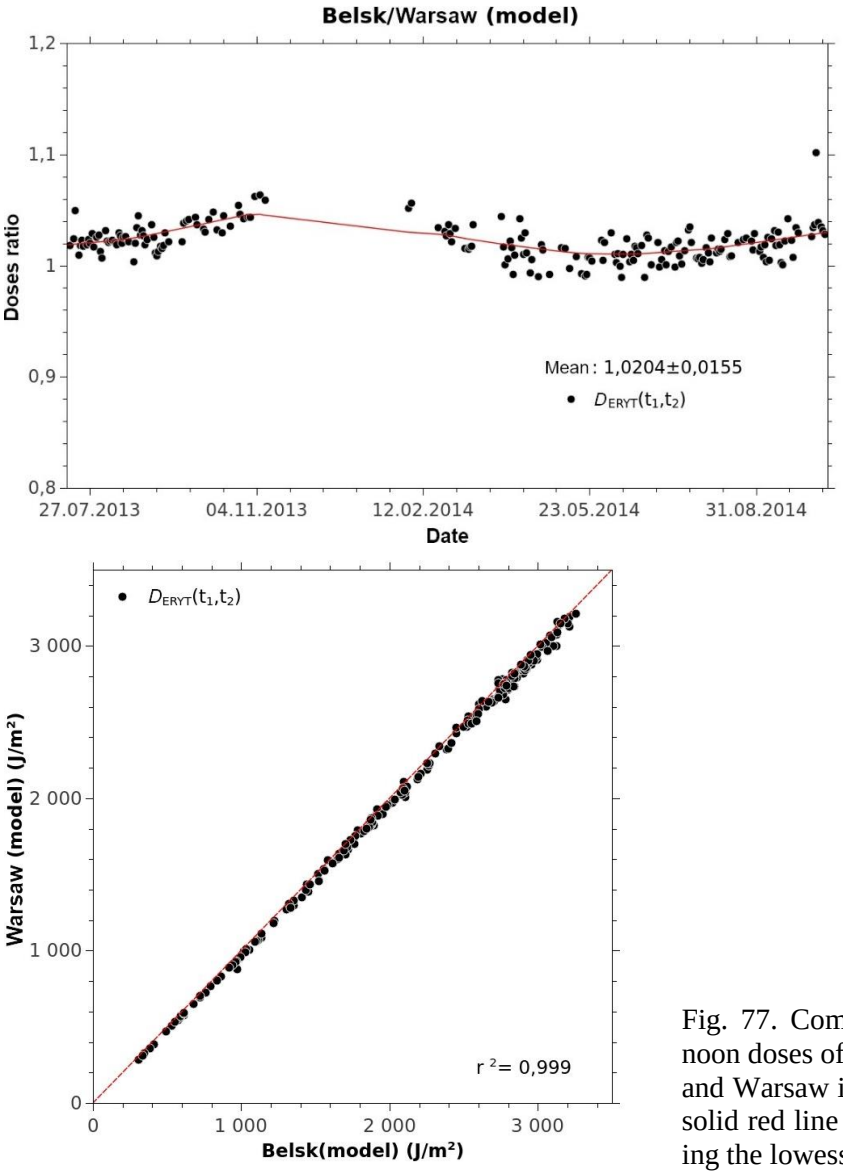

Fig. 77. Comparison of the modelled near-noon doses of erythemal irradiation for Belsk and Warsaw in the cloudless conditions. The solid red line indicates a curve smoothed using the lowess function.

TO_3, and the value of the β parameter referring to the aerosol content in the atmosphere were included into the model input. The value of the β parameter is constant (for both locations) and is 0.09 (which is the mean value obtained from the AERONET network for Belsk from the period of simultaneous Brewer measurements). The mean daily total ozone for individual days was obtained from Brewers' TO_3 measurements using the direct sun method (DirectSun). For calculating the daily mean, values were taken from hours when the optical mass μ did not exceed 3. A comparison of the daily values of TO_3 is demonstrated in Fig. 76. Calculations reveal that the total ozone was approximately the same at Belsk and in Warsaw. Thus, it can be concluded that for the comparison of the near-noon erythemal doses between these locations, the differences in total ozone are of secondary importance.

Subsequently, the influence of the geographical location of Warsaw (52.25°N) and Belsk (51.84°N) on the differences between the erythemal doses is assessed. Figure 77 presents a comparison of modelled values of the near-noon erythemal doses for Belsk and Warsaw, determined on the basis of the measured TO_3 values.

Figure 77 indicates that the mean ratio between the near-noon doses determined from the cloudless sky model, when the total ozone used in the model is obtained from observations, is around 1. The coefficient of determination is 0.999 and the mean modelled value difference

between Belsk and Warsaw for a cloudless sky is 2%, with the coefficient of variation not exceeding 1.5%. Based on the presented comparison of the modelled erythemal doses, it can be concluded that the combined differences due to the geographical location and TO_3 cause that the doses at Belsk are higher by approx. 2%.

5.3 Comparison of erythemal doses of UV radiation measured at Belsk and Warsaw

For the days when both instruments worked simultaneously at Belsk and Warsaw, the near-noon erythemal doses are calculated according to the method described in Chapter 4. These values are subsequently compared for all-sky conditions (Fig. 78). Calculations show that the level of UV radiation at Belsk for all-sky conditions is approx. 6% higher than in Warsaw, with the coefficient of variation of approx. 17%. The coefficient of determination is 0.96.

Subsequently, the mean ratio of the near-noon doses, calculated on the basis of measurements by the Brewer 064 and 207 spectrophotometers at Belsk, is compared with the mean ratio of doses, when both instruments were in different locations. For this purpose, a statistical test is carried out to determine if two population means are equal for a random distribution of samples (Balicki and Makać 2004). The test statistics are calculated according to Eq. (17):

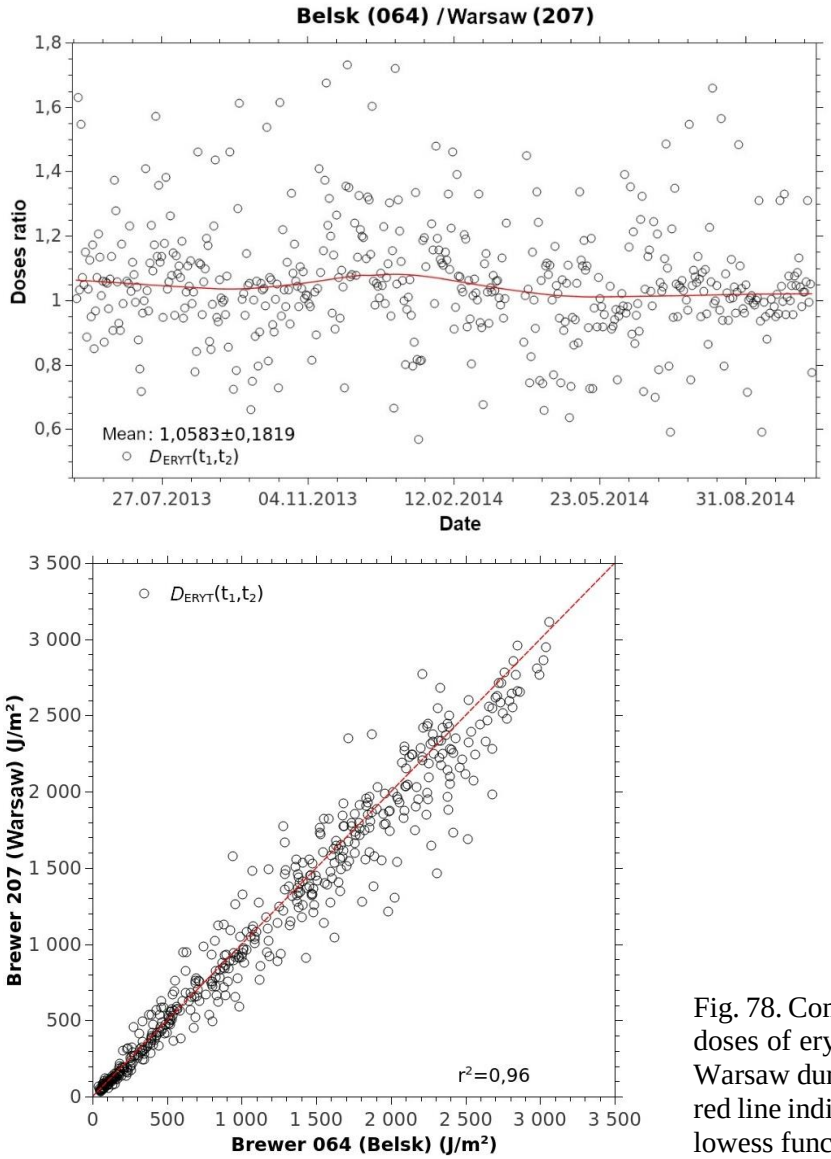

Fig. 78. Comparison of the measured midday doses of erythemal irradiation for Belsk and Warsaw during all-sky conditions. The solid red line indicates a curve smoothed using the lowess function.

$$Z = \frac{\overline{X_1} - \overline{X_2}}{\sqrt{\frac{S_1^2}{n_1} \frac{S_2^2}{n_2}}}, \tag{17}$$

where X_1 and X_2 are the means from the samples, S_1 and S_2 are corresponding standard deviations, and n_1 and n_2 are the sample sizes.

The critical value ($Z_\alpha = 1.96$) is read from the standardised normal distribution table and for the significance level $\alpha = 0.05$. The null hypothesis is that these means are equal, while the alternative hypothesis is that the means are significantly different. The alternative hypothesis is confirmed by satisfying the following inequality: $|Z| > Z_\alpha$. Statistic $Z = -4.63$ is calculated for the mean dose ratio from the Belsk intercomparison, 1.0177 ±0.0659 and the mean dose ratio between Belsk and Warsaw is 1.0583 ±0.1819. Therefore, an alternative hypothesis with a significant difference in the means can be confirmed. Based on the analysis of the mean dose ratios, it can be concluded that higher near-noon doses at Belsk are not only a consequence of technical differences.

Figure 79 shows a comparison of the near-noon erythemal doses for cloudless sky conditions. After eliminating cloudy days, the standard deviation between the measured values at

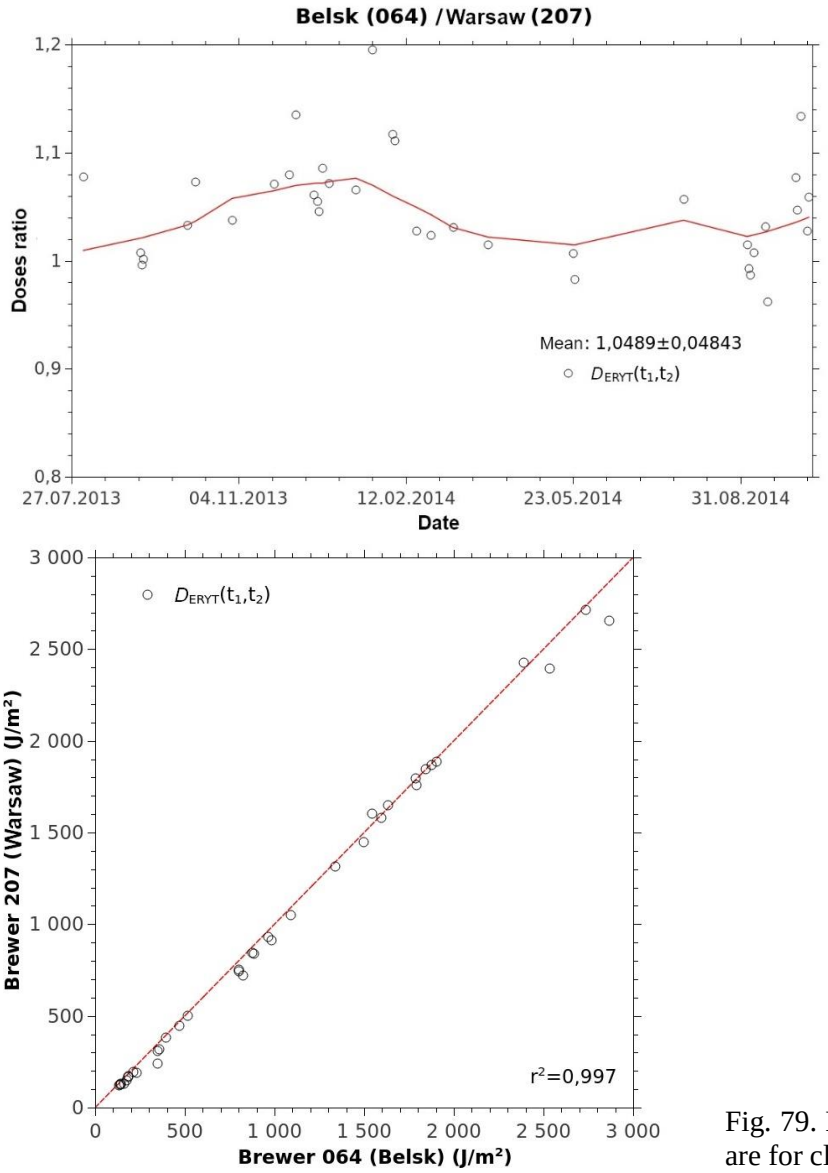

Fig. 79. Markings as in Fig. 78 but doses are for cloudless conditions.

Belsk and Warsaw is significantly reduced. The coefficient of determination amounts to 0.997. The dose difference between Belsk and Warsaw amounts to 5% with the coefficient of variation not exceeding 5%. The coefficient of variation for a cloudless sky is considerably lower than the one determined for all-sky conditions. A similar relationship was also observed when comparing the measurements from the instruments situated in the same site.

For the cloudless sky, as in the case of the measurements for all-sky conditions, a statistical test of the similarity of the mean dose ratios between the instruments is carried out for the period when both Brewers were located at Belsk and when they were operated at Belsk and in Warsaw, respectively. Statistic $Z = -4.19$ was calculated for the mean dose ratio from Belsk = 1.0118 ± 0.0344 and the mean dose ratio between Belsk and Warsaw = 1.0489 ± 0.0484. Thus, also in this case, the alternative hypothesis with a significant difference between the means can be confirmed. After eliminating the cloudy days, it can be concluded that in addition to technical parameters of the instruments, there are other factors which could affect the difference between near-noon doses measured at Belsk and in Warsaw.

5.4 Summary

When comparing the near-noon erythemal doses between Belsk and Warsaw, atmospheric conditions, geographical location as well as technical parameters of the instruments should be taken into account. The mean difference between the instruments does not exceed 5%, for a cloudless sky, while this difference is over 1% when the instruments operated simultaneously at Belsk. Model calculations demonstrated that the mean difference reaches ~2% due to geographical location. Therefore, it can be concluded that the effect of a specific urban aerosol on biologically active ultraviolet radiation in the case of Warsaw is minor (~2%) and comparable to the difference resulting from the geographical location.

For measurements performed during all-sky conditions, the mean difference of the near-noon erythemal doses between the two stations is 1% higher than for the cloudless sky, with a simultaneous increase in the coefficient of variation, which is a result of variability of the local cloudiness.

Haberlie et al. (2015) demonstrated on the example of Atlanta that a metropolitan area can generate the formation of additional convection centres and, thus, increased cloudiness compared to the area outside the city. Nonetheless, by averaging the results of measurements carried out at Belsk and in Warsaw during all-sky conditions, it can be concluded that Warsaw does not generate specific clouds affecting UV radiation. Thus, carrying out pro-healthy heliotherapy is also possible in Warsaw and it is just as effective as in the sites located near Warsaw.

6. SUMMARY OF THE RESULTS

The subject of the study was undertaken as a result of the on-going global debate on balancing the beneficial and harmful effects of solar ultraviolet radiation on the human health. This is crucial because of the growing interest in the level of vitamin D_3 in the body, which largely depends on UV-B irradiation of the skin (Norval and Wulf 2009). Currently, it is proved that 90% of Poles suffer from deficiencies of this vitamin (Płudowski et al. 2014). The exceptions are the groups with the greatest attention of doctors, i.e. newborns and pregnant women. It is widely believed that one of the reasons of vitamin D_3 deficiency is a growing social campaign against skin cancer, recommending to avoid solar radiation during midday hours, as well as to use sunscreen with a high SPF value 15 minutes before going outdoor (Janda et al. 2007; Baggerly et al. 2015). Baggerly et al. (2015) quotes the results of mortality statistics among the United States population. According to them, only by increasing the level of vitamin D_3 in the body, the number of people dying would decrease by 336 thousand a year (out of 2 million dead

from diseases associated with the deficit of this vitamin), while among 5 million people suffering from skin cancer, 13 thousand die every year. It is estimated that on the list of the 30 causes of death in the United States in 2010, 19 were associated with vitamin D_3 deficiency.

Some skin diseases, e.g. psoriasis or albinism are treated with UV-B rays from artificial sources. Similar therapy can be employed utilising solar radiation. The theoretical foundations for conducting anti-psoriatic heliotherapy in Poland were determined by Krzyścin et al. (2014). In practice, anti-psoriatic heliotherapy has been used for a long time in selected treatment centres. The radiation doses received during solar heliotherapy in the Canary Islands and at the Dead Sea are higher than the doses causing erythema and much higher than those needed to produce the adequate level of vitamin D_3. However, based on research and many years of observations of patients participating in anti-psoriatic heliotherapy, no increasing incidence of skin cancer was noted among them (Larko and Swanbeck 1982; Kushelevsky et al. 1998).

This study presents pro-healthy scenarios for balancing the health-promoting and harmful effects of UV radiation during controlled exposure to sun radiation in order to limit its harmful effects (destruction of the DNA structure, erythema) and to achieve maximum benefits, such as an increase of vitamin D_3 levels in the body or treatment of psoriatic lesions. The need to introduce actions in this area, as well as to find optimal scenario that enables the simultaneous assessment of risks and benefits of UV exposures are indicated in the literature (Springbett et al. 2010; Baggerly et al. 2015).

The paper determines a method for converting erythema radiation from, e.g. broadband biometers commonly used at meteorological stations or low-cost hand-held personal UV index meters, to other biologically active radiation used to describe, for example: the destruction of DNA structures, skin synthesis of vitamin D_3, and removal of psoriatic lesions.

In Chapter 2, a procedure allowing the conversion of erythemal doses into doses of different biological efficacy is developed. The procedure is created based on many years of measurements using the Brewer spectrophotometer at Belsk. Tables of ratios between the DNA-damaging, anti-psoriatic and vitaminal irradiation and the intensity of erythemal irradiation (Tables 1A–3A in the Appendix) are determined. Similar tables for vitaminal irradiation can be found in the literature. However, those are based on model values rather than measured ones (McKenzie et al. 2009). Until now there was no conversion procedure for intensities with anti-psoriatic efficacy. In addition, tables of daily dose quotients (Tables 7A–9A in the Appendix) are also developed.

Monitoring of the intensity of UV irradiation has been carried out around the world for many years. At the beginning of the 1970s, a Robertson–Berger meter was constructed to measure the intensity of erythemal ultraviolet radiation. It was a precursor of currently widely used broadband meters, e.g. SL501 or Kipp and Zonen UVS-E-T. Irradiation for other biological processes could only be determined from spectral measurements using expensive instruments, for example a Brewer or Bentham spectrophotometer. Because of the associated costs, such UV spectrophotometers are not suitable for setting a dense measuring network. Hence, it was not possible to assess the conditions for conducting heliotherapy anywhere in Poland, except for places where such spectrophotometers were installed (Belsk, Warsaw). Thanks to the proposed method, personal pro-healthy tanning can be carried out in order to improve the health status.

Using the procedure described in Chapter 2 and having the series of measured doses of erythemal irradiation from 1976–2014 at Belsk, non-erythemal daily doses are reconstructed (Chapter 3). Subsequently, UV radiation trends are calculated for erythemal, vitaminal, anti-psoriatic and DNA destruction efficacy. It is observed that in 2005 there was an overturning in the trend direction, from increasing to decreasing. Therefore, a non-standard (non-linear) trend testing method is used. The approach is based on the generation of hypothetical time series with features similar to the measurement series, and then determining the statistical significance of

the linear trend coefficient in years 1976–2005 and 2005–2014 based on the properties of a set consisting of many such hypothetical series (in our case 100,000). This methodology is known as bootstrapping.

Using this procedure (Chapter 2) as well as the results of the measurements conducted in this study during the Baltic 2014 campaign, pro-healthy scenarios of tanning in order to achieve the adequate dose of vitamin D_3 and performing anti-psoriatic heliotherapy at the Baltic Sea are presented (Chapter 4). The previous researches focused on measuring the level of the vitamin D_3 in the serum (e.g. Kligman et al. 1989; Marx et al. 1995; Farrerons et al. 2001). Sayre and Dowdy (2007) carried out calculations of the hypothetical vitamin doses achieved after application of a cream with SPF 15 based on ultraviolet radiation spectra measured in Kuwait during the period of over two years. Usually, the UV measurements are conducted in order to assess workers' exposure to the erythemal radiation (e.g. Thieden et al. 2005). Within the presented study, contrary to the examples presented, the measurements with selected, low-cost hand-held personal meters, which may possibly be found in a widespread use to assess vitaminal and anti-psoriatic irradiation directly at the tanning site, are presented. The duration of safe tanning as well as the time of self-administered vitaminal and anti-psoriasis heliotherapy can be determined by means of these intruments.

In the next part of research, the influence of the urban environment on the erythemal doses is assessed on the example of Warsaw. A comparison is made with a rural site located outside the city, Belsk (Chapter 5). Haberlie et al. (2015) demonstrated that the large city can cause an increasing cloudiness, while Acosta and Evans (2000), using Mexico as the example, described that ultraviolet radiation can be more than 20% smaller in the city than in suburban areas. However, the examination of the difference in doses of erythemal radiation between Warsaw and Belsk shows that Warsaw does not generate increased cloudiness and specific aerosols loading that attenuates ultraviolet radiation. Thus, heliotherapy in the city can be as effective as in non-urban areas.

The most important conclusions and achievements resulting from the study reported here are presented below:

- a procedure for determining dose rate with vitaminal, anti-psoriatic and anti-DNA efficacy based on the erythemal dose rate measurements is developed;
- in 2005, an overturning of the UV trend from increasing to decreasing is observed for most of the biological effects discussed. This change is not the result of a reversal of the trend in total ozone but is probably due to an increase in cloudiness or the optical depth of the atmospheric aerosol;
- properly calibrated personal hand-held meters can be used to determine non-erythemal irradiation doses directly at the place of outdoor activities;
- during the summer period at the Baltic Sea coast, anti-psoriatic heliotherapy can be effectively performed;
- safe tanning scenario determined strictly according to dermatologists' recommendations, i.e. applying SPF 30 sunscreen according to the instructions (15 minutes before going out into the sun, and then repeating it every 2 hours and after playing sports or bathing), does not provide the recommended vitamin dose even for a few hours stay on the beach;
- it is possible to produce the adequate dose of vitamin D_3 due to the skin synthesis during a stay on the beach, following a scenario of short (~20–30 minutes) tanning without photoprotection and next applying a cream with SPF > 15;
- in Warsaw, the conditions for heliotherapy are the same as in "clean" suburban areas of the Mazowieckie voivodeship;
- Warsaw does not generate a specific aerosol or cloudiness affecting the UV radiation.

The results presented here are an important contribution to the state of knowledge in the field of photobiology and at the same time have a direct link with practical applications. In response to the scientific needs (Baggerly et al. 2015), a method to assess the duration of self-administered anti-psoriatic and vitaminal heliotherapy using personal *UVI* meters, which are widely available for a small price, is proposed. In the future, it is possible to introduce a smartphone application that would significantly simplify the administration of anti-psoriatic heliotherapy.

APPENDIX

The tables presented below include coefficients used for the determination of the dose rate with non-erythemal efficacy from the erythemal dose rate values: Tables 1A–3A. The corresponding standard deviations for the presented coefficients are in Tables 4A–6A.

Tables 7A–9A show coefficients for determining daily non-erythemal UV radiation doses from the values of erythemal doses. Tables 10A–12A contain the standard deviations for the determined coefficients.

Figures 1A–6A present a visualisation of the dependence of coefficients on TO_3 and SZA.

Table 1A
DR_{DNA}/DR_{ERYT} quotient matrix

SZA/TO_3	27.5	32.5	37.5	42.5	47.5	52.5	57.5	62.5	67.5	72.5	77.5	82.5	87.5
245	0.627	0.599	0.595	0.586	0.587	0.572	0.517	0.469	0.424	0.356	0.292	0.267	0.307
255	0.627	0.599	0.595	0.586	0.587	0.54	0.522	0.452	0.403	0.34	0.278	0.257	0.296
265	0.627	0.599	0.595	0.586	0.568	0.536	0.486	0.439	0.39	0.33	0.275	0.253	0.288
275	0.627	0.599	0.595	0.587	0.56	0.52	0.471	0.426	0.372	0.316	0.265	0.246	0.281
285	0.627	0.599	0.586	0.577	0.542	0.505	0.458	0.411	0.362	0.308	0.26	0.241	0.274
295	0.627	0.613	0.585	0.558	0.527	0.486	0.441	0.399	0.351	0.301	0.253	0.237	0.275
305	0.62	0.601	0.576	0.549	0.512	0.474	0.426	0.385	0.337	0.289	0.248	0.232	0.267
315	0.601	0.59	0.565	0.536	0.5	0.459	0.416	0.373	0.331	0.285	0.243	0.229	0.263
325	0.593	0.58	0.551	0.523	0.487	0.447	0.403	0.364	0.32	0.277	0.238	0.225	0.258
335	0.574	0.563	0.537	0.507	0.476	0.436	0.391	0.353	0.314	0.269	0.233	0.222	0.256
345	0.568	0.551	0.526	0.498	0.463	0.425	0.381	0.343	0.303	0.263	0.23	0.219	0.249
355	0.554	0.541	0.514	0.486	0.451	0.413	0.372	0.338	0.297	0.26	0.226	0.216	0.245
365	0.551	0.53	0.507	0.474	0.445	0.407	0.364	0.329	0.29	0.254	0.222	0.214	0.242
375	0.534	0.517	0.486	0.464	0.431	0.396	0.355	0.323	0.285	0.249	0.218	0.21	0.238
385	0.505	0.504	0.478	0.456	0.423	0.385	0.343	0.312	0.277	0.241	0.214	0.208	0.235
395	0.508	0.491	0.47	0.444	0.417	0.381	0.341	0.308	0.273	0.239	0.213	0.206	0.232
405	0.468	0.47	0.458	0.428	0.407	0.368	0.33	0.301	0.268	0.235	0.209	0.204	0.228
415	0.499	0.478	0.452	0.418	0.399	0.36	0.322	0.297	0.264	0.234	0.209	0.205	0.226
425	0.499	0.473	0.443	0.413	0.388	0.354	0.319	0.288	0.255	0.224	0.204	0.2	0.221
435	0.499	0.48	0.44	0.411	0.382	0.35	0.308	0.284	0.251	0.221	0.2	0.196	0.213
445	0.499	0.467	0.402	0.392	0.377	0.346	0.314	0.278	0.242	0.221	0.201	0.194	0.206
455	0.499	0.467	0.426	0.4	0.37	0.333	0.299	0.281	0.242	0.22	0.205	0.201	0.214
465	0.499	0.467	0.426	0.389	0.346	0.315	0.293	0.264	0.237	0.213	0.195	0.192	0.211
475	0.499	0.467	0.426	0.364	0.354	0.319	0.284	0.258	0.232	0.207	0.193	0.188	0.207
485	0.499	0.467	0.426	0.346	0.35	0.319	0.274	0.245	0.22	0.201	0.191	0.191	0.208
495	0.499	0.467	0.426	0.346	0.336	0.305	0.274	0.251	0.229	0.203	0.19	0.19	0.205
505	0.499	0.467	0.426	0.346	0.322	0.3	0.275	0.256	0.229	0.203	0.19	0.19	0.205
515	0.499	0.467	0.426	0.346	0.335	0.3	0.275	0.256	0.229	0.203	0.19	0.19	0.205

Table 2A

DR_{AP}/DR_{ERYT} quotient matrix

SZA/TO_3	27.5	32.5	37.5	42.5	47.5	52.5	57.5	62.5	67.5	72.5	77.5	82.5	87.5
245	0.774	0.754	0.753	0.748	0.747	0.736	0.695	0.659	0.623	0.572	0.534	0.534	0.567
255	0.774	0.754	0.753	0.748	0.747	0.712	0.693	0.645	0.607	0.561	0.526	0.528	0.563
265	0.774	0.754	0.753	0.748	0.732	0.709	0.672	0.635	0.597	0.554	0.524	0.527	0.557
275	0.774	0.754	0.753	0.747	0.727	0.697	0.66	0.623	0.584	0.545	0.519	0.524	0.553
285	0.774	0.754	0.744	0.74	0.714	0.686	0.65	0.614	0.577	0.54	0.516	0.521	0.55
295	0.774	0.764	0.745	0.726	0.703	0.672	0.637	0.604	0.569	0.536	0.513	0.52	0.548
305	0.77	0.756	0.739	0.72	0.692	0.663	0.625	0.594	0.559	0.529	0.511	0.517	0.545
315	0.756	0.749	0.731	0.71	0.682	0.651	0.617	0.585	0.555	0.527	0.509	0.517	0.543
325	0.751	0.742	0.72	0.7	0.672	0.642	0.608	0.578	0.548	0.522	0.506	0.516	0.54
335	0.738	0.729	0.71	0.688	0.664	0.633	0.598	0.571	0.543	0.518	0.505	0.515	0.538
345	0.734	0.72	0.702	0.681	0.654	0.624	0.591	0.563	0.536	0.514	0.503	0.512	0.535
355	0.723	0.713	0.693	0.672	0.645	0.616	0.584	0.559	0.533	0.512	0.501	0.511	0.531
365	0.721	0.705	0.688	0.662	0.64	0.611	0.578	0.553	0.529	0.509	0.501	0.511	0.531
375	0.708	0.695	0.672	0.655	0.629	0.603	0.572	0.549	0.525	0.507	0.499	0.509	0.527
385	0.686	0.686	0.666	0.648	0.623	0.594	0.563	0.542	0.521	0.504	0.498	0.508	0.526
395	0.689	0.675	0.659	0.64	0.618	0.591	0.561	0.539	0.519	0.502	0.498	0.508	0.524
405	0.657	0.66	0.649	0.627	0.611	0.582	0.554	0.535	0.515	0.501	0.497	0.506	0.522
415	0.683	0.668	0.645	0.619	0.605	0.575	0.548	0.532	0.513	0.5	0.496	0.507	0.521
425	0.683	0.657	0.639	0.615	0.597	0.571	0.545	0.526	0.509	0.497	0.496	0.505	0.519
435	0.683	0.666	0.637	0.615	0.592	0.567	0.539	0.524	0.507	0.495	0.494	0.502	0.516
445	0.683	0.659	0.608	0.6	0.589	0.565	0.542	0.521	0.502	0.496	0.493	0.5	0.51
455	0.683	0.659	0.626	0.604	0.583	0.557	0.534	0.521	0.503	0.495	0.497	0.506	0.515
465	0.683	0.659	0.626	0.595	0.567	0.547	0.529	0.513	0.5	0.493	0.493	0.502	0.513
475	0.683	0.659	0.626	0.579	0.571	0.546	0.524	0.51	0.498	0.491	0.493	0.501	0.51
485	0.683	0.659	0.626	0.564	0.568	0.546	0.519	0.503	0.494	0.491	0.495	0.502	0.513
495	0.683	0.659	0.626	0.564	0.558	0.537	0.52	0.506	0.495	0.489	0.492	0.501	0.51
505	0.683	0.659	0.626	0.564	0.547	0.532	0.518	0.508	0.495	0.489	0.492	0.501	0.51
515	0.683	0.659	0.626	0.564	0.557	0.532	0.518	0.508	0.495	0.489	0.492	0.501	0.51

Table 3A
$DR_{VIT\text{-}D3}/DR_{ERYT}$ quotient matrix

SZA/TO_3	27.5	32.5	37.5	42.5	47.5	52.5	57.5	62.5	67.5	72.5	77.5	82.5	87.5
245	2.112	2.055	2.077	1.997	2.068	2.058	1.977	1.886	1.774	1.549	1.237	0.976	1.033
255	2.112	2.055	2.077	1.997	2.068	2.012	1.957	1.85	1.718	1.491	1.174	0.933	0.999
265	2.112	2.055	2.077	1.997	2.058	2.011	1.92	1.819	1.678	1.454	1.157	0.912	0.977
275	2.112	2.055	2.077	2.069	2.043	1.983	1.893	1.773	1.623	1.396	1.107	0.87	0.952
285	2.112	2.055	2.06	2.063	2.019	1.959	1.865	1.745	1.587	1.361	1.082	0.853	0.926
295	2.112	2.095	2.07	2.036	1.993	1.922	1.823	1.709	1.543	1.325	1.046	0.828	0.922
305	2.091	2.083	2.054	2.021	1.967	1.899	1.786	1.665	1.494	1.273	1.021	0.804	0.897
315	2.084	2.077	2.043	2.005	1.947	1.864	1.753	1.624	1.466	1.253	0.986	0.781	0.892
325	2.073	2.065	2.029	1.987	1.922	1.836	1.722	1.595	1.425	1.217	0.959	0.766	0.876
335	2.056	2.043	2.007	1.958	1.9	1.813	1.685	1.559	1.391	1.177	0.926	0.749	0.865
345	2.046	2.024	1.982	1.941	1.871	1.784	1.653	1.522	1.351	1.144	0.91	0.737	0.837
355	2.029	2.015	1.969	1.919	1.847	1.753	1.628	1.504	1.33	1.128	0.884	0.718	0.818
365	2.026	1.994	1.961	1.897	1.836	1.736	1.602	1.471	1.294	1.094	0.86	0.705	0.812
375	2.017	1.98	1.919	1.877	1.801	1.705	1.567	1.444	1.272	1.065	0.837	0.688	0.797
385	1.959	1.956	1.904	1.861	1.778	1.671	1.528	1.398	1.233	1.023	0.806	0.674	0.784
395	1.958	1.926	1.893	1.831	1.765	1.66	1.52	1.383	1.211	1.006	0.797	0.661	0.769
405	1.868	1.877	1.87	1.792	1.736	1.616	1.474	1.353	1.187	0.982	0.771	0.651	0.753
415	1.95	1.899	1.85	1.762	1.714	1.592	1.444	1.331	1.165	0.976	0.774	0.655	0.737
425	1.95	1.983	1.822	1.752	1.682	1.568	1.436	1.294	1.118	0.915	0.735	0.629	0.726
435	1.95	1.948	1.817	1.736	1.667	1.558	1.388	1.278	1.094	0.895	0.712	0.61	0.692
445	1.95	1.865	1.708	1.688	1.649	1.545	1.419	1.241	1.042	0.888	0.718	0.607	0.653
455	1.95	1.865	1.784	1.731	1.624	1.482	1.342	1.27	1.035	0.889	0.743	0.63	0.683
465	1.95	1.865	1.784	1.712	1.53	1.391	1.323	1.171	1.012	0.842	0.667	0.572	0.674
475	1.95	1.865	1.784	1.602	1.566	1.435	1.28	1.139	0.976	0.794	0.652	0.553	0.639
485	1.95	1.865	1.784	1.555	1.553	1.438	1.225	1.059	0.895	0.744	0.619	0.575	0.653
495	1.95	1.865	1.784	1.555	1.506	1.373	1.213	1.098	0.963	0.773	0.633	0.568	0.645
505	1.95	1.865	1.784	1.555	1.45	1.363	1.24	1.125	0.963	0.773	0.633	0.568	0.645
515	1.95	1.865	1.784	1.555	1.504	1.363	1.24	1.125	0.963	0.773	0.633	0.568	0.645

Table 4A
Standard deviation matrix for DR_{DNA}/DR_{ERYT} quotients

SZA/TO_3	27.5	32.5	37.5	42.5	47.5	52.5	57.5	62.5	67.5	72.5	77.5	82.5	87.5
245	0.016	0.079	0.036	0.023	0.034	0.006	0.013	0.015	0.016	0.021	0.016	0.005	0.017
255	0.016	0.079	0.036	0.023	0.034	0.023	0.108	0.02	0.021	0.022	0.015	0.009	0.012
265	0.016	0.079	0.036	0.023	0.013	0.023	0.02	0.018	0.021	0.02	0.015	0.007	0.018
275	0.016	0.079	0.036	0.027	0.023	0.02	0.019	0.063	0.021	0.02	0.014	0.007	0.016
285	0.016	0.079	0.057	0.024	0.02	0.02	0.019	0.019	0.02	0.019	0.014	0.008	0.015
295	0.016	0.028	0.029	0.023	0.026	0.025	0.023	0.025	0.028	0.026	0.02	0.019	0.066
305	0.031	0.034	0.036	0.036	0.022	0.019	0.022	0.023	0.023	0.02	0.014	0.007	0.038
315	0.028	0.025	0.032	0.024	0.024	0.025	0.048	0.025	0.035	0.029	0.02	0.016	0.018
325	0.028	0.023	0.026	0.024	0.022	0.021	0.02	0.021	0.022	0.019	0.015	0.012	0.016
335	0.03	0.029	0.028	0.024	0.023	0.021	0.021	0.023	0.056	0.021	0.012	0.009	0.012
345	0.026	0.028	0.034	0.032	0.025	0.02	0.024	0.02	0.02	0.017	0.014	0.008	0.013
355	0.033	0.03	0.028	0.026	0.023	0.021	0.02	0.018	0.018	0.014	0.011	0.007	0.014
365	0.03	0.03	0.02	0.023	0.021	0.018	0.017	0.02	0.019	0.015	0.01	0.005	0.012
375	0.034	0.033	0.031	0.024	0.019	0.017	0.02	0.019	0.018	0.014	0.01	0.006	0.014
385	0.031	0.027	0.021	0.022	0.017	0.02	0.019	0.022	0.018	0.014	0.009	0.008	0.011
395	0.028	0.03	0.025	0.019	0.021	0.017	0.021	0.018	0.019	0.014	0.01	0.005	0.011
405	0.028	0.03	0.026	0.025	0.018	0.02	0.018	0.019	0.017	0.013	0.009	0.006	0.01
415	0.004	0.042	0.024	0.016	0.016	0.019	0.012	0.02	0.015	0.017	0.012	0.017	0.009
425	0.004	–	0.032	0.019	0.017	0.02	0.017	0.015	0.02	0.01	0.006	0.005	0.012
435	0.004	0.032	0.001	0.022	0.014	0.014	0.009	0.014	0.014	0.011	0.007	0.005	0.009
445	0.004	0.042	0.031	0.025	0.015	0.012	0.011	0.014	0.013	0.021	0.005	0.003	0.007
455	0.004	0.042	–	0.019	0.014	0.009	0.013	0.018	0.011	0.01	0.017	0.01	0.01
465	0.004	0.042	–	0.03	0.015	0.012	0.01	0.013	0.013	0.01	0.006	0.004	0.006
475	0.004	0.042	–	0.011	0.02	0.01	0.007	0.015	0.016	0.012	0.007	0.004	0.006
485	0.004	0.042	–	0.006	0.006	0.014	–	–	–	–	–	–	–
495	0.004	0.042	–	0.006	0.014	0.01	0.007	0.013	0.011	0.008	0.005	0.004	0.006
505	0.004	0.042	–	0.006	–	–	–	–	0.011	0.008	0.005	0.004	0.006
515	0.004	0.042	–	0.006	0.001	–	–	–	0.011	0.008	0.005	0.004	0.006

Table 5A
Standard deviation matrix for DR_{AP}/DR_{ERYT} quotients

SZA/TO_3	27.5	32.5	37.5	42.5	47.5	52.5	57.5	62.5	67.5	72.5	77.5	82.5	87.5
245	0.011	0.059	0.026	0.015	0.025	0.004	0.01	0.012	0.012	0.015	0.009	0.003	0.012
255	0.011	0.059	0.026	0.015	0.025	0.017	0.051	0.015	0.016	0.015	0.008	0.004	0.007
265	0.011	0.059	0.026	0.015	0.01	0.018	0.015	0.014	0.016	0.014	0.007	0.005	0.012
275	0.011	0.059	0.026	0.021	0.018	0.015	0.015	0.027	0.016	0.013	0.006	0.004	0.01
285	0.011	0.059	0.042	0.017	0.015	0.015	0.015	0.015	0.014	0.012	0.006	0.006	0.01
295	0.011	0.021	0.021	0.017	0.019	0.019	0.018	0.019	0.019	0.018	0.011	0.011	0.024
305	0.023	0.025	0.026	0.025	0.016	0.014	0.017	0.017	0.015	0.011	0.005	0.007	0.021
315	0.02	0.019	0.022	0.019	0.018	0.019	0.02	0.018	0.024	0.019	0.011	0.009	0.01
325	0.021	0.018	0.02	0.018	0.017	0.016	0.015	0.015	0.015	0.011	0.006	0.006	0.01
335	0.023	0.022	0.021	0.019	0.017	0.016	0.016	0.016	0.021	0.01	0.004	0.005	0.008
345	0.02	0.021	0.024	0.024	0.017	0.015	0.015	0.013	0.013	0.01	0.006	0.005	0.008
355	0.026	0.023	0.021	0.019	0.018	0.016	0.014	0.013	0.011	0.007	0.003	0.005	0.01
365	0.022	0.023	0.016	0.018	0.016	0.013	0.012	0.014	0.011	0.007	0.002	0.004	0.007
375	0.026	0.025	0.022	0.019	0.014	0.013	0.014	0.012	0.01	0.006	0.003	0.005	0.008
385	0.025	0.021	0.016	0.017	0.013	0.014	0.013	0.014	0.01	0.006	0.003	0.004	0.008
395	0.021	0.024	0.019	0.014	0.016	0.012	0.015	0.012	0.011	0.006	0.002	0.004	0.008
405	0.024	0.025	0.02	0.019	0.014	0.014	0.012	0.012	0.009	0.005	0.002	0.004	0.007
415	0.002	0.03	0.018	0.011	0.012	0.013	0.008	0.013	0.008	0.007	0.004	0.006	0.009
425	0.002	–	0.021	0.014	0.013	0.014	0.011	0.009	0.011	0.003	0.002	0.003	0.007
435	0.002	0.022	0.001	0.016	0.01	0.01	0.007	0.008	0.006	0.004	0.002	0.004	0.004
445	0.002	0.034	0.021	0.018	0.01	0.008	0.006	0.008	0.007	0.009	0.001	0.003	0.006
455	0.002	0.034	–	0.011	0.01	0.008	0.008	0.009	0.005	0.002	0.005	0.004	0.005
465	0.002	0.034	–	0.021	0.01	0.007	0.006	0.007	0.005	0.002	0.002	0.002	0.003
475	0.002	0.034	–	0.007	0.014	0.006	0.004	0.008	0.006	0.002	0.002	0.001	0.004
485	0.002	0.034	–	0.005	0.003	0.01	–	–	–	–	–	–	–
495	0.002	0.034	–	0.005	0.01	0.006	0.008	0.008	0.004	0.002	0.003	0.002	0.003
505	0.002	0.034	–	0.005	–	–	–	–	0.004	0.002	0.003	0.002	0.003
515	0.002	0.034	–	0.005	0.001	–	–	–	0.004	0.002	0.003	0.002	0.003

Table 6A
Standard deviation matrix for $DR_{VIT\text{-}D3}/DR_{ERYT}$ quotients

SZA/TO_3	27.5	32.5	37.5	42.5	47.5	52.5	57.5	62.5	67.5	72.5	77.5	82.5	87.5
245	0.014	0.123	0.034	0.07	0.039	0.006	0.023	0.03	0.043	0.083	0.089	0.025	0.045
255	0.014	0.123	0.034	0.07	0.039	0.038	0.029	0.046	0.063	0.087	0.088	0.062	0.047
265	0.014	0.123	0.034	0.07	0.019	0.045	0.048	0.05	0.071	0.088	0.089	0.047	0.058
275	0.014	0.123	0.034	0.023	0.038	0.041	0.046	0.057	0.075	0.089	0.089	0.043	0.054
285	0.014	0.123	0.111	0.044	0.04	0.049	0.05	0.057	0.072	0.091	0.093	0.052	0.052
295	0.014	0.039	0.048	0.041	0.063	0.065	0.062	0.075	0.104	0.106	0.109	0.097	0.123
305	0.065	0.065	0.089	0.114	0.05	0.05	0.067	0.079	0.108	0.111	0.094	0.042	0.094
315	0.047	0.05	0.1	0.057	0.065	0.06	0.07	0.086	0.104	0.121	0.116	0.085	0.094
325	0.06	0.048	0.062	0.055	0.058	0.061	0.064	0.079	0.097	0.103	0.101	0.073	0.077
335	0.062	0.062	0.066	0.059	0.065	0.062	0.066	0.084	0.095	0.119	0.093	0.056	0.051
345	0.067	0.066	0.106	0.105	0.097	0.066	0.109	0.084	0.095	0.094	0.095	0.048	0.053
355	0.073	0.074	0.073	0.084	0.074	0.071	0.073	0.074	0.088	0.087	0.089	0.036	0.064
365	0.079	0.082	0.053	0.064	0.065	0.061	0.064	0.084	0.099	0.09	0.085	0.03	0.053
375	0.085	0.078	0.107	0.073	0.059	0.06	0.08	0.083	0.093	0.091	0.081	0.035	0.075
385	0.089	0.079	0.064	0.065	0.058	0.07	0.077	0.107	0.098	0.096	0.078	0.041	0.053
395	0.078	0.079	0.08	0.065	0.067	0.062	0.087	0.081	0.097	0.091	0.087	0.03	0.05
405	0.058	0.072	0.084	0.079	0.057	0.074	0.078	0.091	0.099	0.089	0.076	0.031	0.054
415	0.002	0.147	0.086	0.06	0.057	0.077	0.054	0.087	0.085	0.106	0.089	0.069	0.063
425	0.002	–	0.129	0.069	0.055	0.081	0.076	0.073	0.107	0.072	0.057	0.021	0.039
435	0.002	0.124	0.008	0.084	0.045	0.062	0.037	0.069	0.081	0.076	0.062	0.034	0.054
445	0.002	0.082	0.117	0.091	0.065	0.048	0.063	0.072	0.077	0.13	0.049	0.018	0.046
455	0.002	0.082	–	0.086	0.056	0.038	0.068	0.103	0.072	0.077	0.121	0.055	0.044
465	0.002	0.082	–	0.125	0.069	0.067	0.047	0.075	0.091	0.077	0.066	0.018	0.034
475	0.002	0.082	–	0.049	0.077	0.045	0.035	0.08	0.104	0.093	0.07	0.019	0.033
485	0.002	0.082	–	0.016	0.031	0.056	–	–	–	–	–	–	–
495	0.002	0.082	–	0.016	0.054	0.045	0.026	0.069	0.075	0.061	0.051	0.026	0.027
505	0.002	0.082	–	0.016	–	–	–	–	0.075	0.061	0.051	0.026	0.027
515	0.002	0.082	–	0.016	0.011	–	–	–	0.075	0.061	0.051	0.026	0.027

Table 7A
D_{DNA}/D_{ERYT} quotient matrix

SZA/TO_3	27.5	32.5	37.5	42.5	47.5	52.5
245	0.558	0.553	0.521	0.536	0.574	0.449
255	0.558	0.553	0.521	0.536	0.574	0.449
265	0.558	0.553	0.521	0.504	0.471	0.449
275	0.558	0.553	0.527	0.493	0.459	0.449
285	0.558	0.535	0.513	0.475	0.447	0.449
295	0.543	0.524	0.5	0.468	0.439	0.449
305	0.545	0.521	0.488	0.46	0.421	0.449
315	0.535	0.513	0.48	0.461	0.412	0.459
325	0.519	0.502	0.474	0.462	0.435	0.435
335	0.507	0.493	0.471	0.457	0.442	0.436
345	0.492	0.489	0.472	0.465	0.437	0.425
355	0.487	0.478	0.454	0.447	0.436	0.402
365	0.477	0.468	0.458	0.435	0.418	0.398
375	0.451	0.457	0.446	0.428	0.409	0.388
385	0.442	0.445	0.435	0.418	0.398	0.378
395	0.434	0.441	0.422	0.408	0.396	0.382
405	0.409	0.423	0.42	0.404	0.374	0.38
415	0.409	0.433	0.403	0.404	0.365	0.35
425	0.409	0.433	0.405	0.372	0.349	0.347
435	0.409	0.443	0.406	0.371	0.347	0.332
445	0.409	0.35	0.406	0.371	0.344	0.348
455	0.409	0.35	0.406	0.371	0.354	0.309
465	0.409	0.35	0.406	0.371	0.333	0.304
475	0.409	0.35	0.406	0.371	0.325	0.325
485	0.409	0.35	0.406	0.371	0.308	0.312
495	0.409	0.35	0.406	0.371	0.308	0.304
505	0.409	0.35	0.406	0.371	0.308	0.304
515	0.409	0.35	0.406	0.371	0.308	0.304

Table 8A
D_{AP}/D_{ERYT} quotient matrix

SZA/TO_3	27.5	32.5	37.5	42.5	47.5	52.5
245	0.724	0.732	0.713	0.72	0.716	0.655
255	0.724	0.732	0.713	0.72	0.716	0.655
265	0.724	0.732	0.713	0.691	0.677	0.655
275	0.724	0.732	0.715	0.686	0.667	0.655
285	0.724	0.715	0.699	0.674	0.654	0.655
295	0.721	0.704	0.688	0.667	0.646	0.655
305	0.722	0.705	0.681	0.66	0.635	0.655
315	0.712	0.697	0.676	0.659	0.63	0.678
325	0.705	0.69	0.672	0.663	0.642	0.653
335	0.694	0.686	0.672	0.656	0.649	0.64
345	0.685	0.683	0.671	0.663	0.641	0.629
355	0.68	0.673	0.655	0.65	0.638	0.62
365	0.677	0.67	0.661	0.643	0.63	0.62
375	0.668	0.665	0.65	0.636	0.625	0.611
385	0.66	0.648	0.644	0.627	0.617	0.601
395	0.644	0.646	0.64	0.619	0.605	0.594
405	0.613	0.627	0.63	0.61	0.594	0.592
415	0.613	0.633	0.609	0.611	0.594	0.593
425	0.613	0.608	0.627	0.596	0.582	0.578
435	0.613	0.633	0.623	0.586	0.584	0.568
445	0.613	0.608	0.623	0.586	0.566	0.569
455	0.613	0.608	0.623	0.586	0.573	0.569
465	0.613	0.608	0.623	0.586	0.559	0.539
475	0.613	0.608	0.623	0.586	0.553	0.553
485	0.613	0.608	0.623	0.586	0.541	0.544
495	0.613	0.608	0.623	0.586	0.541	0.539
505	0.613	0.608	0.623	0.586	0.541	0.539
515	0.613	0.608	0.623	0.586	0.541	0.539

Table 9A
$D_{VIT\text{-}D3}/D_{ERYT}$ quotient matrix

SZA/TO_3	27.5	32.5	37.5	42.5	47.5	52.5
245	1.997	1.967	1.9	1.958	1.921	1.791
255	1.997	1.967	1.9	1.958	1.921	1.791
265	1.997	1.967	1.9	1.912	1.829	1.791
275	1.997	1.967	1.926	1.885	1.803	1.791
285	1.997	1.956	1.92	1.848	1.789	1.791
295	1.955	1.943	1.906	1.836	1.778	1.791
305	1.967	1.932	1.878	1.823	1.729	1.791
315	1.963	1.918	1.863	1.826	1.697	1.798
325	1.924	1.901	1.846	1.818	1.76	1.749
335	1.904	1.882	1.834	1.817	1.779	1.777
345	1.877	1.874	1.84	1.836	1.777	1.756
355	1.876	1.858	1.809	1.795	1.779	1.679
365	1.846	1.829	1.814	1.764	1.723	1.662
375	1.77	1.798	1.794	1.748	1.698	1.637
385	1.755	1.788	1.766	1.73	1.671	1.609
395	1.748	1.78	1.719	1.701	1.679	1.635
405	1.71	1.728	1.732	1.701	1.603	1.636
415	1.71	1.776	1.698	1.701	1.57	1.508
425	1.71	1.776	1.676	1.591	1.515	1.513
435	1.71	1.806	1.7	1.599	1.501	1.454
445	1.71	1.47	1.7	1.599	1.515	1.523
455	1.71	1.47	1.7	1.599	1.544	1.352
465	1.71	1.47	1.7	1.599	1.464	1.349
475	1.71	1.47	1.7	1.599	1.434	1.433
485	1.71	1.47	1.7	1.599	1.372	1.385
495	1.71	1.47	1.7	1.599	1.372	1.349
505	1.71	1.47	1.7	1.599	1.372	1.349
515	1.71	1.47	1.7	1.599	1.372	1.349

Table 10A
Standard deviation matrix for D_{DNA}/D_{ERYT} quotients

SZA/TO_3	27.5	32.5	37.5	42.5	47.5	52.5
245	0.035	0.011	0.02	0.015	0.14	0.046
255	0.035	0.011	0.02	0.015	0.14	0.046
265	0.035	0.011	0.02	0.015	0.03	0.046
275	0.035	0.011	0.014	0.021	0.03	0.046
285	0.035	0.021	0.021	0.02	0.021	0.046
295	0.043	0.029	0.02	0.024	0.018	0.046
305	0.02	0.02	0.021	0.026	0.029	0.046
315	0.019	0.027	0.021	0.031	0.039	–
325	0.021	0.024	0.027	0.033	0.028	0.024
335	0.025	0.024	0.028	0.033	0.022	0.013
345	0.023	0.025	0.028	0.023	0.016	0.012
355	0.02	0.025	0.026	0.024	0.016	0.017
365	0.016	0.026	0.021	0.018	0.025	0.019
375	0.018	0.017	0.017	0.022	0.018	0.012
385	0.028	0.02	0.02	0.015	0.027	0.015
395	0.028	0.016	0.022	0.018	0.013	0.009
405	–	0.019	0.014	0.021	0.012	0.013
415	–	0.015	0.033	0.008	0.016	0.014
425	–	0.015	0.008	0.022	0.023	0.023
435	–	–	0.029	0.004	0.022	0.02
445	–	–	0.029	0.004	0.012	0.006
455	–	–	0.029	0.004	0.01	0.025
465	–	–	0.029	0.004	0.002	–
475	–	–	0.029	0.004	0.002	–
485	–	–	0.029	0.004	–	0.008
495	–	–	0.029	0.004	–	–
505	–	–	0.029	0.004	–	–
515	–	–	0.029	0.004	–	–

Table 11A

Standard deviation matrix for D_{AP}/D_{ERYT} quotients

SZA/TO_3	27.5	32.5	37.5	42.5	47.5	52.5
245	0.026	0.006	0.009	0.004	0.067	0.017
255	0.026	0.006	0.009	0.004	0.067	0.017
265	0.026	0.006	0.009	0.006	0.014	0.017
275	0.026	0.006	0.011	0.013	0.017	0.017
285	0.026	0.014	0.015	0.012	0.008	0.017
295	0.026	0.02	0.013	0.017	0.015	0.017
305	0.015	0.011	0.013	0.019	0.013	0.017
315	0.014	0.015	0.014	0.023	0.024	–
325	0.011	0.017	0.019	0.028	0.023	0.001
335	0.012	0.017	0.018	0.024	0.021	0.005
345	0.014	0.016	0.022	0.011	0.009	0.009
355	0.012	0.016	0.023	0.017	0.013	0.013
365	0.011	0.014	0.012	0.015	0.01	0.014
375	0.016	0.012	0.011	0.016	0.011	0.01
385	0.01	0.013	0.014	0.011	0.017	0.008
395	0.012	0.008	0.009	0.011	0.01	0.006
405	–	0.013	0.008	0.015	0.009	0.009
415	–	0.011	0.024	0.007	0.011	0.01
425	–	0.011	0.014	0.006	0.011	0.005
435	–	–	0.002	0.003	0.009	0.013
445	–	–	0.002	0.003	0.009	0.004
455	–	–	0.002	0.003	0.006	0.007
465	–	–	0.002	0.003	0.003	–
475	–	–	0.002	0.003	0.002	–
485	–	–	0.002	0.003	–	0.004
495	–	–	0.002	0.003	–	–
505	–	–	0.002	0.003	–	–
515	–	–	0.002	0.003	–	–

Table 12A
Standard deviation matrix for $D_{VIT\text{-}D3}/D_{ERYT}$ quotients

SZA/TO_3	27.5	32.5	37.5	42.5	47.5	52.5
245	0.054	0.054	0.055	0.049	0.038	0.137
255	0.054	0.054	0.055	0.049	0.038	0.137
265	0.054	0.054	0.055	0.055	0.086	0.137
275	0.054	0.054	0.047	0.064	0.086	0.137
285	0.054	0.057	0.054	0.065	0.075	0.137
295	0.096	0.064	0.053	0.07	0.057	0.137
305	0.05	0.055	0.06	0.071	0.097	0.137
315	0.048	0.054	0.061	0.078	0.119	–
325	0.059	0.061	0.071	0.078	0.075	0.09
335	0.052	0.066	0.079	0.086	0.062	0.055
345	0.065	0.069	0.073	0.072	0.06	0.045
355	0.061	0.072	0.064	0.073	0.048	0.066
365	0.056	0.08	0.069	0.062	0.095	0.076
375	0.054	0.062	0.062	0.076	0.068	0.063
385	0.108	0.067	0.069	0.059	0.097	0.068
395	0.091	0.062	0.08	0.068	0.043	0.036
405	–	0.057	0.067	0.07	0.052	0.046
415	–	0.04	0.105	0.018	0.071	0.071
425	–	0.04	0.043	0.098	0.101	0.104
435	–	–	0.113	0.018	0.096	0.09
445	–	–	0.113	0.018	0.042	0.027
455	–	–	0.113	0.018	0.036	0.123
465	–	–	0.113	0.018	0.004	–
475	–	–	0.113	0.018	0.007	–
485	–	–	0.113	0.018	–	0.045
495	–	–	0.113	0.018	–	–
505	–	–	0.113	0.018	–	–
515	–	–	0.113	0.018	–	–

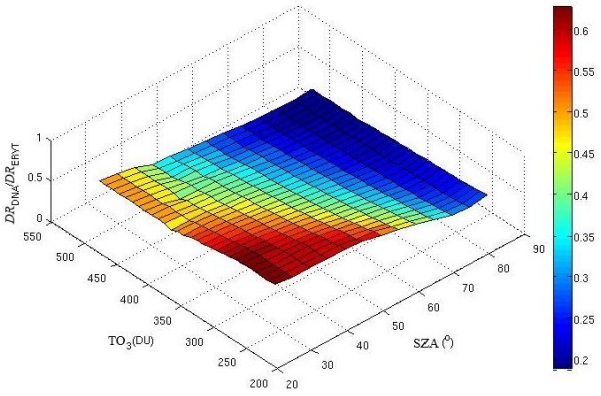

Fig. 1A. Visualisation of the dependence of DR_{DNA}/DR_{ERYT} coefficients on total ozone and solar zenith angle.

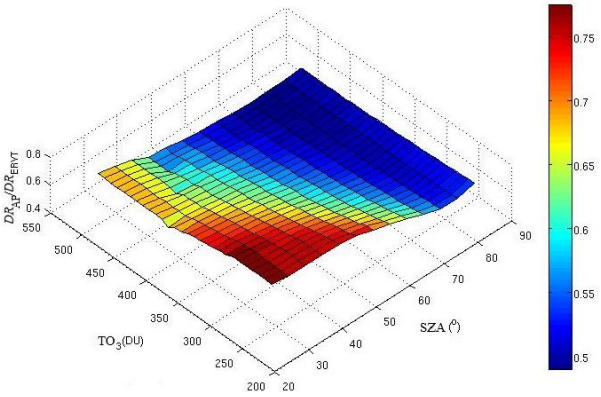

Fig. 2A. Visualisation of the dependence of DR_{AP}/DR_{ERYT} coefficients on total ozone and solar zenith angle.

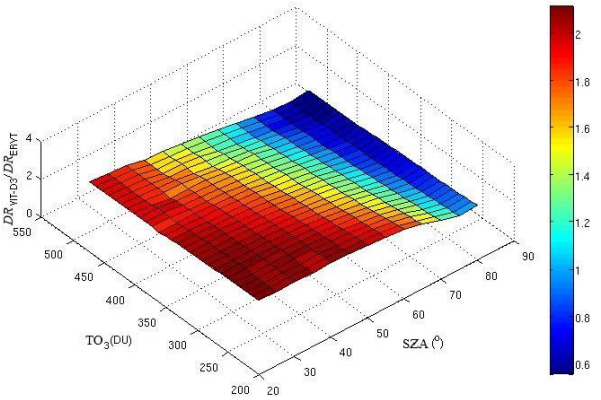

Fig. 3A. Visualisation of the dependence of DR_{VIT-D3}/DR_{ERYT} coefficients on total ozone and solar zenith angle.

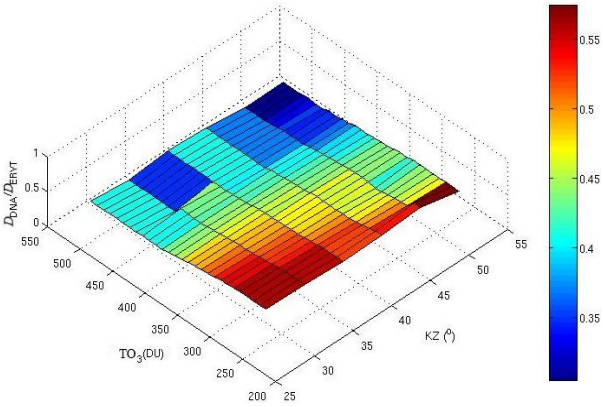

Fig. 4A. Visualisation of the dependence of D_{DNA}/D_{ERYT} coefficients on total ozone and solar zenith angle.

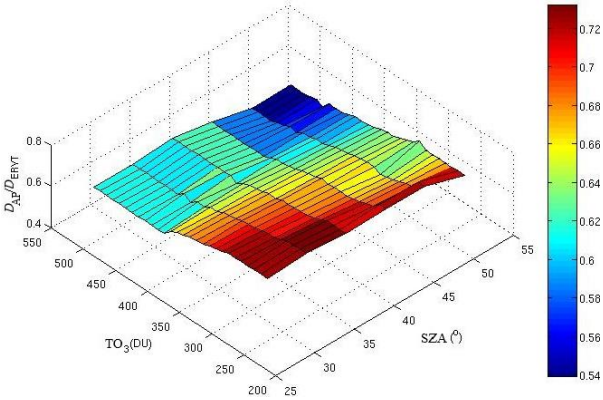

Fig. 5A. Visualisation of the dependence of D_{AP}/D_{ERYT} coefficients on total ozone and solar zenith angle.

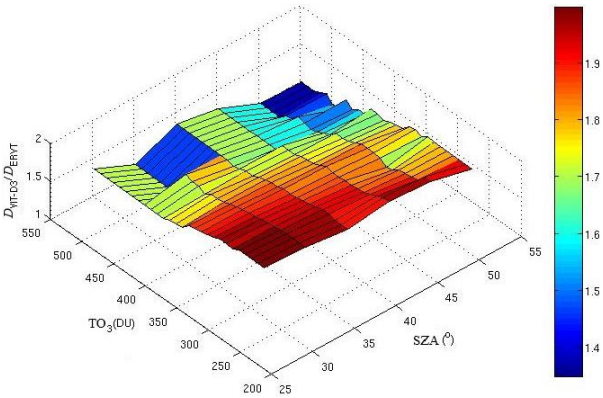

Fig. 6A. Visualisation of the dependence of D_{VIT-D3}/D_{ERYT} coefficients on total ozone and solar zenith angle.

List of abbreviations and terms used in text

AERONET – an international network for monitoring parameters that determine the properties of atmospheric aerosol (Aerosol RObotic NETwork),
"AP" index – a biological effect of UV radiation – removal of psoriatic lesions (anti-psoriatic effect),
"BIOL" index – any chosen biological effect of UV radiation,
CGO – Central Geophysical Observatory located at Belsk,
CIE – the International Commission on Illumination (the Commission Internationale de l´Eclairage),
D_{BIOL} – irradiation dose causing a given biological effect,
"DNA" index – a biological effect of UV radiation – destruction of the DNA structure,
DR_{BIOL} – irradiation intensity, so-called dose rate causing a given biological effect,
DU – an unit expressing the total ozone content in the atmosphere (Dobson Unit),
EISC – Erythemal Irradiation Strengthening Coefficient,
"ERYT" Index – a biological effect of UV radiation – erythema formation on the skin,
FastRT – a model for ultraviolet radiation simulation (http://nadir.nilu.no/~olaeng/fastrt/fastrt.html),
FR_{AREA} – a coefficient for calculating the individual dose of vitamin D_3 referring to the percentage value of the body surface area exposed to radiation,
$FR_{POSTURE}$ – a coefficient for calculating the personal dose of vitamin D_3, dependent on the position relative to the Sun,
GFS – the Global Forecast System,
GMT – Greenwich Mean Time,
IU – an International Unit of vitamin D_3 content, 1000 IU = 25μg,
loess – a function in the R program, based on the improved LOWESS method,
LOWESS – a smoothing method (Locally Weighted Scatterplot Smoothing),
MAPD – minimum anti-psoriatic dose,
MED – minimum erythemal dose,
MODIS – a spectroradiometer on the Aqua and Terra satellite platform (Moderate Resolution Imaging Spectroradiometer),
MVD_3D – minimal vitamin (vit. D_3) dose,
OMI – an instrument monitoring total ozone on the Aura satellite platform (Ozone Monitor Instrument),
PUV-A – phototherapy with UV-A radiation using a photosensitising substance (Psoralen),
SDD – (standard vitamin D dose),
SPF – sun protection factor against UV-B radiation (Sun Protection Factor),
SUP – Selective UV-B Phototherapy,
SZA – the solar zenith angle,
TO_3 – total ozone,
UV – ultraviolet,
UV-A – ultraviolet in the 315–400 nm range (long wave),
UV-B – ultraviolet in the 280–315 nm range (medium wave),
UV-C – ultraviolet in the 100–280 nm range (short wave),
UVI – UV index,
"VIT_D3" index – a biological effect of UV radiation – induction of vitamin D_3 synthesis,
WHO – World Health Organisation.

References

Acosta, L.R., and W.F.J. Evans (2000), Design of the Mexico City UV monitoring network: UV-B measurements at ground level in the urban environment, *J. Geophys. Res*. **105**, D4, 5017–5026, DOI: 10.1029/1999JD900250.

Akaike, H. (1973), Information theory and an extension of the maximum likelihood principle. **In:** B.N. Petrov and F. Csaki (eds.), *Proc. Second International Symp. on Information Theory*, Akademiai Kiado, Budapest, 267–281, DOI: 10.1007/978-1-4612-1694-0_15.

Albert, M.R., and K.G. Ostheimer (2002), The evolution of current medical and popular attitudes toward ultraviolet light exposure: Part 1, *J. Am. Acad. Dermatol.* **47**, 6, 930–937, DOI: 10.1067/mjd.2002.127254.

Albert, M.R., and K.G. Ostheimer (2003), The evolution of current medical and popular attitudes toward ultraviolet light exposure: Part 3, *J. Am. Acad. Dermatol.* **49**, 6, 1096–1106, DOI: 10.1016/S0190-9622(03)00021-5.

Baggerly, C.A., R.E. Cuomo, C.B. French, C.F. Garland, E.D. Gorham, W.B. Grant, R.P. Heaney, M.F. Holick, B.W Hollis, S.L. McDonnell, M. Pittaway, P. Seaton, C.L. Wagner, and A. Wunsch (2015), Sunlight and vitamin D: necessary for public health, *J. Am. Coll. Nutrition* **34**, 4, 359–365, DOI: 10.1080/07315724.2015.1039866.

Balicki, A., and W. Makać (2004), *Metody Wnioskowania Statystycznego*, Wydawnictwo Uniwersytetu Gdańskiego, Gdańsk (in Polish).

Bowszyc-Dmochowska, M. (2010), Działanie promieniowania ultrafioletowego na skórę. Ostre i przewlekłe uszkodzenie posłoneczne, *Homines Hominibus* **6**, 29–42 (in Polish).

Brannon, H.L. (2015), SPF – Sun Protection Factor, available from: http://dermatology.about.com/od/glossarys/g/spf.htm (accessed: 23 January 2015).

CIE (1987), A reference action spectrum for ultraviolet induced erythema in human skin (A.F. MacKinley and B.L. Diffey (eds.)), *CIE J.* **6**, 1, 17–22.

CIE (2006), Action spectrum for the production of previtamin D3 in human skin, Tech. Rep. No. 174, CIE Publications, International Commission on Illumination, Vienna.

Cleveland, W.S. (1979), Robust locally weighted regression and smoothing scatterplots, *J. Am. Statist. Assoc*. **74**, 368, 829–836, DOI: 10.1080/01621459.1979.10481038.

Cleveland, W.S., E. Grosse, and W.M. Shyu (1992), Local regression models. Chp. 8. **In:** J.M. Chambers and T.J. Hastie (eds.), *Statistical Models in S*,Wadsworth & Brooks/Cole.

Cohen, A.D., J. Shapiro, D. Michael, E. Hodak, D. Van-Dijk, L. Naggan, and D.A. Vardy (2008), Outcome of "short-term" Dead Sea climatotherapy for psoriasis, *Acta Derm.-Venereol*. **88**, 1, 90–91, DOI: 10.2340/00015555-0340.

Dowdy, J.C., R.M. Sayre, and M.F. Holick (2010), Holick's rule and vitamin D from sunlight, *J. Steroid Biochem. Mol. Biol*. **121**, 1-2, 328–330, DOI: 10.1016/j.jsbmb.2010.04.002.

Engelsen, O., and A. Kylling (2005), Fast simulation tool for ultraviolet radiation at the Earth's surface, *Opt. Eng*. **44**, 4, 041012, DOI: 10.1117/1.1885472.

Farrerons, J., M. Barnadas, A. López-Navidad, A. Renau, J. Rodríguez, B. Yoldi, and A. Alomar (2001), Sunscreen and risk of osteoporosis in the elderly: A two-year follow-up, *Dermatology* **202**, 27–30, DOI: 10.1159/000051580.

Fioletov, V.E., L.J.B. McArthur, T.W. Mathews, and L. Marrett (2009), On the relationship between erythemal and vitamin D action spectrum weighted ultraviolet radiation, *J. Photochem. Photobiol. B: Biology* **95**, 1, 9–16, DOI: 10.1016/j.jphotobiol.2008.11.014.

Fitzpatrick, T.B. (1988), The validity and practicality of sun-reactive skin types I through VI, *Arch. Dermatol*. **124**, 6, 869–871, DOI: 10.1001/archderm.1988.01670060015008.

Garland, C.F., F.C. Garland, E.D. Gorham, M. Lipkin, H. Newmark, S.B. Mohr, and M.F. Holick (2006), The role of vitamin D in cancer prevention, *Am. J. Public Health* **96**, 2, 252–261, DOI: 10.2105/AJPH.2004.045260.

Haberlie, A.M., W.S. Ashley, and T.J. Pingel (2015), The effect of urbanisation on the climatology of thunderstorm initiation, *Q. J. R. Meteorol. Soc*. **141**, 688, 663–986, DOI: 10.1002/qj.2499.

Hockberger, P.E. (2002), A history of ultraviolet photobiology for humans, animals and microorganisms, *Photochem. Photobiol*. **76**, 6, 561–579, DOI: 10.1562/0031-8655(2002)076<0561: AHOUPF>2.0.CO;2.

Holick, M.F. (1989), Will 1,25-dihydroxyvitamin D3, MC 903, and their analogues herald a new pharmacologic era for the treatment of psoriasis? *Arch Dermatol*. **125**, 12, 1692–1697, DOI: 10.1001/archderm.1989.01670240092022.

Holick, M.F., and Tai C. Chen (2008), Vitamin D deficiency: a worldwide problem with health consequences, *Am. J. Clin. Nutr*. **87** (Suppl.), 4, 1080S-1086S.

Horn, E.J., K.M. Fox, V. Patel, Chiun-Fang Chiou, F. Dann, and M. Lebwohl (2007), Are patients with psoriasis undertreated? Results of National Psoriasis Foundation survey, *J. Am. Acad. Dermatol*. **57**, 6, 957–962, DOI: 10.1016/j.jaad.2007.06.042.

Janda, M., M. Kimlin, D. Whiteman, J. Aitken, and R. Neale (2007), Sun protection and low levels of vitamin D: are people concerned? *Cancer Causes Control* **18**, 9, 1015–1019, DOI: 10.1007/s10552-007-9042-4.

Jarosławski, J. (2015), personal communication.

Kimlin, M.G., W.J. Olds, and M.R. Moore (2007), Location and vitamin D synthesis: is the hypothesis validated by geophysical data?, *J. Photochem. Photobiol. B* **86**, 3, 234–239, DOI: 10.1016/j.jphotobiol.2006.10.004.

Kligman, E.W., A. Watkins, K. Johnson, and R. Kronland (1989), The impact of lifestyle factors on serum 25-hydroxy vitamin D levels in older adults: a preliminary study, *Fam. Pract. Res. J*. **9**, 1, 11–19.

Krzyścin, J.W., J. Jarosławski, and P.S. Sobolewski (2011a), A mathematical model for seasonal variability of vitamin D due to solar radiation, *J. Photochem. Photobiol. B* **105**, 1, 106–112, DOI: 10.1016/j.jphotobiol.2011.07.008.

Krzyścin, J.W., P.S. Sobolewski, J. Jarosławski, J. Podgórski, and B. Rajewska-Więch (2011b), Erythemal UV observations at Belsk, Poland, in the period 1976–2008: Data homogenization, climatology, and trends, *Acta Geophys.* **59**, 1, 155–182, DOI: 10.2478/s11600-010-0036-3.

Krzyścin, J.W., J. Narbutt, A. Lesiak, J. Jarosławski, P.S. Sobolewski, B. Rajewska-Więch, A. Szkop, J. Wink, and A. Czerwińska (2014), Perspectives of the antipsoriatic heliotherapy in Poland, *J. Photochem. Photobiol. B: Biology* **140**, 111–119, DOI: 10.1016/j.jphotobiol.2014.07.017.

Kushelevsky, A.P., M. Harari, A.I. Kudish, E. Hristakieva, A. Ingber, and J. Shani (1998), Safety of solar phototherapy at the Dead Sea, *J. Am. Acad. Dermatol*. **38**, 3, 447–452, DOI: 10.1016/S0190-9622(98)70504-3.

Larkö, O., and G. Swanbeck (1982), Is UVB treatment of psoriasis safe? A study of extensively UVB-treated psoriasis patients compared with a matched control group, *Acta Derm.-Venereol.* **62**, 6, 507–512.

Marks, R., P.A. Foley, D. Jolley, K.R. Knight, J. Harrison, and S.C. Thompson (1995), The effect of regular sunscreen use on vitamin D levels in an Australian population, *Arch. Dermatol*. **131**, 4, 415–21, DOI: archderm.1995.01690160043006.

Matsuoka, L.Y., L. Ide, J. Wortsman, J.A. Maclaughlin, and M.F. Holick (1987), Sunscreens suppress cutaneous vitamin D3 synthesis, *J. Clin. Endocrinol. Metab*. **64**, 6, 1165–1168, DOI: 10.1210/jcem-64-6-1165.

Matsuoka, L.Y., J. Wortsman, N. Hanifan, and M.F. Holick (1988), Chronic sunscreen use decreases circulating concentrations of 25-hydroxyvitamin D. A preliminary study, *Arch. Dermatol*. **124**, 12, 1802–1804, DOI: 10.1001/archderm.1988.01670120018003.

Mayer, B., and A. Kylling (2005), Technical note: The libRadtran software package for radiative transfer calculations – description and examples of use, *Atmos. Chem. Phys*. **5**, 7, 1855–1877, DOI: 10.5194/acp-5-1855-2005.

McKenzie, R.L., J.B. Liley, and L.O. Björn (2009), UV radiation: Balancing risks and benefits, *Photochem. Photobiol*. **85**, 1, 88–98, DOI: 10.1111/j.1751-1097.2008.00400.x.

Metropolis, N., and S. Ulam (1949), The Monte Carlo Method, *J. Am. Statistic. Assoc*. **44**, 247, 335–341, DOI: 10.1080/01621459.1949.10483310.

Ministerstwo Środowiska (2012), Rozporządzenia Ministra Środowiska z dnia 24 sierpnia 2012 r. w sprawie poziomów niektórych substancji w powietrzu, Dz. U. z dnia 18.09.2012 r., poz. 1031 (in Polish).

Nilsen, L.T.N., E. Søyland, and A.L. Krogstad (2009), Estimated ultraviolet doses to psoriasis patients during climate therapy, *Photodermatol. Photoimmunol. Photomed*. **25**, 4, 202–208, DOI: 10.1111/j.1600-0781.2009.00443.x.

Noonan, F.P., M.R. Zaidi, A. Wolnicka-Glubisz, M.R. Anver, J. Bahn, A. Wielgus, J. Cadet, T. Douki, S. Mouret, M.A. Tucker, A. Popratiloff, G. Merlino, and E.C. De Fabo (2012), Melanoma induction by ultraviolet A but not ultraviolet B radiation requires melanin pigment, *Nat. Commun*. **3**, 884, DOI: 10.1038/ncomms1893.

Norval, M., and and H.C. Wulf (2009), Does chronic sunscreen use reduce vitamin D production to insufficient levels?, *Br. J. Dermatol*. **161**, 4, 732–736, DOI: 10.1111/j.1365-2133.2009.09332.x.

Norval, M., L.O. Björn, and F.R. de Gruijl (2010), Is the action spectrum for the UV-induced production of previtamin D_3 in human skin correct?, *Photochem. Photobiol. Sci*. **9**, 11–17, DOI: 10.1039/B9PP00012G.

Papayannis, A., D. Balis, A. Bais, H. Van Der Bergh, B. Calpini, E. Durieux, L. Fiorani, L. Jaquet, I. Ziomas, and C.S. Zerefos (1998), Role of urban and suburban aerosols on solar UV radiation over Athens, Greece, *Atmosph. Environ*. **32**, 12, 2193–2201, DOI: 10.1016/S1352-2310(97)00411-1.

Parrish, J.A., and K.F. Jaenicke (1981), Action spectrum for phototherapy of psoriasis, *J. Invest. Dermatol*. **76**, 5, 359–362, DOI: 10.1111/1523-1747.ep12520022.

Parrish, J.A., T.B. Fitzpatrick, L. Tanenbaum, and M.A. Pathak (1974), Photochemotherapy of psoriasis with oral methoxsalen and longwave ultraviolet light, *N. Engl. J. Med*. **291**, 1207–1211, DOI: 10.1056/NEJM197412052912301.

Płudowski, P., E. Karczmarewicz, D. Chlebna-Sokół, J. Czech-Kowalska, R.Dębski, A. Dobrzańska, E. Franek, P. Głuszko, J. Konstantynowicz, J. Książyk, K. Księżopolska-Orłowska, A. Lewiński, M. Litwin, R.S. Lorenc, J. Łukaszkiewicz, E. Marcinowska-Suchowierska, A. Milewicz, W. Misiorowski, M. Nowicki, P. Rozentryt, P. Socha, B. Solnica, M. Szalecki, M. Tałałaj. and M.A. Żmijewski (2013), Vitaminum D supplementation in healthy population and risk gripups of vitamin D deficiency – practice guidelines for Central Europe 2013 [Witamina D: Rekomendacje dawkowania w populacji osób zdrowych oraz w grupach ryzyka deficytów – wytyczne dla Europy Środkowej 2013 r.], *Standardy Medyczne. Pediatria* **10**, 5, 573–578 (in Polish).

Płudowski, P., W.B. Grant, H. Pal Bhattoa, M. Bayer, V. Povoroznyuk, E. Rudenka, H. Ramanau, S. Varbiro, A. Rudenka, E. Karczmarewicz, R. Lorenc, J. Czech-Kowalska, and J. Konstantynowicz (2014), Vitamin D status in Central Europe, *Int. J. Endocrinol*. **2014**, Article ID 589587, 12 pp., DOI: 10.1155/2014/589587.

Pope, S.J., M.F. Holick, S. Mackin, and D.E. Godar (2008), Action spectrum conversion factors that change erythemally weighted to previtamin D_3-weighted UV doses, *Photochem. Photobiol*. **84**, 5, 1277–1283, DOI: 10.1111/j.1751-1097.2008.00373.x.

Raab, W. (1997), History of therapeutic UV radiation. **In:** P. Altmeyer, K. Hoffmann, and M. Stücker (eds.), *Skin Cancer and UV Radiation*, Springer-Verlag, Berlin Heidelberg, 13–19.

Reisch, M. (2002), Sunscreens: active ingredients prevent skin damage, *Chem. Eng. News* **80**, 38-41.

Ripley, B.D. (2002), Time series in R 1.5.0, *R News* **2/2**, 2–7, available from: http://r-project.org/doc/Rnews/Rnews_2002-2.pdf.

Sajkowska, J.J., and K. Paradowska (2014), Wielokierunkowe działanie witaminy D, *Biul. Wydz. Farm. WUM* **1**, 1–6 (in Polish).

Sayre, R.M., and J.C. Dowdy (2007), Darkness at noon: sunscreens and vitamin D_3, *Photochem. Photobiol.* **83**, 2, 459–463, DOI: 10.1562/2006-06-29-RC-956.

Setlow, R.B. (1974), The wavelengths in sunlight effective in producing skin cancer: A theoretical analysis, *Proc. Natl. Acad. Sci. U.S.A.* **71**, 9, 3363–3366, DOI: 10.1073/pnas.71.9.3363.

Slaper, H. (2002), The SHICrivm software package, National Institute for Public Health and the Environment, available from: http://www.rivm.nl/shicrivm.

Slaper, H., H.A.J.M. Reinen, M. Blumthaler, M. Huber, and F. Kuik (1995), Comparing ground-level spectrally resolved UV measurements using various instruments: A technique resolving effects of wavelength shifts and slit width, *Geophys. Res. Lett*. **22**, 20, 2721–2724, DOI: 10.1029/95GL02824.

Sobolewski, P.S., J.W. Krzyścin, J. Jarosławski, J. Wink, A. Lesiak, and J. Narbutt (2014), Controlling adverse and beneficial effects of solar UV radiation by wearing suitable clothes – Spectral transmission of different kinds of fabrics, *J. Photochem. Photobiol. B* **140**, 105–110, DOI: 10.1016/j.jphotobiol.2014.07.009.

Springbett, P., S. Buglass, and A.R. Young (2010), Photoprotection and vitamin D status, *J. Photochem. Photobiol. B* **101**, 2, 160–168, DOI: 10.1016/j.jphotobiol.2010.03.006.

Szramka-Pawlak, B. (2008), Historia badań nad łuszczycą, *Nowiny Lekarskie* **77**, 6, 480–482 (in Polish).

Śniadecki, J. (2002), *On the Physical Upbringing of Children [O Fizycznym Wychowaniu Dzieci]*, Wyd. Akademii Wychowania Fizycznego im. Bronisława Czecha w Krakowie, Kraków (reprint Ossolineum, Wrocław, 1956) (in Polish).

Thieden, E., P.A. Philipsen, J. Sandby-Møller, and H.C. Wulf (2005), Sunscreen use related to UV exposure, age, sex, and occupation based on personal dosimeter readings and sun-exposure behavior diaries, *Arch. Dermatol*. **141**, 8, 967–973, DOI: 10.1001/archderm.141.8.967.

Webb, A.R. (2006), Who, what, where and when—influences on cutaneous vitamin D synthesis, *Progress Biophys. Molecul. Biol.* **92**, 1, 17–25, DOI: 10.1016/j.pbiomolbio.2006.02.004.

WHO (2008), *Vitamin D and Cancer*, World Health Organization, International Agency for Research on Cancer, IARC Working Group Reports, WHO Press, 5, 148 pp.

Wicha, J. (2012), Droga pod słońce. Wczesna historia witaminy D, *Wiad. Chem.* **66**, 7–8, 671–696 (in Polish).

WIOŚ (2015), Roczna ocena jakości powietrza w województwie mazowieckim. Raport za rok 2014, Wojewódzki Inspektorat Ochrony Środowiska w Warszawie, available from: http://www.wios.warszawa.pl (in Polish).

Wolnicka-Głubisz, A., and P.M. Płonka (2007), Rola promieniowania UV w etiopatogenezie czerniaka skóry, *Wsp. Onkol*. **11**, 9, 419–429 (in Polish).

Zawadzka, O., K.M. Markowicz, A. Pietruczuk, T. Zielinski, and J. Jaroslawski (2013), Impact of urban pollution emitted in Warsaw on aerosol properties, *Atmos. Environ*. **69**, 15–28, DOI: 10.1016/j.atmosenv.2012.11.065.

Received 21 January 2020
Received in revised form 10 June 2020
Accepted 24 June 2020

"Publications of the Institute of Geophysics, Polish Academy of Sciences: Geophysical Data Bases, Processing and Instrumentation" appears in the following series:

A – Physics of the Earth's Interior

B – Seismology

C – Geomagnetism

D – Physics of the Atmosphere

E – Hydrology (formerly Water Resources)

P – Polar Research

M – Miscellanea

Every volume has two numbers: the first one is the consecutive number of the journal and the second one (in brackets) is the current number in the series.